

**PURDUE UNIVERSITY**  
**GRADUATE SCHOOL**  
**Thesis/Dissertation Acceptance**

This is to certify that the thesis/dissertation prepared

By Shan Cong

Entitled  
MORPHOMETRIC ANALYSIS OF HIPPOCAMPAL SUBFIELDS: SEGMENTATION,  
QUANTIFICATION AND SURFACE MODELING

For the degree of Master of Science in Electrical and Computer Engineering

Is approved by the final examining committee:

Maher E. Rizkalla \_\_\_\_\_

Li Shen \_\_\_\_\_

Eliza Y. Du \_\_\_\_\_

To the best of my knowledge and as understood by the student in the *Thesis/Dissertation Agreement, Publication Delay, and Certification/Disclaimer (Graduate School Form 32)*, this thesis/dissertation adheres to the provisions of Purdue University's "Policy on Integrity in Research" and the use of copyrighted material.

Approved by Major Professor(s): \_\_\_\_\_

Approved by: \_\_\_\_\_

Head of the Department Graduate Program

Date

MORPHOMETRIC ANALYSIS OF HIPPOCAMPAL SUBFIELDS:  
SEGMENTATION, QUANTIFICATION AND SURFACE MODELING

A Dissertation

Submitted to the Faculty

of

Purdue University

by

Shan Cong

In Partial Fulfillment of the

Requirements for the Degree

of

Master of Science in Electrical and Computer Engineering

May 2014

Purdue University

Indianapolis, Indiana

I dedicate this thesis to my parents, Xubo Cong and Xiang Li. Because of your support, I can pursue every dream in my life and make them come true.

## ACKNOWLEDGMENTS

First of all, I want to express my sincere gratitude to Dr. Eliza Y. Du for introducing me into the exciting research area of image processing. She is always knowledgeable and always has the eager to learn, which encourages me a lot. Thank her for the inspirations that she brought to me, and because of this I decided to dedicate myself in biometrics and image processing field. I miss her enthusiasm and her insights.

I am very grateful to Dr. Maher E. Rizkalla for the consistant support, patient guidance, and encouragement. I appreciate his tremendous caring about his students, and hope to keep working with him in the future.

I am especially grateful to Dr. Li Shen for providing such an interesting project to me. My thesis could not have been done without his intellectual, spiritual, and financial support. He created a great learning environment for me, and I have learned a lot from him.

I also want to express my gratitude to my colleagues at Biometrics and Pattern Recognition lab who supported me in my research: Zhi Zhou, Kai Yang, Pingge Jiang, Feng Jiang; my colleagues at Center for Neuroimaging: Lei Du, Jingwen Yan, Xiaohui Yao, Sungeun Kim, John West, Shannon Risacher, Andrew Saykin, Rui Chen, Yuese Zheng; and my friend John Michael Palmer.

## TABLE OF CONTENTS

	Page
LIST OF TABLES . . . . .	vi
LIST OF FIGURES . . . . .	vii
SYMBOLS . . . . .	xi
ABBREVIATIONS . . . . .	xii
ABSTRACT . . . . .	xiii
1 INTRODUCTION . . . . .	1
1.1 Neuroimaging Analysis in Biomedical Studies . . . . .	1
1.1.1 Image Segmentation and Quantification . . . . .	1
1.1.2 Shape Modeling and Analysis . . . . .	2
1.2 Previous Work . . . . .	4
1.3 Main Contributions of The Thesis . . . . .	5
1.3.1 Hippocampal Segmentation and Subfield Quantification . . . . .	5
1.3.2 3D Hippocampal Surface Atlas Modeling . . . . .	7
1.4 Potential Applications . . . . .	9
1.5 Organization . . . . .	9
2 HIPPOCAMPUS SEGMENTATION, QUANTIFICATION, AND RELIABILITY ANALYSIS . . . . .	10
2.1 Dataset Acquisition . . . . .	11
2.2 Hippocampal Segmentation and Subfield Quantification . . . . .	11
2.2.1 Hippocampal Segmentation . . . . .	11
2.2.2 Subfield Quantification . . . . .	14
2.3 Reliability Analysis . . . . .	15
2.4 Results and Discussions . . . . .	16

	Page
3 OPTIMIZATION AND RELIABILITY ANALYSIS OF HIPPOCAMPAL SUBFIELD SEGMENTATIONS . . . . .	19
3.1 Fixing Holes . . . . .	20
3.2 Results and Discussions . . . . .	25
3.2.1 Map Smoothing . . . . .	25
3.2.2 Reliability Analysis . . . . .	27
4 HIPPOCAMPAL SURFACE ATLAS MODELING . . . . .	32
4.1 Data preparation . . . . .	32
4.2 SPHARM Parameterization . . . . .	35
4.3 SPHARM Expansion . . . . .	37
4.4 SPHARM Registration . . . . .	40
4.5 Building Hippocampal Surface Atlas Models . . . . .	42
4.5.1 Construct A Mean Hippocampus . . . . .	42
4.5.2 Creating Hippocampal Surface Atlas . . . . .	44
5 CONCLUSIONS AND FUTURE WORK . . . . .	49
LIST OF REFERENCES . . . . .	51
A DEMONSTRATE RESULTS . . . . .	56
B DEMONSTRATE PROGRAMS . . . . .	76

## LIST OF TABLES

Table	Page
3.1 The comparison of ICCs results based on segmentations from FreeSurfer: before and after holes were fixed (left hippocampi) . . . . .	28
3.2 The comparison of ICCs results based on segmentations from FreeSurfer: before and after holes were fixed (right hippocampi) . . . . .	29
3.3 The comparison of ICCs results based on segmentations from FIRST: before and after holes were fixed (left hippocampi) . . . . .	30
3.4 The comparison of ICCs results based on segmentations from FIRST: before and after holes were fixed (right hippocampi) . . . . .	31

## LIST OF FIGURES

Figure	Page
1.1 Sample MRI scan of a human brain in axial, coronal, and sagittal view. (a) The axial view is a slice taken horizontally of the brain as seen from the top. (b) The coronal view is a slice taken vertically of the brain as seen from the front. (c-d) The sagittal view is a slice taken vertically of the brain as seen from its left side. Highlighted areas are left (brown) and right (red) hippocampi. . . . .	3
1.2 Example of the hippocampus represented as a 3D binary object. . . . .	4
1.3 Automatic segmentation results from (a) FreeSurfer (b) FIRST. There are noisy boundaries on the FreeSurfer segmentation results compared with the FIRST result . . . . .	6
1.4 Entire modeling procedure . . . . .	8
2.1 A brief diagram of the structure of hippocampus segmentation, quantification and reliability analysis process. . . . .	10
2.2 The left and right hippocampi segmentations from FreeSurfer. . . . .	12
2.3 Hippocampal subfields mapped onto the surface of hippocampi segmentations. . . . .	13
2.4 The left and right hippocampi segmentations from FIRST. . . . .	14
2.5 Hippocampal subfield quantification results and volumetric distributions.	17
2.6 ICCs results using original (blue) hippocampal subfield segmentations, then these subfield segmentations were masked by FreeSurfer (red) and FIRST (green) . . . . .	18
3.1 The structure of Chapter 3: a procedure with fixed probability maps . . . . .	19
3.2 Example holes for subfield CA1 (black areas within blue area) . . . . .	20
3.3 A demonstration on holes is found on one image . . . . .	21
3.4 A comparison between two smoothing methods: (a) the original hippocampal subfields overlapped with entire hippocampi mask, the dark green areas indicate holes; (b) subfield maps were fixed using the probability values and Euclidean distance; (c) subfield maps were fixed using Gaussian Kernel . . . . .	26



Figure	Page
3.5 The ICCs comparison based on FreeSurfer results, measured on left hippocampi . . . . .	28
3.6 The ICCs comparison based on FreeSurfer results, measured on right hippocampi . . . . .	29
3.7 The ICCs comparison based on FIRST results, measured on left hippocampi . . . . .	30
3.8 The ICCs comparison based on FIRST results, measured on right hippocampi . . . . .	31
4.1 The structure of Chapter 4: a procedure to build a surface atlas of hippocampal subfields using SPHARM . . . . .	33
4.2 Several conditions that show the voxel-based structures need to be topology fixed . . . . .	35
4.3 A spherical unit: $\theta$ is defined as the polar (or co-latitudinal) coordinate with $\theta \in [0, \pi]$ , and $\phi$ is taken as the azimuthal (or longitudinal) coordinate with $\phi \in [0, 2\pi)$ . . . . .	36
4.4 Hippocampal surface (left) and its spherical parameterization (right). Color indicates the correspondence between the surface and parameterization	36
4.5 An example of degree 1 reconstruction (an ellipsoid) and the degree 15 reconstruction of the same object . . . . .	39
4.6 The object on left is the original hippocampus, the object in the middle is the unit sphere, and the object on the right is the reconstructed hippocampus using SPHARM expansion . . . . .	40
4.7 SPHARM registration using First Order Ellipsoids (FOEs). Each of (a-c) shows the FOE on left and degree 15 reconstruction on right. Parameterization is indicated by the mesh and color on the surface. . . . .	41
4.8 Subfields mapped onto an individual SPHARM model . . . . .	43
4.9 As each participant has two repeated scans (Groups A and B), (a - b) are models reconstructed from Group A, which contains 26 images. . . . .	46
4.10 As each participant has two repeated scans (Groups A and B), (a - b) are models reconstructed from Group B, which contains 26 images. . . . .	47
4.11 As each participant has two repeated scans (Groups A and B), (a - b) are models reconstructed both from Groups A and B, which contains 52 images. . . . .	48

Figure	Page
A.1 Axial view of MRI scans with labeled left (red) and right (brown) hippocampi. . . . .	57
A.2 Coronal view of MRI scans with labeled left (red) and right (brown) hippocampi. . . . .	58
A.3 Sagittal view of MRI scans with labeled right (brown) hippocampi. . . . .	59
A.4 Sagittal view of MRI scans with labeled left (red) hippocampi. . . . .	60
A.5 Subfields masked by entire hippocampal segmentation result from FreeSurfer, noises can be viewed around the edges. . . . .	61
A.6 Subfields masked by entire hippocampal segmentation result from FIRST, some unreasonable quantifications are made. . . . .	62
A.7 Subfields masked by entire hippocampal segmentation result from FIRST, after Gaussin Kernel is applied. . . . .	63
A.8 The distributions of hippocampal subfields on the 3D surface (left hippocampi). . . . .	64
A.9 The distributions of hippocampal subfields on the 3D surface (right hippocampi). . . . .	65
A.10 The distributions of hippocampal subfields on the 3D surface (left hippocampi). . . . .	66
A.11 The distributions of hippocampal subfields on the 3D surface (right hippocampi). . . . .	67
A.12 The voxel-based structures after topology fix. . . . .	68
A.13 The voxel-based structures after topology fix. . . . .	69
A.14 SPHARM parameterization: bijective mapping from object surface to the surface of unit sphere. . . . .	70
A.15 The hippocampal subfields distributions labeled on the surface, as each participant has two scans, (a) is obtained from group A and (b) is obtained from group B. . . . .	71
A.16 Bijective mapping results from hippocampi surface to spherical surface: (a) is mapped from left hippocampi and (b) is mapped from right hippocampi. . . . .	72
A.17 The flat view of hippocampal subfields distributions labeled on the surface: (a) is obtained from left hippocampi and (b) is obtained from right hippocampi. . . . .	73

Figure	Page
A.18 The SPHARM expansion examples: (a) is obtained from left hippocampi and (b) is obtained from right hippocampi. . . . .	74
A.19 SPHARM registration: fist group (first two images) is the original pose and parameterization, second group is aligned in parameter space, third group is aligned in object space. . . . .	75

## SYMBOLS

$\mu$	unobserved overall mean
$\alpha$	unobserved random effect
$\epsilon$	unobserved noise term
$\sigma$	standard deviation
$\theta$	polar coordinate
$\phi$	azimuthal coordinate
$c$	coefficients of harmonic functions

## ABBREVIATIONS

3D	Three Dimensional
AD	Alzheimer's Disease
ADNI	Alzheimer's Disease Neuroimaging Initiative
CAT	Computed Axial Tomography
EFD	Elliptic Fourier Descriptor
FOE	First Order Ellipsoid
FSL	FMRIB Software Library
FMRI	Functional Magnetic Resonance Imaging
FWHM	Full Width at Half Maximum
FIRST	Functional magnetic resonance imaging of the brain's Integrated Registration and Segmentation Tool
GLM	General Linear Model
HC	Health Control
ICCs	Intraclass Correlation Coefficients
MRI	Magnetic Resonance Imaging
PET	Positron Emission Tomography
ROIs	Regions Of Interest
SBM	Surface-Based Morphometry
SPHARM	Spherical Harmonic
SPSS	Statistical Package for the Social Sciences

## ABSTRACT

Cong, Shan M.S.E.C.E., Purdue University, May 2014. Morphometric Analysis of Hippocampal Subfields: Segmentation, Quantification and Surface Modeling . Major Professors: Maher E. Rizkalla, and Li Shen.

Object segmentation, quantification, and shape modeling are important areas in medical image processing. By combining these techniques, researchers can find valuable ways to extract and represent details on user-desired structures, which can function as the base for subsequent analyses such as feature classification, regression, and prediction.

This thesis presents a new framework for building a three-dimensional (3D) hippocampal atlas model with subfield information mapped onto its surface, with which hippocampal surface registration can be done, and the comparison and analysis can be facilitated and easily visualized. This framework combines three powerful tools for automatic subcortical segmentation and 3D surface modeling. Freesurfer and Functional magnetic resonance imaging of the brain's Integrated Registration and Segmentation Tool (FIRST) are employed for hippocampal segmentation and quantification, while SPHERICAL HARMONICS (SPHARM) is employed for parametric surface modeling. This pipeline is shown to be effective in creating a hippocampal surface atlas using the Alzheimer's Disease Neuroimaging Initiative Grand Opportunity and phase 2 (ADNI GO/2) dataset. Intra-class Correlation Coefficients (ICCs) are calculated for evaluating the reliability of the extracted hippocampal subfields.

The complex folding anatomy of the hippocampus offers many analytical challenges, especially when informative hippocampal subfields are usually ignored in detailed morphometric studies. Thus, current research results are inadequate to accurately characterize hippocampal morphometry and effectively identify hippocampal

structural changes related to different conditions. To address this challenge, one contribution of this study is to model the hippocampal surface using a parametric spherical harmonic model, which is a Fourier descriptor for general a 3D surface. The second contribution of this study is to extend hippocampal studies by incorporating valuable hippocampal subfield information. Based on the subfield distributions, a surface atlas is created for both left and right hippocampi. The third contribution is achieved by calculating Fourier coefficients in the parametric space. Based on the coefficient values and user-desired degrees, a pair of averaged hippocampal surface atlas models can be reconstructed. These contributions lay a solid foundation to facilitate a more accurate, subfield-guided morphometric analysis of the hippocampus and have the potential to reveal subtle hippocampal structural damage associated with different conditions.

## 1. INTRODUCTION

Segmentation, quantification, and shape modeling techniques are important areas in computer vision, and have been widely used in many biomedical studies [1] [2] [3]. In this study, a creative framework for building a hippocampal surface atlas is introduced using widely recognized segmentation and shape modeling methods. This thesis introduces the issues that shape analysis can be applied to biomedical studies, provides a brief description on related works, explains the contributions of this work, and sketches the organization of this thesis.

### 1.1 Neuroimaging Analysis in Biomedical Studies

The hippocampus is widely studied with large varieties of neuroimaging techniques, such as Computed Axial Tomography (CAT), Diffuse Optical Imaging, Event-related Optical Signal, Magnetoencephalography, Magnetic Resonance Imaging (MRI), Functional Magnetic Resonance Imaging (fMRI), Positron Emission Tomography (PET), Single-Photon Emission Computed Tomography (SPECT) [4] [5] [6] [7] [8] [9], etc. The development of these image acquisition techniques, has resulted in a large body of studies that employ manual or automated methods to extract Regions Of Interest (ROIs) from high-resolution images, and apply 3D morphometric analysis on these ROIs.

#### 1.1.1 Image Segmentation and Quantification

Identifying the morphological abnormalities is always a fundamental problem in medical image analysis, but it is useful for disease prediction, diagnosis, and treatment. In order to obtain the morphological changes, several classic methods can



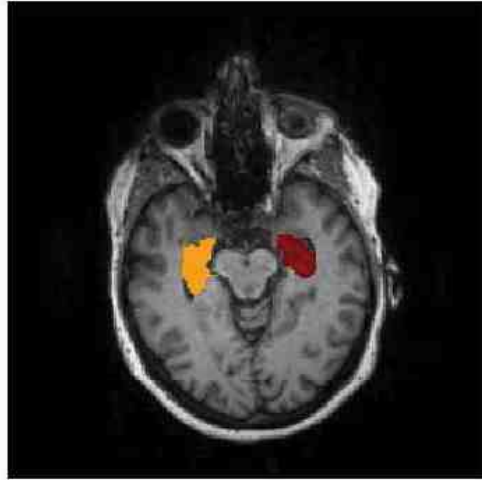
be applied. A common method based on volumetric analysis counts the volumetric changes which have happened in the interested areas or the partition changes of the structure. The most obvious benefit of volumetric analysis is simplicity. However, the disadvantages are also obvious in that this measurement may not contain enough information for some certain conditions, especially for complex conditions. For example, even though different objects have similar volume numbers, they may have totally different morphological structures; because of that, the differences between structure may be overlooked if one only considers volumetric measures.

To overcome that problem and perform shape modeling and analysis, a structure of the interested area needs to be extracted from volumetric images; this process is done by image segmentation. The image segmentation is the process of partitioning one image into several segments based on labeling an image, so a corresponding relationship is created between label values and different object areas in the real world. The classic methods for automatic image segmentation includes thresholding, region growing, classifiers, clustering, Markov random field models, artificial neural networks, deformable models, atlas based approaches [10], and many other methods.

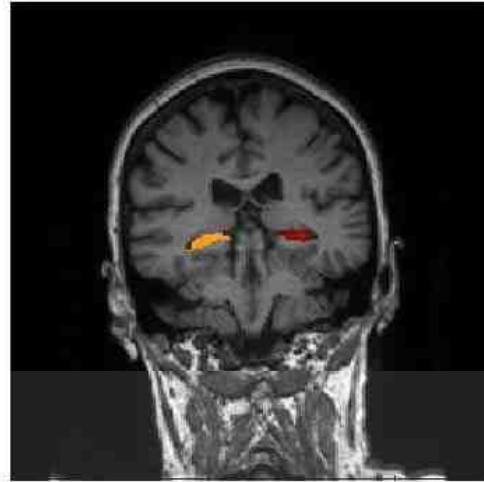
Fig. 1.1 shows an MRI scan from different views, and label information is added on the left and right hippocampus areas. However, as the goal of this study is to build 3D models of the segmentation results, shape modeling and analysis techniques are employed.

### **1.1.2 Shape Modeling and Analysis**

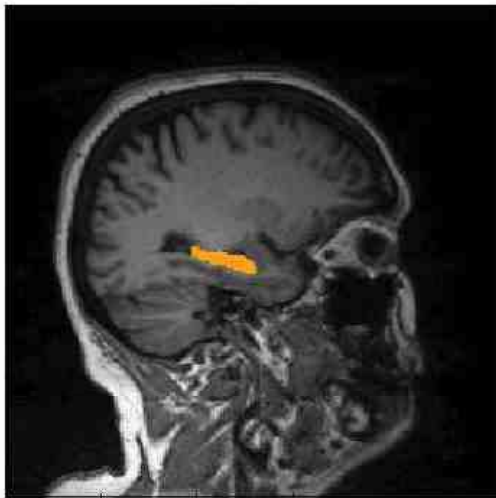
In order to examine the shape abnormalities in hippocampal structures, sliced images from MRI scans need to be aligned based on certain features, especially when landmarks are used. After that, the comparison among different individuals can be performed. To achieve this goal, shape modeling and visualization techniques are introduced to model objects extracted from original segmented images.



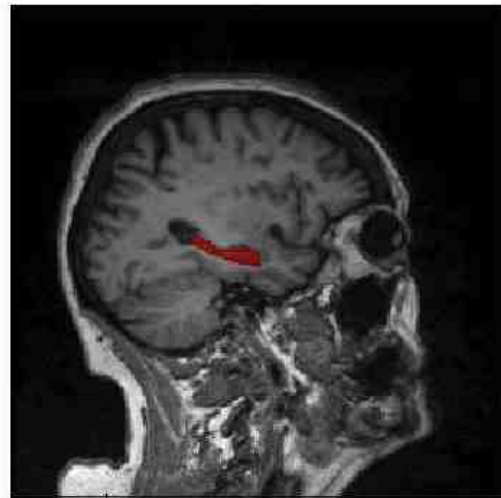
(a) Axial view



(b) Coronal view



(c) Sagittal view



(d) Sagittal view

Fig. 1.1.: Sample MRI scan of a human brain in axial, coronal, and sagittal view. (a) The axial view is a slice taken horizontally of the brain as seen from the top. (b) The coronal view is a slice taken vertically of the brain as seen from the front. (c-d) The sagittal view is a slice taken vertically of the brain as seen from its left side. Highlighted areas are left (brown) and right (red) hippocampi.

3D modeling is the process of representing object surface using a computational framework that simulates two-dimensional images through 3D rendering. Models can be visualized by various geometric entities based on mesh or solid renderings, see Fig. 1.2 for an example 3D hippocampal structure.

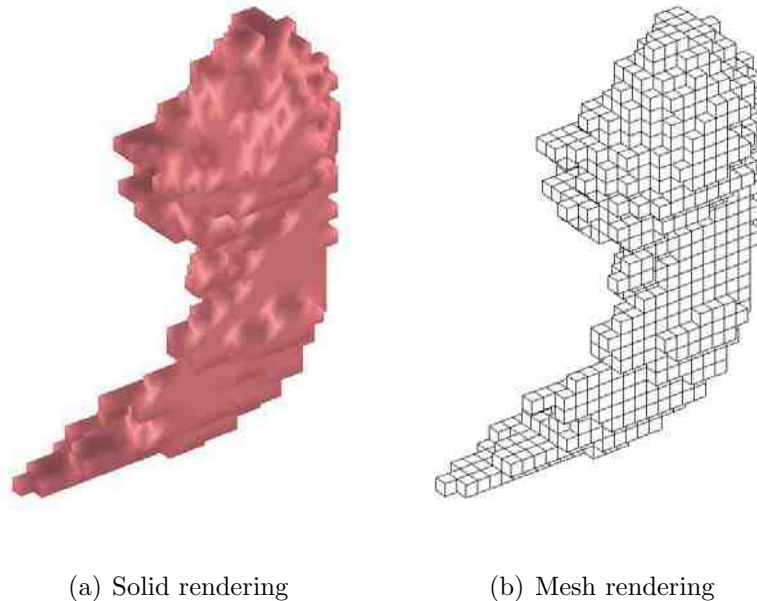


Fig. 1.2.: Example of the hippocampus represented as a 3D binary object.

## 1.2 Previous Work

Because of the low contrast between tissues in certain human organs on images such as brain scans, manually segmented structures were performed to ensure accuracy [11], and to avoid problems caused by individual topological variations in these structures, which may puzzle automatic methods. Thus, much previous work is done manually [12] [11] or semi-automatically [13] [14] [15], but manual or semi-automatic segmentation cannot be used to process a large amount of data since it is very time consuming. With the explosive development of imaging techniques, microscopy, laser scanning, CAT, and MRI, high quality morphological data can be obtained quickly

and easily from almost any structure, automatic segmentation approaches are proposed to quickly quantify complex 3D shapes, such as [16], [17], [18], and [19].

Many 3D shape modeling and visualization techniques have been reported based on computer vision and biomedical imaging analysis. Some of them are volumetric studies such as den Heijer, et al. 2010; Dewey, et al. 2010; Holland, et al. 2009; Jack, et al. 2004; Ridha, et al. 2008; Wolz, et al. 2010. However, many studies have suggested that surface-based analysis may offer advantages over volume measures because the surface-based methods are able to localize patterns of hippocampal atrophy and detailed point-wise correlation between atrophy and cognitive functions/biological markers [20]. So using parametric surface as a shape descriptor is well recognized, and many studies have been performed using different descriptors such as landmark-based descriptors [21] [22], deformation fields [23] [24], distance transforms [25], medial axes [26] [27] [28], and parametric surfaces [25] [29] [30].

### **1.3 Main Contributions of The Thesis**

In this thesis, a creative framework is proposed that combines powerful segmentation and shape modeling techniques. The main contributions include:

- High quality hippocampal subfield segmentation results generated by combining effective segmentation tools Freesurfer and RIRST.
- The study of hippocampal subfields, which are usually ignored during registration in existing surface-based or voxel-based morphometric studies.
- A 3D surface atlas of hippocampal subfields built using the SPHARM method.

#### **1.3.1 Hippocampal Segmentation and Subfield Quantification**

Critical hippocampal subfield information is usually ignored by hippocampal registration in existing surface-based or voxel-based morphometric studies. Such an approach is thus inadequate to accurately characterize hippocampal morphometry and effectively identify hippocampal structural changes related to different conditions.

Even though many recent studies provide solutions for extracting hippocampal subfields based on MRI technologies [31] [32] [33] [34], these methods are not applicable to a large cohort. Automated extraction of hippocampal subfields from 1.5T or 3T MRI brain scans is still a challenging task [35], and there are very few tools available. FreeSurfer (<http://freesurfer.net/>) is a widely recognized brain segmentation and cortical parcellation tool, it recently released a promising routine (<http://freesurfer.net/fswiki/HippocampalSubfieldSegmentation>) where hippocampal subfields can be automatically segmented from regular MRI scans with a Bayesian framework [36].

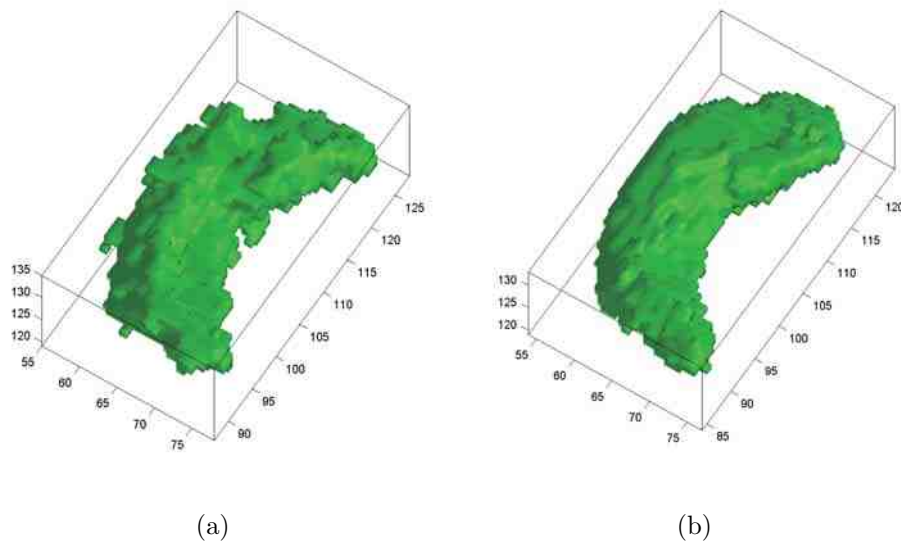


Fig. 1.3.: Automatic segmentation results from (a) FreeSurfer (b) FIRST. There are noisy boundaries on the FreeSurfer segmentation results compared with the FIRST result

However, as reported by many groups using FreeSurfer for hippocampal volume measures, the segmentation results turned out to have noisy boundaries 1.3 (a), thus it is not suitable for surface study or detailed shape analysis [37]. There is another well-developed automatic hippocampal segmentation tool, FIRST ([www.fmrib.ox.ac.uk](http://www.fmrib.ox.ac.uk)) which was published as a part of the Functional Magnetic Resonance Imaging of the

Brain (FMRIB) Software Library (FSL), and it generates satisfactory hippocampal segmentation results 1.3 (b). Because of the successful hippocampal segmentation, FIRST is employed in several of the latest hippocampal shape studies [38] [20]. The disadvantage of FIRST is that it does not provide hippocampal subfield segmentation results. In this thesis, both FreeSurfer and FSL are employed in generating smooth hippocampal surface and its subfields.

### 1.3.2 3D Hippocampal Surface Atlas Modeling

SPHARM is employed for 3D hippocampal modeling and Surface-Based Morphometry (SBM) studies, it is based on the Elliptic Fourier Descriptor (EFD) [39] but extended to the 3D space. By using SPHARM, specific shape changes among different hippocampi can be localized through aligning all objects together. Thus morphological abnormalities can be easily identified. Fig. 1.4 shows the surface modeling procedures used in this study.

Compared with image-based or voxel-based methods, surface-based approaches have several advantages. First, surface-based approaches can be employed in more general situations where a surface is not embedded in an image but instead is defined by segmented boundaries, triangulations, or other information as described in [40] [41] [42]. Second, as the boundary or surface of a 3D volumetric object actually defines the shape, a surface-based representation may be more appropriate for studying shape unless the appearance or tissue inside the object is also a focus of interest. Third, scaling operation is not a challenging problem for surface-based approaches. Unlike image or voxel-based approaches, scaling operations are done by re-sampling 3D volumetric images that usually introduce fatal quantification errors. For surface-based methods, accurate scaling operations can be achieved for parametric surfaces and polygonal surfaces, while no error is introduced during the scaling process.

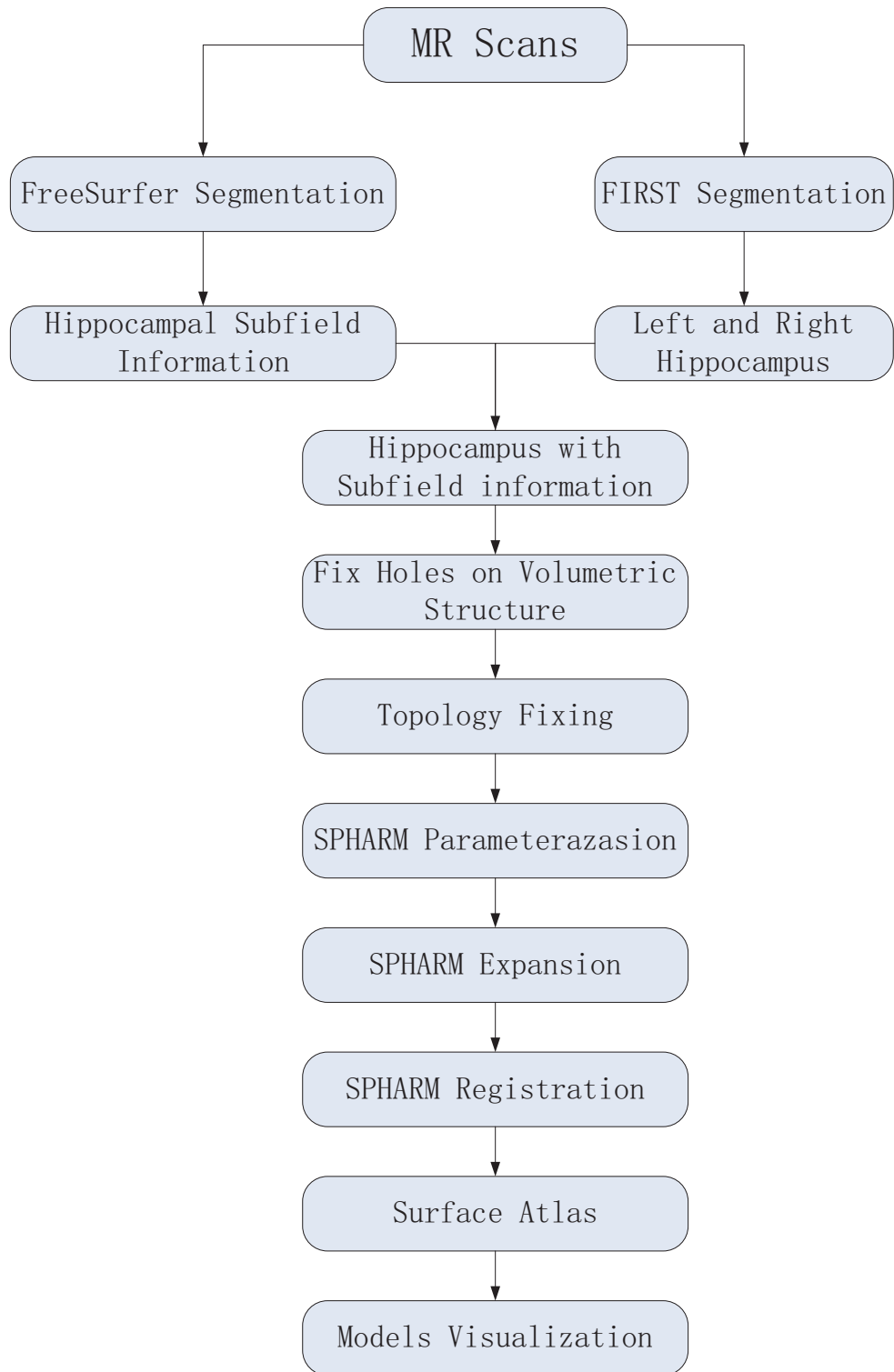


Fig. 1.4.: Entire modeling procedure

## 1.4 Potential Applications

The research introduced in this thesis is an initial effort towards building a computational framework for subfield-guided hippocampal morphometry. This initial effort is focused on surface-based morphometry and aims to build a surface atlas of hippocampal subfields. Thus the surface atlas can be used for structural comparison among different test groups to identify morphological abnormalities such as the comparison between disease and health controls. Compared with the volumetric studies, surface-based studies are more suitable for localizing the structural changes on the surface. The long-term goal is to find the relationship between shape morphological changes and brain function. Thus, as an imaging biomarker, it has the potential to detect brain diseases such as AD [14], epilepsy [43], and schizophrenia [44], and provide critical information for clinical use.

## 1.5 Organization

The rest of the thesis is organized as follows. Chapter 2 introduces the MRI-based hippocampus segmentation, quantification and stability analysis of the hippocampus and its subfields. Chapter 3 describes a method for refining the volume-based hippocampal subfield segmentation. Chapter 4 is dedicated to creating a surface atlas of hippocampal subfields using SPHARM-based surface modeling. Chapter 5 concludes the work with a plan for future work.



## 2. HIPPOCAMPUS SEGMENTATION, QUANTIFICATION, AND RELIABILITY ANALYSIS

In order to segment and quantify the hippocampus and its subfields, the following three major steps were performed: (1) *hippocampus segmentation*, which provided segmented hippocampus images from 3T MR scans. The results were generated from FreeSurfer and FIRST separately. (2) *hippocampal subfield information acquisition*, which provided probabilistic maps for each hippocampal subfield area based on FreeSurfer computation. (3) *hippocampal subfield mapping*. Each subfield map was masked by the entire hippocampus generated by either FreeSurfer or FIRST to obtain two new sets of subfield volume measures. Based on the measurement results of two repeated scans, ICCs were calculated for reliability evaluation. Fig. 2.1 illustrates the segmentation, quantification, and reliability analysis procedures.

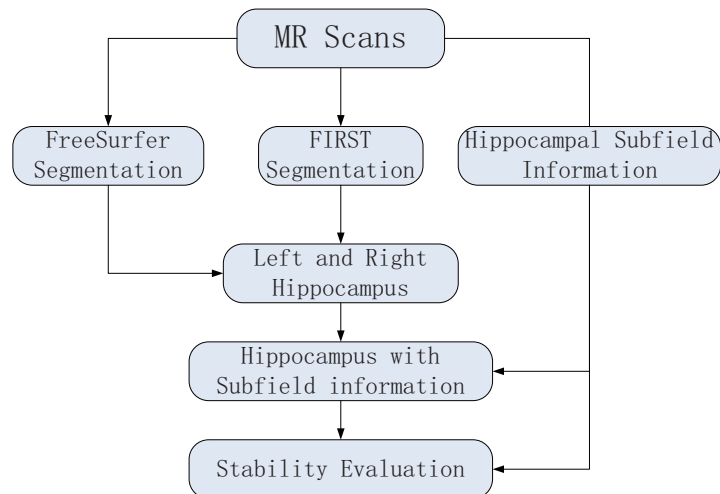


Fig. 2.1.: A brief diagram of the structure of hippocampus segmentation, quantification and reliability analysis process.

## 2.1 Dataset Acquisition

The experimental data came from the Alzheimer’s Disease Neuroimaging Initiative (ADNI) database. ADNI is a multiple years, public-private partnership that is aiming to test if PET, biological markers, serial MRI, neuropsychological and clinical assessment can be combined to measure the progression of amnesic Mild Cognitive Impairment (MCI) and early probable AD. ADNI longitudinal phenotype data includes structural, functional, diffusion and perfusion MRI scans, molecular imaging scans (e.g., AV45-PET and FDG-PET), fluid bio-markers from cerebrospinal fluid and blood, clinical data, and neuropsychological assessments. In this work, the baseline MRI scans of the ADNI GO/2 cohort were downloaded, which was designed to understand the very earliest stages of memory loss by enrolling individuals ages 55 to 90 who are in the earliest stages of AD and MCI, which included 195 health control (HC), 466 MCI, and 131 AD participants from approximately 50 sites from the United States and Canada [45]. We randomly picked 26 participants from the HC group. Two repeated baseline 3T MRI scans were downloaded for each participant. The experiments were performed on a Dell Precision T7500 workstation running Unix OS, and a Dell PWS670 workstation running WinXP.

## 2.2 Hippocampal Segmentation and Subfield Quantification

In this section, in order to describe the shape of the hippocampus, left and right hippocampi were extracted from the original MRI scans. FreeSurfer and FIRST were employed for segmentation of the hippocampus and its subfields.

### 2.2.1 Hippocampal Segmentation

FreeSurfer is a powerful package for analysis and visualization of structural and functional brain imaging data. A fully automatic structural imaging stream is contained within FreeSurfer tools package in order to process cross longitudinal and

sectional data. It has been widely used and recognized for extracting the cortical/subcortical surface between white and gray matter, segmenting of white matter from the rest of the brain, rendering the pial surface, skull stripping, nonlinear registration of the cortical surface of an individual with a stereotaxic atlas, B1 bias field correction, statistical analysis of group morphometry differences, labeling of regions of the cortical surface and subcortical brain structures [46]. In this study, FreeSurfer will be employed for the segmentation of the hippocampus and its subfields.

The hippocampal segmentations were obtained using a statistical model of image formation around the hippocampal area based on Bayesian theory. The model was built from manually traced segmentations of the right hippocampus with  $0.38 \times 0.38 \times 0.8mm^3$  in vivo MRI scans in 10 subjects. The process of building the left hippocampus was to mirror the model of right hippocampus [36].

An example, hippocampal segmentation results from FreeSurfer are shown in Fig. 2.2, while Fig. 2.3 shows the hippocampal subfields mapped onto the surface.

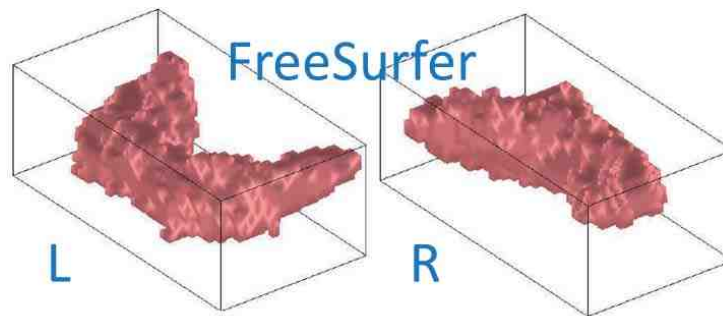


Fig. 2.2.: The left and right hippocampi segmentations from FreeSurfer.

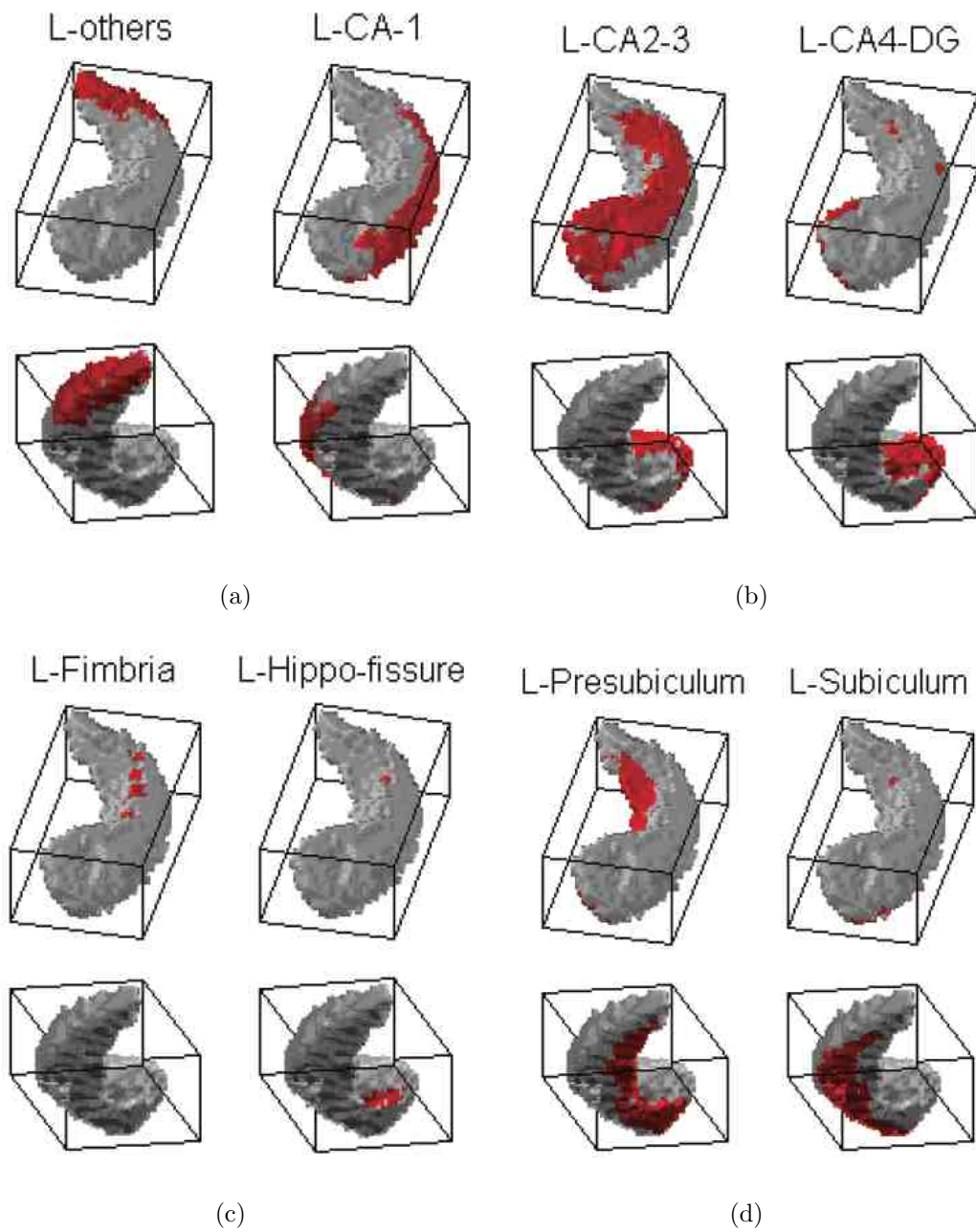


Fig. 2.3.: Hippocampal subfields mapped onto the surface of hippocampi segmentations.

The segmentation/registration function is also model-based for FIRST. The shape models used in FIRST were constructed from manually segmented images provided by the Center for Morphometric Analysis. The labels on each segment were marked manually and were parameterized as surface meshes, thus a point distribution model could be built. The surfaces of the model were deformable and used to automatically parameterize the volumetric labels in terms of meshes. Furthermore, the deformable surfaces were constrained in order to preserve vertex correspondence across the training data. Moreover, normalized intensities along the surface normals were sampled and modeled. The shape and appearance model were built within a multivariate Gaussian framework. As a result, shape model was expressed as a mean after averaging the modes of variation. Based on the pre-trained models, FIRST searches through linear combinations of shape models of variation for the most similar shape instance, when it was given the observed intensities from the test images [47].

An example hippocampal segmentation result from FIRST is shown in Fig. 2.4.

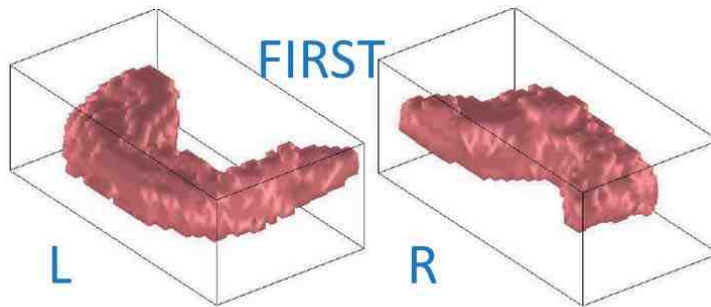


Fig. 2.4.: The left and right hippocampi segmentations from FIRST.

### 2.2.2 Subfield Quantification

An initial segmentation of the subfields of the hippocampus from each MRI scan using FreeSurfer was performed during the last section. Two sets of entire hippocampi segmentation results from FreeSurfer and FIRST were also obtained.

For the subfield segmentation results, each hippocampus (left or right) includes 8 probability maps based on the FreeSurfer output. These were then masked by the entire hippocampus generated from FreeSurfer and FIRST segmentation processes. Each probability map was represented by a matrix with the same size as that of the hippocampus image, which means that each voxel on the hippocampus has one or more probability values from different subfield probability maps, since they may have overlapping areas especially around the boundary areas between different subfields. The quantification work was to define the area and boundary of each subfield based on the comparison results among all 8 probability maps. One probability map was introduced first, all voxels with values bigger than 0 were set as label “1”, and the probability map was saved as the original template. Then, the second probability map was introduced to be compared with the template, for each voxel that second map value larger than the value from the template, label “1” was replaced by label “2”, and the template was updated by the bigger probability values. This process was repeated until all 8 maps were compared. As the output, a label map was obtained with the labels from “1”-“8”, which represented different subfields.

### **2.3 Reliability Analysis**

ICCs [48] were calculated to evaluate the reproducibility of the volume measures of these extracted structures, including hippocampal subfield measures and the subfield measures after they were masked by the entire hippocampus segmentations generated by FreeSurfer and FIRST. ICCs was used to describe how strongly units in the same group resemble each other, while, for the sampled data in this study, each individual had two sets of repeated scans. By performing the calculation, a two-way mixed model was selected to configure Statistical Package for the Social Sciences (SPSS) 20.0, due to the two raters (repeated MRI scans Group A and Group B), and volumetric measure is considered as the single measure in this study. The higher ICCs leads to better reliability.

The calculation procedure is showed in Equation 2.3, where  $Y_{ij}$  is the  $i_{th}$  observation in the  $j_{th}$  group,  $\mu$  is an unobserved overall mean,  $\alpha_j$  is an unobserved random effect shared by all values in group  $j$ , and  $\epsilon_{ij}$  is an unobserved noise term [49].

$$Y_{ij} = \mu + \alpha_j + \epsilon_{ij},$$

For this model to be identified,  $\alpha_j$  and  $\epsilon_{ij}$  are assumed to have expected value zero and to be uncorrelated with each other. Also, the  $\alpha_j$  is assumed to be identically distributed, and the  $\epsilon_{ij}$  is assumed to be identically distributed. The variance of  $\alpha_j$  is denoted  $\alpha_\alpha^2$  and the variance of  $\epsilon_{ij}$  is denoted  $\alpha_\epsilon^2$ . The ICC is determined in Equation 2.3.

$$ICC = \alpha_\alpha^2 / (\alpha_\alpha^2 + \alpha_\epsilon^2),$$

Fig. 2.6 shows the reproducibility results for subfield volume measures, whereas ICCs range from 0.4 to 0.9 (values ranging from 0.4 to 0.75 are described as "fair to good" [50]). Using FIRST to mask the subfields yielded a set of ICCs (green line) that were better than or similar to the original ones (blue line) because green line had higher ICC values in general. This promising result suggests that FIRST-masked subfields may be suitable for detailed shape analyses.

## 2.4 Results and Discussions

The ICCs were calculated based on the measures of hippocampal subfield volumes. As shown in Fig. 2.5, the histogram chart represents the measures of subfield volume distributions for one hippocampus, and different colors represent for different subfield areas. The entire hippocampus segmentation from FIRST as well as from FreeSurfer were used as a binary mask. For the areas that have a mask value of "1" but have no probability value on any of 8 subfield maps, they were defined as "undefined". More details will be discussed in the next chapter. Based on the results from the histogram measures, among the 8 hippocampal subfields "CA2-3" has the largest volume in the

hippocampus which followed by the “Subiculum”, “presubiculum”, “the 8th area” , “CA4-DG”, “CA-1”, “fimbria”, and “hippocampal fissure”. Note that, (1) “the 8th area” is the area that does not belong to any other subfields, which means it is the area when the other 7 subfields are defined; (2) this order is based on the measure of one individual; for different individuals, the order may change but will be similar to this order. More results can be viewed in the “results demonstration” section; (3) for small subfields, their measurement reliability is easily influenced by noise, as can be seen by the subfields “CA4-DG”, “CA-1”, and “fimbria” usually having low ICCs.

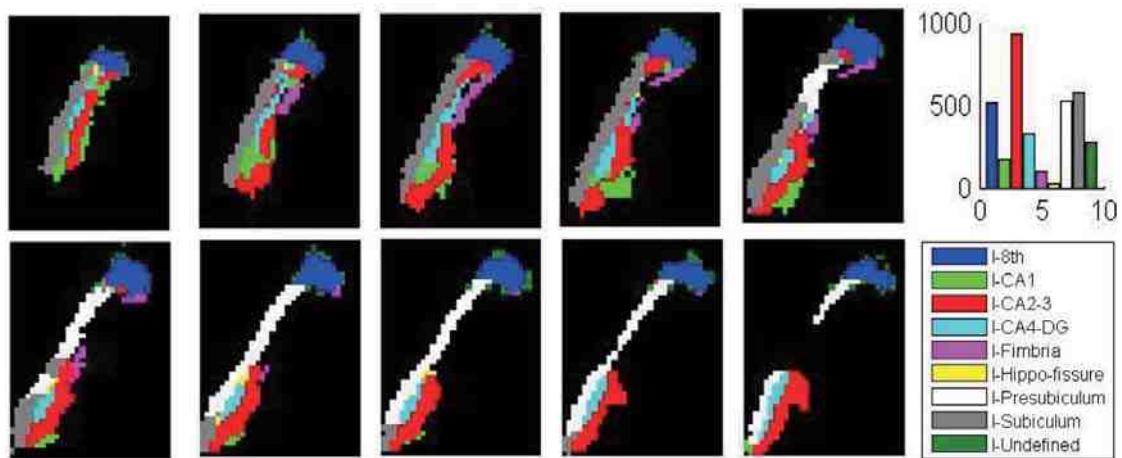


Fig. 2.5.: Hippocampal subfield quantification results and volumetric distributions.

Fig. 2.6 shows the reproducibility/reliability of hippocampal subfield volumes measured by ICCs. Where the ICC curve of original subfield segmentations from FreeSurfer is shown in blue, the curve of original subfields masked by FreeSurfer is shown in red, and the curve of original subfields masked by FIRST is shown in green. Based on the reproducibility measures, using FIRST to mask the subfields yielded a set of ICCs that were better than or similar to the original ones. While most of the ICCs results by using FreeSurfer to mask subfields were similar or worse than the original ones. This promising result suggests that FIRST-masked subfields may have the potential to be used in detailed shape analysis.



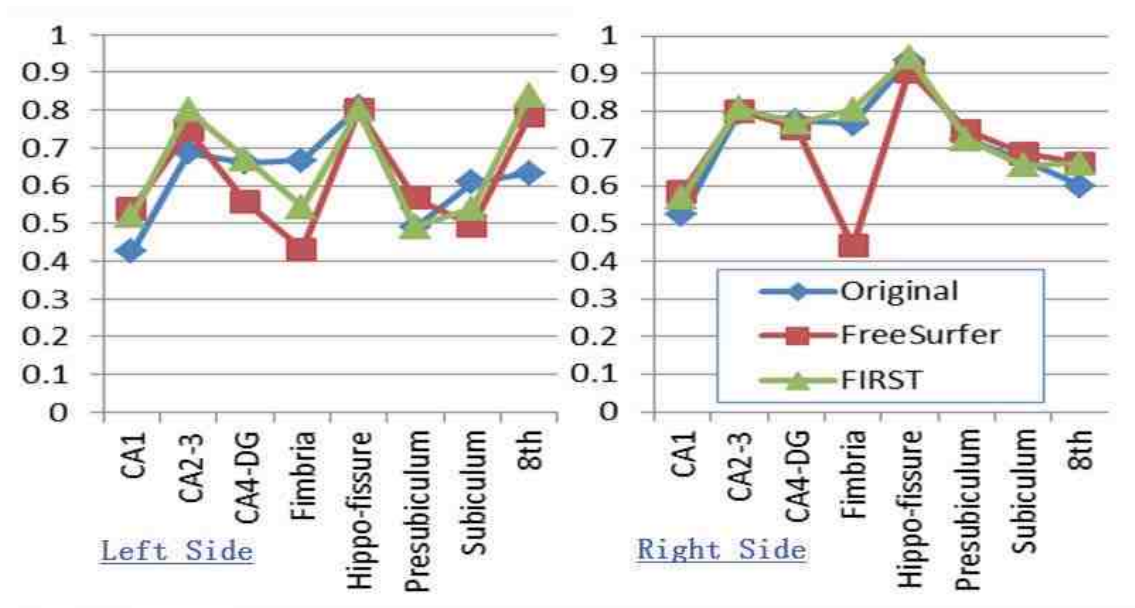


Fig. 2.6.: ICCs results using original (blue) hippocampal subfield segmentations, then these subfield segmentations were masked by FreeSurfer (red) and FIRST (green)

### 3. OPTIMIZATION AND RELIABILITY ANALYSIS OF HIPPOCAMPAL SUBFIELD SEGMENTATIONS

Observed from the previous chapter, not all masked results were fully filled; there might have been some holes inside or on the surface of the hippocampus segmentations, which might introduce some errors to the hippocampal subfield quantification process. Thus, in this chapter, methods for identifying holes and fixing these holes are discussed, by using the fixed results, hippocampal subfield quantification and reliability tests are also performed. The structure of this chapter is shown in Fig. 3.1

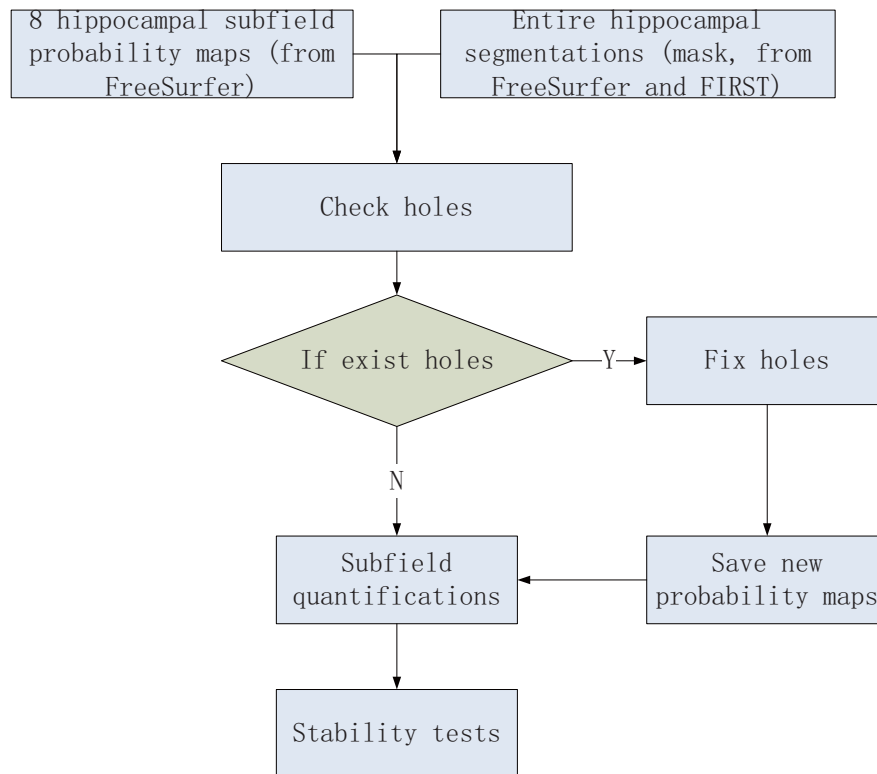


Fig. 3.1.: The structure of Chapter 3: a procedure with fixed probability maps

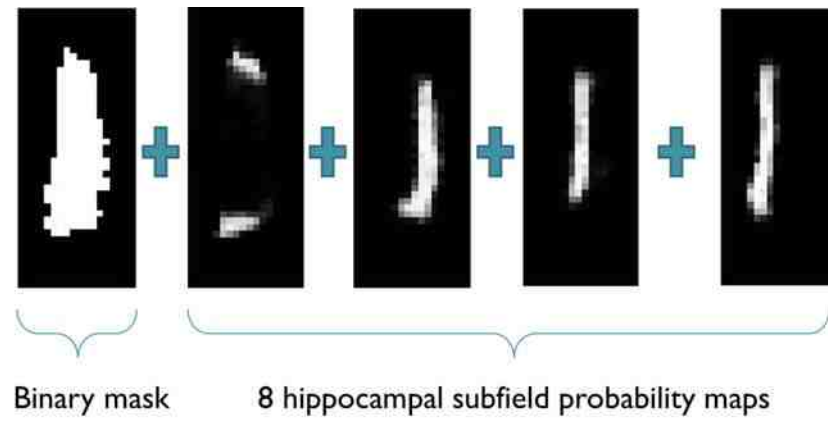
### 3.1 Fixing Holes

Taking a slice from CA1 as an example, Fig. 3.2 roughly shows holes (black areas within the blue area) may exist within a hippocampal subfield area. The existence of the holes may be caused by the limited accuracy that FreeSurfer subfield segmentation can achieve.

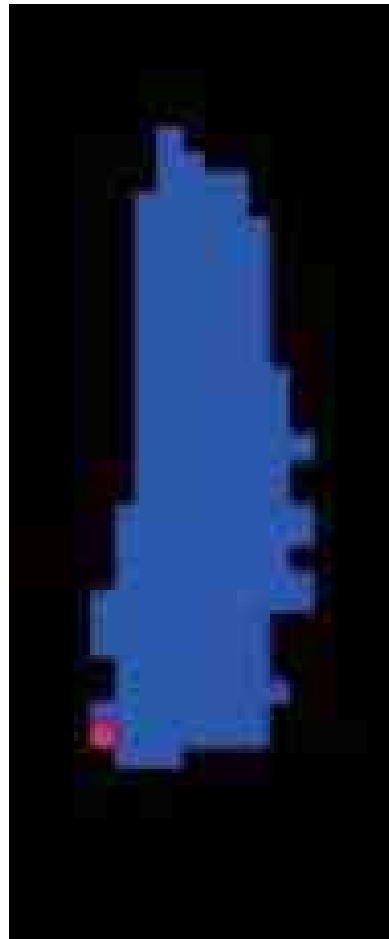


Fig. 3.2.: Example holes for subfield CA1 (black areas within blue area)

Holes can not be defined based only on one subfield probability map. In order to identify holes, the method is to overlap all 8 subfield probability maps together, e.g., shown in Fig. 3.3 (a) and Fig. 3.3 (b). Note that the red area in the Fig. 3.3 (b) shows a hole found on the image (one MRI slice) after overlapping all probability maps.



(a)



(b)

Fig. 3.3.: A demonstration on holes is found on one image

In order to make sure it is a hole, one can superimpose the overlapping result onto the entire hippocampus segmentation (the mask) generated by FreeSurfer or FIRST. A hole is a connected region, where all the 8 probability maps have value “0” (black), but the mask has value “1” (white). In order to fill this hole, each probability map can be smoothed with a 3D Gaussian kernel (a centered Gaussian low-pass filter) to get non-zero values and assign these values to voxels in the holes. The Gaussian lowpass filter of size  $S$  with standard deviations is defined as:

$$\sigma = \frac{S}{4 \times \sqrt{2 \times \log(2)}}, \quad (3.1)$$

Where Full Width at Half Maximum (FWHM) equals half the filter size. Such a FWHM-dependent standard deviation yields a congruous Gaussian shape:

$$H = \exp \left[ - \left( \frac{x^2}{2 \times \sigma_x^2} + \frac{y^2}{2 \times \sigma_y^2} + \frac{z^2}{2 \times \sigma_z^2} \right) \right], \quad (3.2)$$

The algorithm for fixing holes is shown as Algorithm 1:

---

**Algorithm 1** Find holes

---

- 1: read entire hippocampus mask;
  - 2: initialize Sub-map = [ ];
  - 3: **for**  $i = 1 : 8$  **do**
  - 4:   read P(i);
  - 5:   sub-map = P(i) + sub-map;
  - 6: **end for**
  - 7: Check = sub-map + mask;
  - 8: Holes = find(Check = 1);
- 

In Algorithm 1, P denotes the probability map of each hippocampal subfield, and i denotes the  $i_{th}$  map. The basic idea is to identify hole voxels that have value

value of “1” after every subfield is masked. Because the mask is a binary image, and probability maps take values from “0” to “1”, the locations on the mask that have value “1” but have value “0” on all subfield probability maps, are identified as holes.

After identifying all holes, each probability map was smoothed before next step. For each map, it was convolved with a Gaussian kernel (size=5 in our experiments) to get nonzero values and then assigned to voxels in the holes. The algorithm to fix the holes is shown in Algorithm 2:

---

**Algorithm 2** Fix holes

---

- 1: Collect holes location information
  - 2: **for** each probability map **do**
  - 3:   **while** existing holes **do**
  - 4:     apply Gaussian Kernel (size = 5) to smooth the map;
  - 5:   **end while**
  - 6: **end for**
  - 7: save new probability maps;
- 

As a comparison, another algorithm was designed for fixing holes described in Algorithm 3, in which, the *flag* is a condition indicating if a non-zero is found.  $P$  is the biggest non-zero value found within the search window.  $D$  is the Euclidean distance between hole point and the biggest non-zero point.  $N$  is adjusted by an appropriate value that makes the window size not exceed the image size. Algorithm 3 is much more complex than the Algorithm 2. It is also very time consuming and the results are not as ideal as the previous method, example results can be seen in Section .

---

**Algorithm 3** Fix holes
 

---

```

1: collect holes location information
2: initialize  $flag = 0$ ;
3: for each probability map do
4:   for each hole point do
5:     while  $flag = 0$  do
6:       for  $i = 1 : N$  do
7:          $window\ size = i \times i \times i$ ;
8:         Search the nearest non-zero value  $V$ ;
9:         if existing  $V$  then
10:          pick the biggest probability value  $P$  within the window
11:           $new\ value = P^2/D$ 
12:           $flag = 1$ 
13:        end if
14:      end for
15:    end while
16:  end for
17: end for
18: save new probability maps;

```

---

## 3.2 Results and Discussions

As the results of this chapter, based on the segmentation results obtained as Chapter 2 mentioned, all 8 hippocampal subfields probability maps were fixed for the left and right hippocampus of each participant, and two hole fixing methods will be compared in Section 3.2.1 and shows that Gaussian Kernel smoothing is more reasonable and suitable for this study. Using the fixed subfield probability maps, the hippocampal subfield distributions were quantified more accurately. Which will be indicated by the ICCs calculation results as shown in the Section 3.2.2. The following sections presents the comparison results of different hole smoothing methods, and demonstrate the reliability analysis based on the results generated before and after the holes were fixed.

### 3.2.1 Map Smoothing

Fig. 3.4 demonstrates the comparison of the segmentation results before and after holes were fixed, and the comparison of two different hole fixing methods. To illustrate the former issue, there exists some holes (marked as dark green areas) as shown in the Fig. 3.4 (a), then they were fixed by using hole fixing methods mentioned above and the results can be seen in Fig. 3.4 (b) and Fig. 3.4 (c). Fig. 3.4 (b) and Fig. 3.4 (c) demonstrate the results based on two hole smoothing methods: Fig. 3.4 (b) is an example result using probability value and Euclidean distance, while Fig. 3.4 (c) is an example result using Gaussian Kernel smoothing method. Many noises which showed on Fig. 3.4 (b), no longer appear on the Fig. 3.4 (c), thus more reliable results were achieved. Results were improved by applying Gaussian Kernel to smooth subfield probability maps, and more results can be viewed in the demonstration section. After the holes were fixed, the quantification process was similar to the method as proposed in the last chapter, except that the holes were updated with new values smoothed by Gaussian Kernel. Then we measured the volumes of each hippocampal subfield based on the new probability maps. Thus, for each hippocampus, the results after



this step included (1) a binary object to represent the entire hippocampus, and (2) 8 probability maps P1 - P8, one for each subfield (see Fig. 2.3 for mapping it onto the surface, where nonzero values were colored in red). These were the input data for the next chapter.

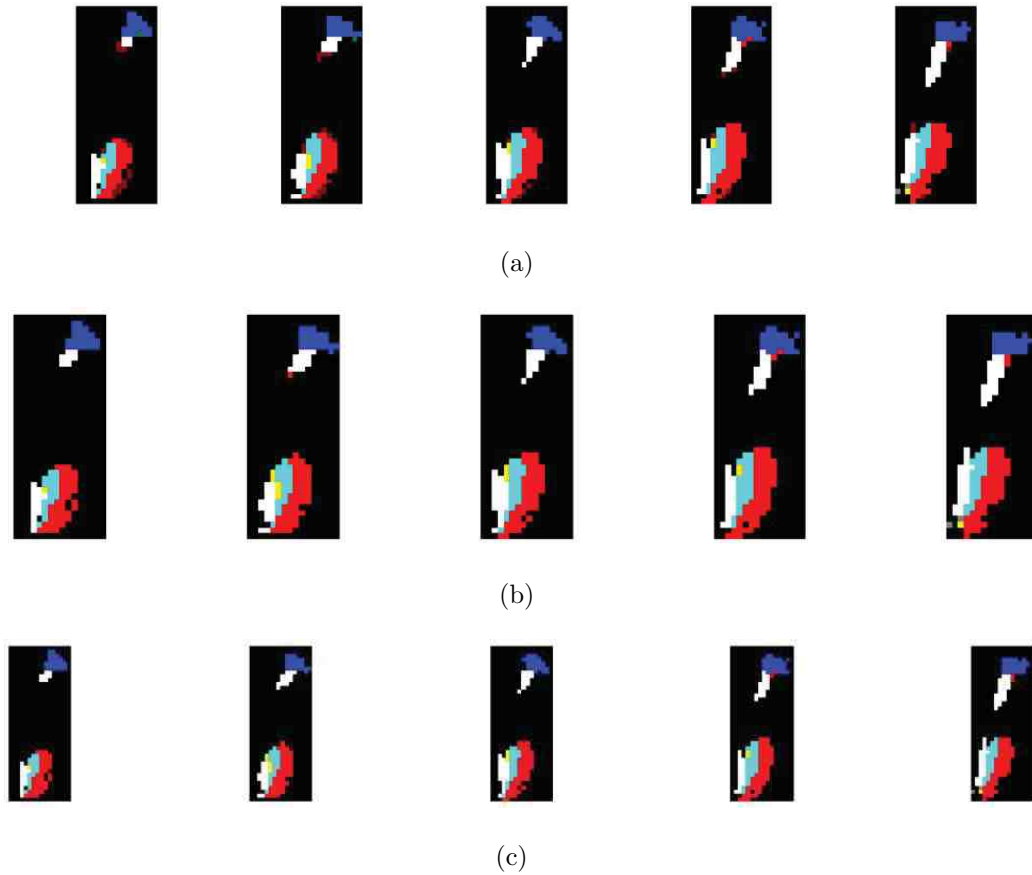


Fig. 3.4.: A comparison between two smoothing methods: (a) the original hippocampal subfields overlapped with entire hippocampi mask, the dark green areas indicate holes; (b) subfield maps were fixed using the probability values and Euclidean distance; (c) subfield maps were fixed using Gaussian Kernel

### 3.2.2 Reliability Analysis

For the reliability test, the sample dataset includes (1) FreeSurfer and FIRST segmentation results before holes are fixed; (2) FreeSurfer and FIRST segmentation results after holes are fixed using Gaussian Kernel smoothing method. And ICCs are used to examine the reliabilities of these models, which is a similar process comparing with the ICCs calculation process performed in last chapter.

The statistical analysis results were performed using Statistical Package for the Social Sciences (SPSS) 20.0, in this experimental scenario, two raters was considered as each individual has two repeated MRI scans. In order to select a set of appropriate ICCs, the experimental procedure followed the procedure suggested in [51] for the reliability analyses. A “two-way mixed model” was selected, due to the two raters just mentioned above, together was a fixed effect when evaluating the target ratings, as the ratings such as hippocampal volumes in this study were a random effect. The “single measure reliability” was selected as a testing factor instead of the average measure reliability, since the goal of this study was to examine the reliability of the ratings for a typical single rater (i.e., volumetric measures before holes were fixed) rather than the mean of all the ratings. “Consistency model type was selected instead of choosing “absolute agreement, because the consistency of the relative standing of the measures is the more important factor in this study, rather than the absolute agreement between two raters. In summary, the SPSS was configured for this study of selecting appropriate ICCs can be described as the “two-way mixed model, “single measure reliability, and “consistency type.

The ICCs results indicate that the overall reliability was slightly increased as there were not many holes existing in the hippocampi segmentations. On the other hand, the existing holes also influence a small number of subfields to have a worse ICCs. As the experiment of this study only take 30 sets of objects, this may be caused by limited sample size. In our future study, a larger scale of dataset (over 700 sets of object are getting to be processed) will be analyzed.

Table 3.1.: The comparison of ICCs results based on segmentations from FreeSurfer: before and after holes were fixed (left hippocampi)

ICCs for left hippocampi	FreeSurfer(fixed)	FreeSurfer(original)
CA1	0.64	0.537
CA2-3	0.808	0.747
CA4-DG	0.591	0.556
Fimbria	0.393	0.431
Hippo-fissure	0.782	0.799
Presubiculum	0.613	0.568
Subiculum	0.437	0.494
8th subfield	0.734	0.784

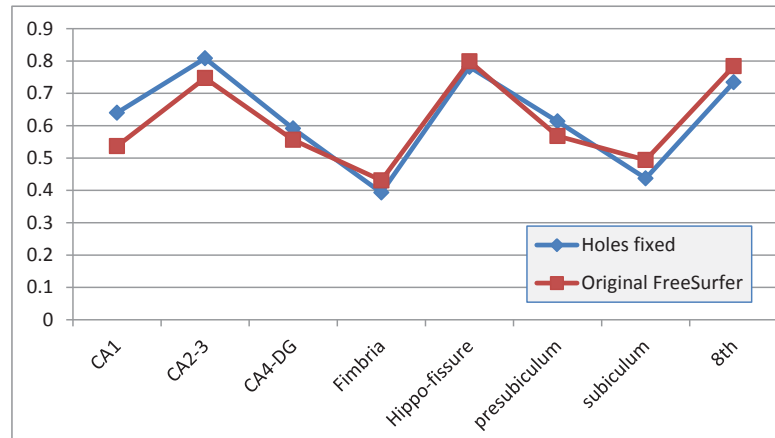


Fig. 3.5.: The ICCs comparison based on FreeSurfer results, measured on left hippocampi

Table 3.2.: The comparison of ICCs results based on segmentations from FreeSurfer: before and after holes were fixed (right hippocampi)

ICCs for right hippocampi	FreeSurfer(fixed)	FreeSurfer(original)
CA1	0.681	0.585
CA2-3	0.775	0.801
CA4-DG	0.756	0.756
Fimbria	0.479	0.441
Hippo-fissure	0.893	0.906
Presubiculum	0.689	0.748
Subiculum	0.671	0.688
8th subfield	0.707	0.662

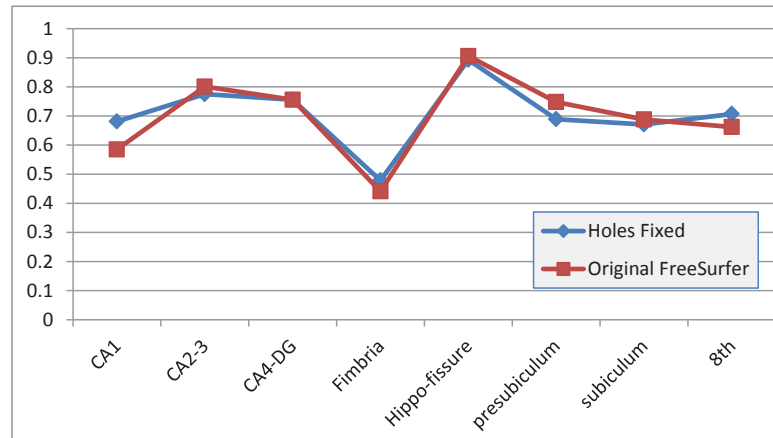


Fig. 3.6.: The ICCs comparison based on FreeSurfer results, measured on right hippocampi

Table 3.3.: The comparison of ICCs results based on segmentations from FIRST: before and after holes were fixed (left hippocampi)

ICCs for left hippocampi	FIRST(fixed)	FIRST(original)
CA1	0.689	0.518
CA2-3	0.773	0.8
CA4-DG	0.695	0.671
Fimbria	0.6	0.544
Hippo-fissure	0.873	0.799
Presubiculum	0.536	0.491
Subiculum	0.584	0.54
8th subfield	0.779	0.837

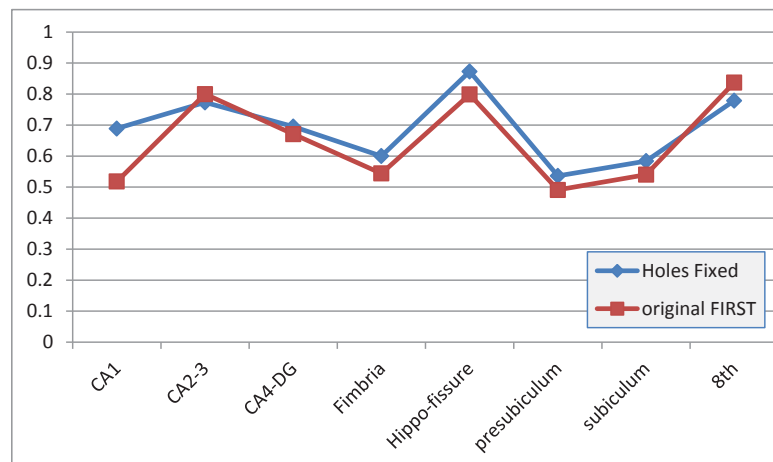


Fig. 3.7.: The ICCs comparison based on FIRST results, measured on left hippocampi

Table 3.4.: The comparison of ICCs results based on segmentations from FIRST: before and after holes were fixed (right hippocampi)

ICCs for right hippocampi	FIRST(fixed)	FIRST(original)
CA1	0.604	0.569
CA2-3	0.804	0.808
CA4-DG	0.762	0.769
Fimbria	0.803	0.804
Hippo-fissure	0.944	0.944
Presubiculum	0.705	0.725
Subiculum	0.609	0.655
8th subfield	0.679	0.662

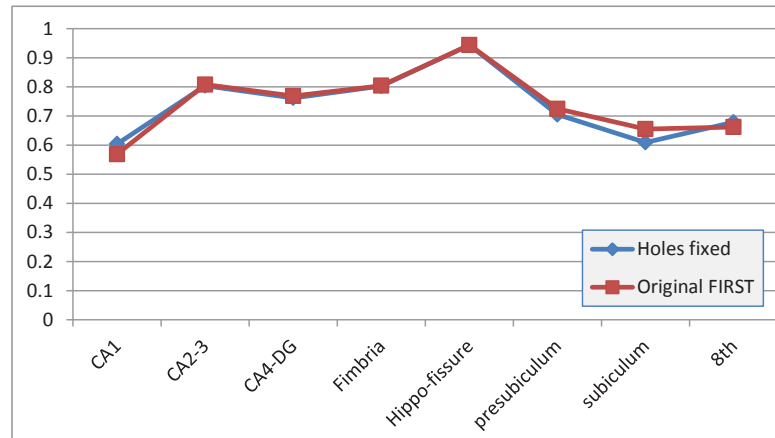


Fig. 3.8.: The ICCs comparison based on FIRST results, measured on right hippocampi

## 4. HIPPOCAMPAL SURFACE ATLAS MODELING

Even though the information of the hippocampus and its subfields has already been obtained, it is still hard to compare the shape among different hippocampi and their subfields, since the goal is to observe the morphometric changes. Since the binary hippocampal objects cannot be compared directly across subjects, the SPHARM method [52] is employed to model their surfaces so that group analysis (e.g., computing an average shape) can be facilitated. This work extends the analysis on single object cases to multiple objects cases, and allows the analysis not only on the individual shape information of each object, but also on spatial relations between or among objects. The SPHARM method was proposed by Brechbuhler et al. [29] to model arbitrarily shaped but simply connected 3D objects. It is essentially a Fourier transform technique that defines a 3D surface using three spherical functions and transforms them into three sets of Fourier coefficients in the frequency domain. Three steps were involved in our SPHARM processing pipeline: (1) spherical parameterization, (2) SPHARM expansion, and (3) SPHARM registration. The structure of Chapter 4 is shown in Fig. 4.1.

### 4.1 Data preparation

The entire hippocampal segmentation results, and the 8 updated hippocampal subfield probability maps generated from Chapter 2 and Chapter 3 will be used in this chapter. Based on SPHARM requirements [52], in order to create shape descriptors that can be compared across different 3D hippocampal structures, appropriate voxel-based structures should meet the following properties:

1. Area preservation: every unit space on the surface of the object must be assigned to the same relative amount of area in the parameter space.

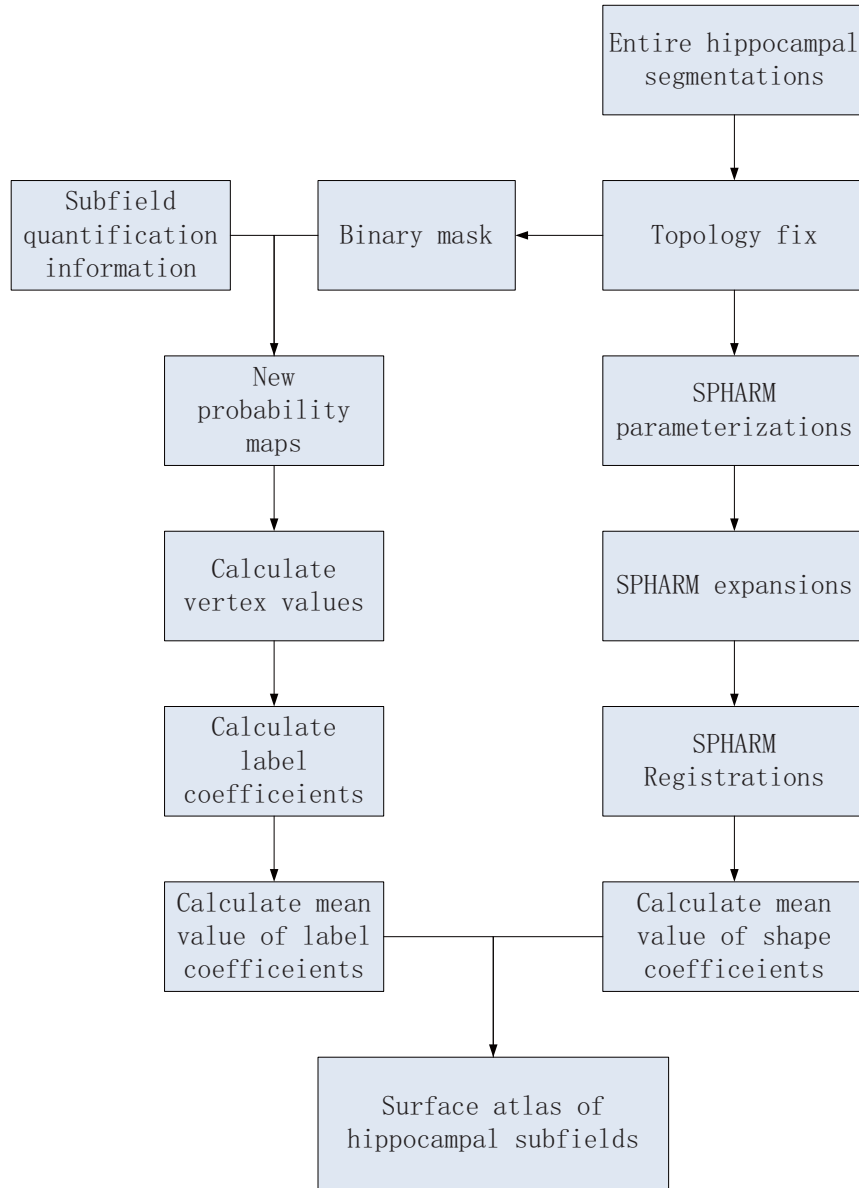


Fig. 4.1.: The structure of Chapter 4: a procedure to build a surface atlas of hippocampal subfields using SPHARM

2. Topology preservation: each square face on the surface of the object must be mapped to a spherical quadrilateral in the parameter space.



3. Bijective mapping: each vertex on the hippocampal segmentation surface must have the unique correspondent relationship exactly mapping from one point onto the sphere, so as the inverse mapping.

4. Minimal angular distortion: the spherical mapping of each square face should be as close to a spherical square as possible.

SPHARM can only model a surface with spherical topology, and not all hippocampal segmentations meet this requirement. The hippocampus segmentations described by voxel-based structures may contain errors due to the voxel quantization or the limited voxel resolution. In some cases, it may cause the mapping process to fail because the voxel surface does not have spherical topology. These cases include: (1) simple cases (e.g., disconnected components); (2) bad edge connectivity; (3) bad vertex connectivity; and (4) 3D holes.

Because the hippocampal segmentations are binary images, value “1” represents the object, while value “0” represents the background. Based on the influencing factors as discussed above, topology fix needs to be performed for the FIRST result to make sure that the hippocampal object is simply-connected and its surface has a spherical topology: (1) Simple cases include disconnected small components, and holes inside the object, such as a zero is completely surrounded by ones. For the former case, the way to resolve this problem is to remove them by changing their values to 0; for the second case, the solution is to replace the zero values by ones. (2) For bad edge connectivity, the solution is to select a voxel from 4 candidates and change its value according to maximum number of different neighbors, illustrated in Fig. 4.2(a). (3) For the bad vertex connectivity, there are two cases shown in Fig. 4.2(b) and Fig. 4.2(c). The solution of the first problem is to change a 1-value-voxel from “1” to “0”, according to the maximum number of different neighbors. While the solution of the second case is to change a 0-value-voxel from “0” to “1”, according to maximum number of different neighbors. (4) For 3D holes shown in Fig. 4.2(d), a hole fixing method proposed by Z. Aktouf et al. [53] is employed.

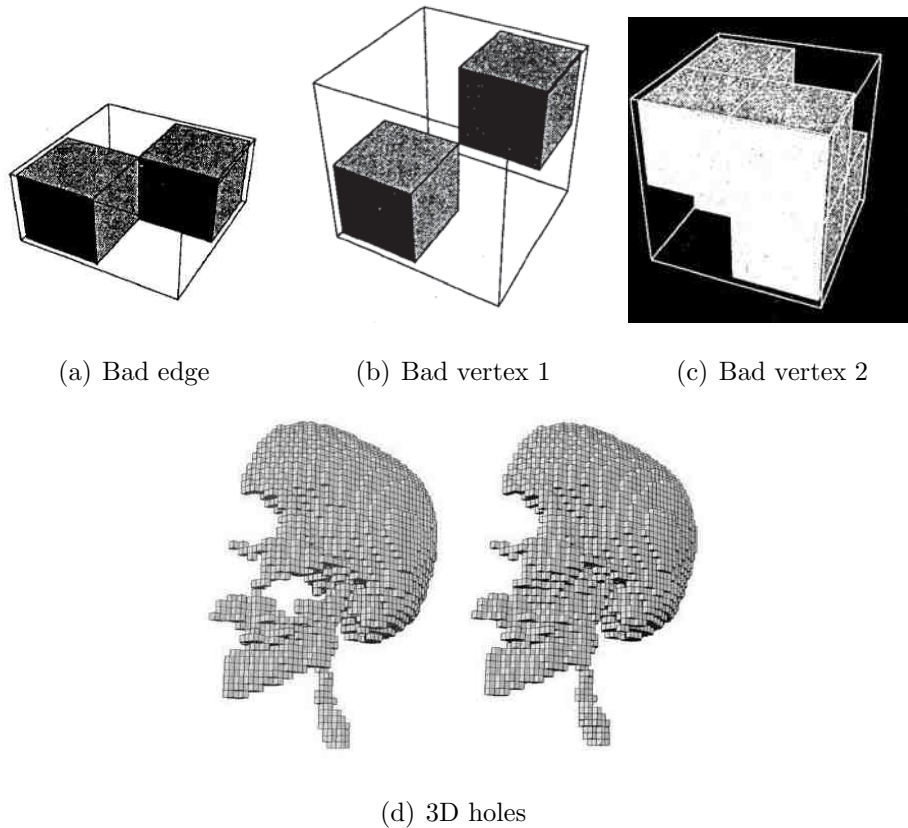


Fig. 4.2.: Several conditions that show the voxel-based structures need to be topology fixed

## 4.2 SPHARM Parameterization

In order to describe a voxel-based hippocampal surface using spherical harmonics, Spherical parameterization was introduced. It created a continuous and uniform mapping from the object surface to the surface of a unit sphere, and it resulted in a bijective mapping between each point  $v$  on a surface and a pair of spherical coordinates  $\theta$  and  $\phi$  that matched the definition of spherical harmonics [54]:

$$\mathbf{v}(\theta, \phi) = (x(\theta, \phi), y(\theta, \phi), z(\theta, \phi))^T, \quad (4.1)$$

Where  $\theta$  is defined as the polar (or co-latitudinal) coordinate with  $\theta \in [0, \pi]$ , and  $\phi$  is taken as the azimuthal (or longitudinal) coordinate with  $\phi \in [0, 2\pi)$ ; As shown

in Fig. 4.3. Thus, the north pole is defined as  $\theta = 0$  and the south pole has  $\theta = \pi$ . Fig. 4.4 shows an example spherical parameterization. This parameterization is an area preserving mapping computed using Brechbuhlers method [29].

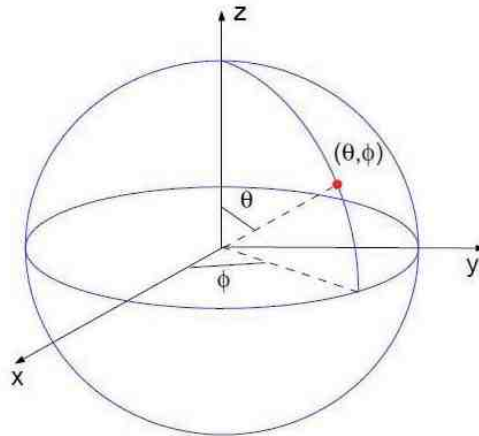


Fig. 4.3.: A spherical unit:  $\theta$  is defined as the polar (or co-latitudinal) coordinate with  $\theta \in [0, \pi]$ , and  $\phi$  is taken as the azimuthal (or longitudinal) coordinate with  $\phi \in [0, 2\pi)$

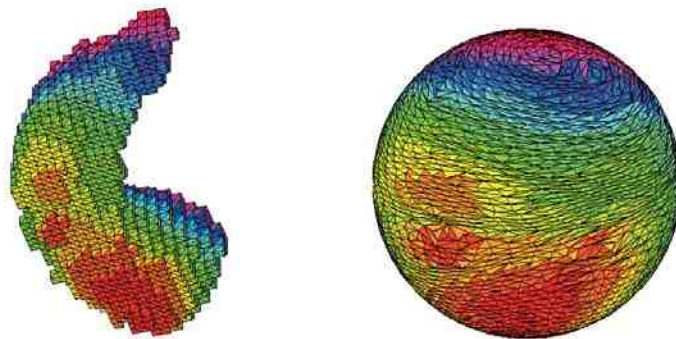


Fig. 4.4.: Hippocampal surface (left) and its spherical parameterization (right). Color indicates the correspondence between the surface and parameterization

### 4.3 SPHARM Expansion

SPHARM expansion expands the object surface into a complete set of spherical harmonic basis functions  $Y_l^m$ , where  $Y_l^m$  denotes the spherical harmonic of degree  $l$  and order  $m$  and it is essentially a Fourier basis function defined on the sphere. Each function is independently decomposed in terms of SPHARM as:

$$x(\theta, \phi) = \sum_{l=0}^{\infty} \sum_{m=-l}^l c_{lx}^m Y_l^m(\theta, \phi), \quad (4.2)$$

$$y(\theta, \phi) = \sum_{l=0}^{\infty} \sum_{m=-l}^l c_{ly}^m Y_l^m(\theta, \phi), \quad (4.3)$$

$$z(\theta, \phi) = \sum_{l=0}^{\infty} \sum_{m=-l}^l c_{lz}^m Y_l^m(\theta, \phi), \quad (4.4)$$

The expansion can be bundled as a single vector-valued form:

$$v(\theta, \phi) = \begin{pmatrix} x(\theta, \phi) \\ y(\theta, \phi) \\ z(\theta, \phi) \end{pmatrix} = \sum_{l=0}^{\infty} \sum_{m=-l}^l \begin{pmatrix} c_{xl}^m \\ c_{yl}^m \\ c_{zl}^m \end{pmatrix} = \sum_{l=0}^{\infty} \sum_{m=-l}^l c_l^m Y_l^m(\theta, \phi), \quad (4.5)$$

where

$$v(\theta, \phi) = \begin{pmatrix} x(\theta, \phi) \\ y(\theta, \phi) \\ z(\theta, \phi) \end{pmatrix}, \quad (4.6)$$

and

$$c_l^m = \begin{pmatrix} c_{xl}^m \\ c_{yl}^m \\ c_{zl}^m \end{pmatrix}, \quad (4.7)$$

The prerequisite for SPHARM expansion is to finish spherical parameterization in advance, as it was introduced in the last section. As the results of spherical parameterization shown in Equation 4.3,  $x(\theta, \phi), y(\theta, \phi), z(\theta, \phi)$  are functions that define the location relationship between voxel-based object and spherical unit. Based on this theory, the object surface can be described through expanding these three spherical functions using SPHARM, as shown in Equation 4.3.

The Fourier coefficients  $c_l^m$  are determined using standard least-square estimation and can be estimated by solving a linear system. To describe how to calculate it, we can pick one dimension,  $x(\theta, \phi)$  as an example. The goal is to compute the coefficients  $c_{lx}^m$  up to a user-desired maximum degree  $L_{max}$ . When an input spherical function  $x(\theta, \phi)$  is described by a set of spherical samples  $(\theta_i, \phi_i)$  and their function values  $x_i = x(\theta_i, \phi_i)$ , for  $1 \leq i \leq n$ . Based on Equation 4.3, a linear system can be described as follows:

$$\begin{pmatrix} y_{1,1} & y_{1,2} & y_{1,3} & \cdots & y_{1,k} \\ y_{2,1} & y_{2,2} & y_{2,3} & \cdots & y_{2,k} \\ \vdots & \vdots & \vdots & \ddots & \vdots \\ y_{n,1} & y_{n,2} & y_{n,3} & \cdots & y_{n,k} \end{pmatrix} \begin{pmatrix} a_1 \\ a_2 \\ a_3 \\ \vdots \\ a_k \end{pmatrix} = \begin{pmatrix} x_1 \\ x_2 \\ x_3 \\ \vdots \\ x_n \end{pmatrix}, \quad (4.8)$$

where  $y_{i,j} = Y_l^m(\theta_i, \phi_i)$ ,  $j = l^2 + l + m + 1$ , and  $k = (L_{max} + 1)^2$ . For every pair  $(l, m)$ , an indexing scheme  $j$  is the unique number assigned to these pairs. The above system is solved by least square fitting for  $(a_1, a_2, \dots, a_k)^T$  as for most cases  $n \neq k$ . As each  $a_j \equiv \hat{c}_{lx}^m$  is an estimation of the original coefficients  $c_{lx}^m$ , for the unique index  $j = l^2 + l + m + 1$ , the original function can be reconstructed as the form:

$$\hat{x}(\theta, \phi) = \sum_{l=0}^{\infty} \sum_{m=-l}^l \hat{c}_{lx}^m Y_l^m(\theta, \phi) \approx x(\theta, \phi), \quad (4.9)$$

The object surface can be reconstructed using these coefficients, and the more degrees (i.e. larger values of  $L_{max}$ ) the user uses, the more coefficients are generated and the more accurate and detailed reconstruction  $\hat{x}(\theta, \phi)$  will be achieved. Applying

least-squares estimation in a same way onto  $y(\theta, \phi)$  and  $z(\theta, \phi)$ , the results  $c_{ly}^m$  and  $c_{lz}^m$  are determined separately. Thus a series of bundled coefficients  $c_l^m$  can be used for approximating the original surface and also used to represent and reconstruct an

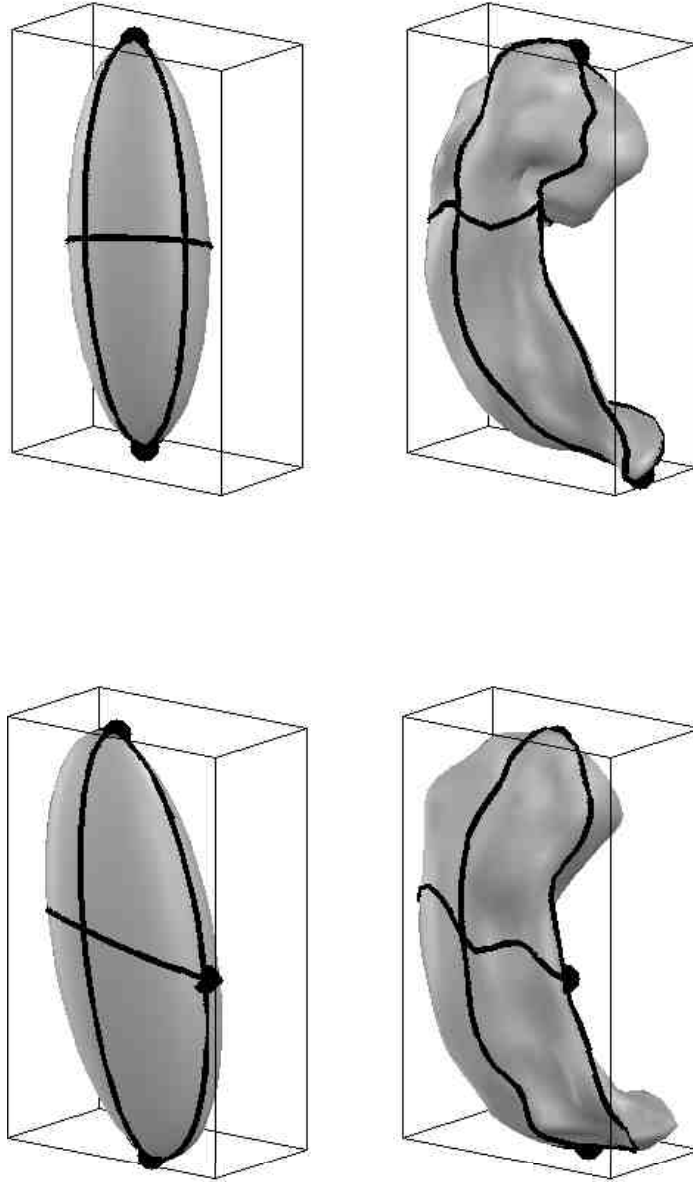


Fig. 4.5.: An example of degree 1 reconstruction (an ellipsoid) and the degree 15 reconstruction of the same object

approximated surface. Fig. 4.5 shows the degree 1 reconstruction and the degree 15 reconstruction for the same object. The SPHARM parametrization and expansion process are demonstrated in Fig. 4.6, the surface of an object (hippocampus) was first bijectively mapped onto the spherical surface (done by SPHARM parameterization), then this object was reconstructed by applying spherical harmonic functions and using the calculated spherical coefficients and user-desired degree(done by SPHARM expansion).

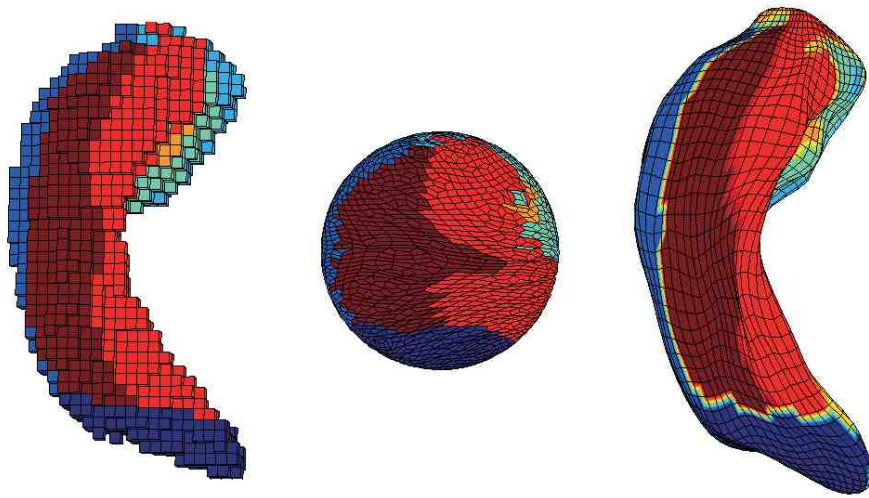


Fig. 4.6.: The object on left is the original hippocampus, the object in the middle is the unit sphere, and the object on the right is the reconstructed hippocampus using SPHARM expansion

#### 4.4 SPHARM Registration

Sections 4.2 and 4.3 describe the working procedures of SPHARM parameterization and expansion that describe a 3D hippocampal surface based on computing coefficients and user-desired degrees. As the goal is to compare different objects, a method that can align all these objects into a common reference system should be introduced; that's the reason why SPHARM registration is proposed.

SPHARM registration creates a shape descriptor (i.e., excluding translation, rotation, and/or scaling) from a normalized set of SPHARM coefficients, which are comparable across objects.

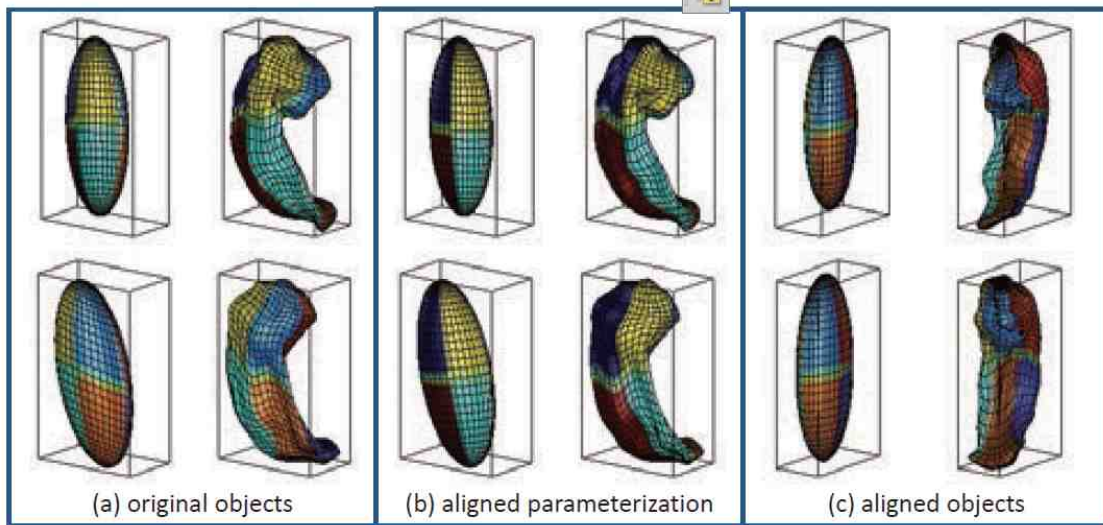


Fig. 4.7.: SPHARM registration using First Order Ellipsoids (FOEs). Each of (a-c) shows the FOE on left and degree 15 reconstruction on right. Parameterization is indicated by the mesh and color on the surface.

The Scaling invariance can be achieved by adjusting the coefficients so that the object volume is normalized. Ignoring the  $0th$  degree coefficient leads to translation invariance. By design, the  $1st$  degree reconstruction is an ellipsoid unit for all SPHARM models (see Fig.4.5), it is also known as FIRST Order Ellipsoid (FOE). The Rotation invariance can be achieved through aligning the FOE [29]. Fig.4.7 demonstrates the registration of SPHARM models by aligning the FOEs. Each of (a-c) shows the FOE at the left and degree 15 reconstruction at right. In (a), the original pose and parameterization are shown. Note that the correspondence between two SPHARM models is implied by the underlying parameterization: two points with the same parameter pair  $(\theta, \phi)$  on two surfaces were defined to be a corresponding pair. Thus, in (b), the FOE was used to align the parameterization in the parameter



space and to establish the surface correspondence; although, the object pose stayed the same, the parameter net on each FOE was rotated to a canonical position such that the north pole was at one end of the longest main axis, and both the crossing point of the zero meridian and the equator were at one end of the shortest main axis. In (c), the FOE was used to adjust the object pose in the object space: the FOE was rotated to make its main axes coincide with the coordinate axes, putting the shortest axis along x and the longest along z. As the result, these two hippocampi were aligned to a canonical position in both parameter space and object space. Algorithmic details about this method are available in Brechbuhler et al. [29] [55].

## 4.5 Building Hippocampal Surface Atlas Models

The goal of this study is to build surface atlas models for left and right hippocampi. In order to achieve this goal, parameterization, expansion and registration techniques discussed above will be used. And as an expansion of previous work, sub-field information is used for generating hippocampal surface atlas by parameterizing the probability maps resulted from last chapter.

### 4.5.1 Construct A Mean Hippocampus

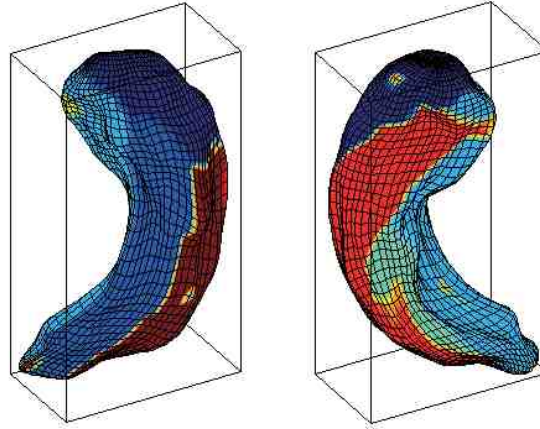
Based on the work discussed in Sections 4.2, 4.3 and 4.4, we are able to reconstruct each hippocampus object with a certain degree, and align them together. After they are well-aligned, given n hippocampal SPHARM models, mean values can be obtained by averaging  $N$  sets of harmonics coefficients  $c_l^m$ , as we have 26 sets of participant data (Groups A and B). The way to calculate Fourier coefficients in in Harmonic functions is as same as it was described in Section 4.3, and shows as the followings:

$$c_{new,lx}^m = \frac{c_{1,lx}^m + c_{2,lx}^m + \dots + c_{n,lx}^m}{N}, \quad (4.10)$$

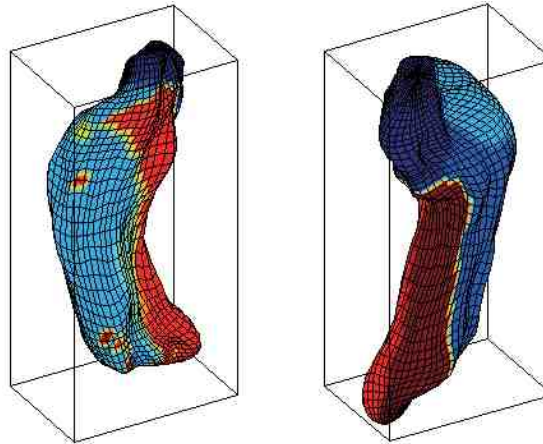
$$c_{new,ly}^m = \frac{c_{1,ly}^m + c_{2,ly}^m + \dots + c_{n,ly}^m}{N}, \quad (4.11)$$

$$c_{new,lz}^m = \frac{c_{1,lz}^m + c_{2,lz}^m + \dots + c_{n,lz}^m}{N}, \quad (4.12)$$

Here  $N = 26$ , and by using the new bundled coefficients  $c_{new,l}^m$ , an averaged hippocampus can be generated, as shown in Fig. 4.8.



(a) Left hippocampi



(b) Right hippocampi

Fig. 4.8.: Subfields mapped onto an individual SPHARM model

### 4.5.2 Creating Hippocampal Surface Atlas

Given  $N$  hippocampal SPHARM models, we can calculate a mean SPHARM model (as shown in Section 4.5.1) and use a similar idea to create a surface atlas. Now we describe our approach to map the subfield information onto the mean surface.

The main idea is to also use spherical harmonic basis functions to expand each subfield probability map. After that, for each surface location, we can assign it with the subfield label which has the largest probability among all eight subfields. In order to compute a SPHARM expansion for each probability map, we need to map a probability value to each vertex on the original voxel surface (see Fig. 4.4). The algorithm to give vertex values is shown in Algorithm 5; note that vertex probability values are not expanded in Algorithm 5 as it demonstrates a process to generate surface atlas for each individual. The process of building an averaged surface atlas will be introduced later.

---

**Algorithm 4** Compute vertex values based on probability maps of each hippocampal subfield

---

```

1: for each subject; do
2:   for each subfield probability map do
3:     give vertex values based on face values;
4:     if two or more faces share the same vertex then
5:       add probabilities together  $P$  and record how many times  $N$  it has been
        added;
6:     end if
7:     mean values =  $\frac{P}{N}$ ;
8:   end for
9: end for
10: compare values on each vertex from each subfield;
11: vertex is labeled as the subfield having biggest probability value;

```

---

Note that each original probability value was defined for each voxel, and thus each face on the original surface has a unique probability value. Based on this, a probability value for each vertex can be calculated by averaging the probability values of its adjacent faces. Thus, a label map was generated in order to create a surface atlas for each individual.

As the goal of this study is to build a mean surface atlas, some further work based on spherical harmonics basis functions is described in Algorithm 5. In this algorithm, the SPHARM expansion process is similar to the method as discussed in Section 4.3. We denote probability map as  $L(\theta, \phi)$ . Based on SPHARM expansion theory, it can be reconstructed as Equation 4.5.2.

---

**Algorithm 5** Generate hippocampal surface atlas information

---

```

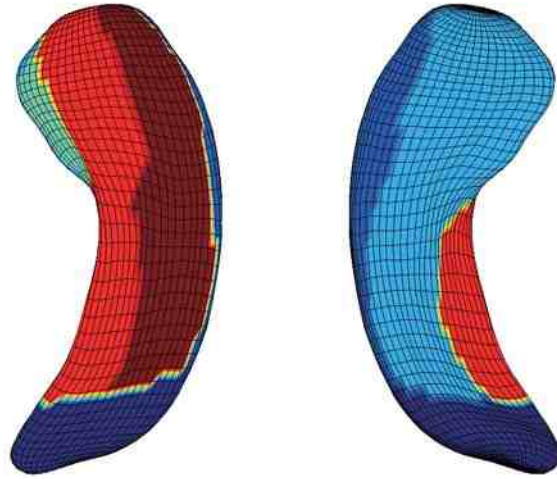
1: for n subject do
2:   for each subfield probability map do
3:     give vertex values based on face values;
4:     if two or more faces share the same vertex then
5:       add probabilities together  $P$  and record how many times  $N$  it has been
         added;
6:     end if
7:     SPHARM expansion and save coefficients;
8:   end for
9:   average coefficient values in parametric space
10: end for
11: compare values on each vertex from each subfield;
12: vertex is labeled as the subfield having biggest probability value;
13: use the vertex label information to reconstruct surface atlas

```

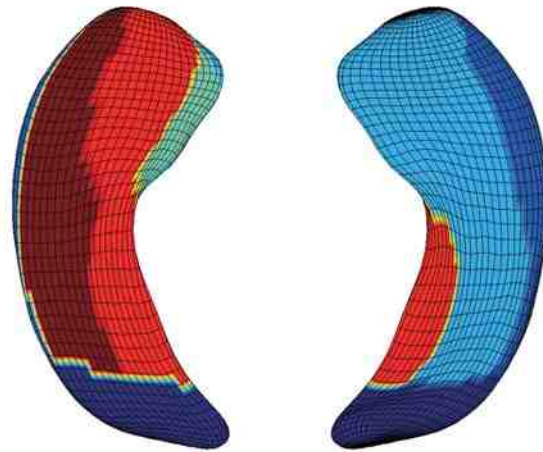
---

$$\hat{L}(\theta, \phi) = \sum_{l=0}^{\infty} \sum_{m=-l}^l \hat{C}_{new,l}^m Y_l^m(\theta, \phi) \approx L(\theta, \phi), \quad (4.13)$$

Where  $\hat{P}$  are coefficients, which are mean values from averaging  $n$  sets of objects. And the models can be viewed in Fig. 4.9, Fig. 4.10, and Fig. 4.11.

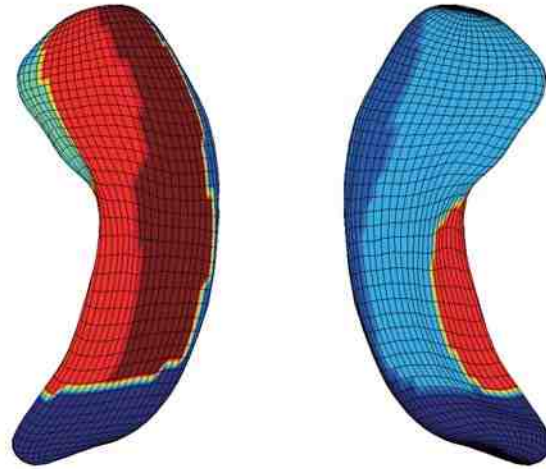


(a) Model A left

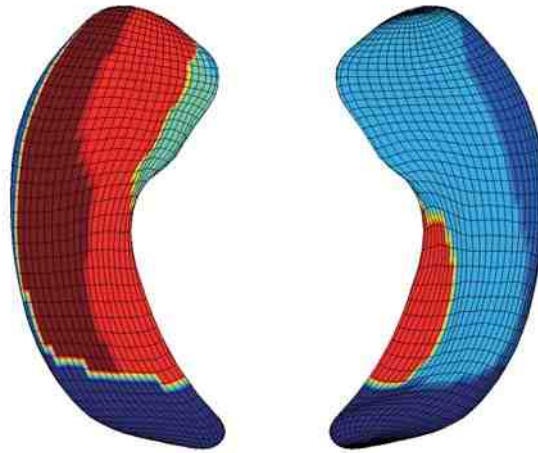


(b) Model A right

Fig. 4.9.: As each participant has two repeated scans (Groups A and B), (a - b) are models reconstructed from Group A, which contains 26 images.

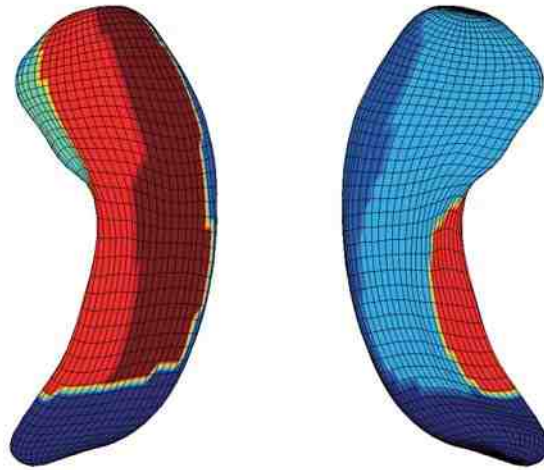


(a) Model B left

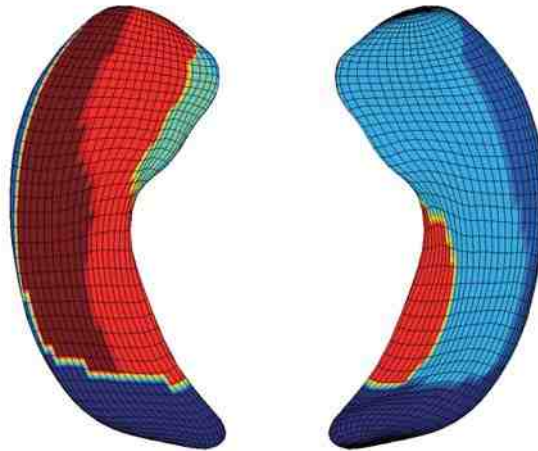


(b) Model B right

Fig. 4.10.: As each participant has two repeated scans (Groups A and B), (a - b) are models reconstructed from Group B, which contains 26 images.



(a) All averaged model left



(b) All averaged model right

Fig. 4.11.: As each participant has two repeated scans (Groups A and B), (a - b) are models reconstructed both from Groups A and B, which contains 52 images.

## 5. CONCLUSIONS AND FUTURE WORK

We have proposed a method for building a surface atlas of hippocampal subfields from MRI scans using FreeSurfer, FIRST and SPHARM methods and tools. Using FreeSurfer, we have obtained valuable hippocampal subfield information. Using FIRST, we have extracted reliable hippocampal surface information. Using SPHARM, we have developed an approach to create an atlas by mapping interpolated subfield information onto an average surface. The empirical result using ADNI data demonstrates good reproducibility of the proposed method.

We presented our initial effort towards building a computational framework for subfield-guided hippocampal morphometry. Based on this work, some more complicated registration methods can be applied as the FOE method registers SPHARM objects in both parameter space and object space. However, it works only if the FOE is a real ellipsoid but not an ellipsoid of revolution or a sphere [56]. In the latter case, we couldn't find a unique set of main axes to align things together. Thus the more advanced registration method such as SHREC (SPHARM Registration ICP) [56] will be studied.

We need to first register all the hippocampal surface to an atlas and then define the surface signals. The hippocampal surface atlas we built in this study was a common reference system where morphometric analysis was performed. All surfaces can be registered to it, then comparable across each other. Let  $X_t$  be our atlas, for an individual complex  $X$ , we can directly use its deformation field  $\delta X = X - X_t$  relative to the atlas  $X_t$  to describe it. Many feature measures will be concluded such as normals, curvatures, and thicknesses.

Multi-scale analysis of hippocampal morphometry is also a goal of future work that will be studied for the hippocampal morphometry at multiple scales, including (1) the total volume, (2) subfield volumes, and (3) the detailed surface-based mor-



phometric features extracted using the above method. We will use a well-established statistical inference to identify hippocampal morphometric changes related to different diagnostic or cognitive conditions while controlling for a few relevant covariates. The following is the General Linear Model (GLM) we will use:  $y = X\Psi + Z\Phi + \varepsilon$ , where the dependent variable is our morphometric measure;  $X = (x_1, \dots, x_p)^T$  are the variables of interest;  $Z = (z_1, \dots, z_k)^T$  are the variables whose effects we want to exclude;  $\Psi = (\Psi_1, \dots, \Psi_p)^T$  and  $\Phi = (\Phi_1, \dots, \Phi_k)^T$  are the coefficients; and  $\varepsilon$  is the error term. In surface-based analysis, the goal is to test if  $X$  is significant (i.e.,  $\Phi \neq 0$ ) for some  $y \in S$ , where  $S$  is our surface manifold. After extracting surface signals, we will perform heat kernel smoothing [57] on the surface to increase signal to noise ratio, run GLM as described above, use random field theory [58] for multiple comparison correction, and finally map statistical analysis results on the surface for an intuitive visualization. We will compare the results from surface-based analysis with those from the analyses of the total volume and subfield volumes.

Furthermore, as the complexity of the hippocampal structure and the multi-modal genetic, imaging, cognitive and clinical data, it remains challenges to develop novel data mining methods to discover the complex relationship between hippocampal morphology and these rich multi-modal data. One direction of our future work will be designed to address this challenge.

## LIST OF REFERENCES

## LIST OF REFERENCES

- [1] M. K. Garvin and X. Wu, “Graph algorithmic techniques for biomedical image segmentation,” in *Advanced Computational Approaches to Biomedical Engineering*. Springer, 2014, pp. 3–45.
- [2] E. Ruiz Pujadas and M. Reiser, “Shape-based normalized cuts using spectral relaxation for biomedical segmentation,” *IEEE Transactions on Image Processing*, pp. 163–170, 2014.
- [3] A. Q. Al-Faris, U. K. Ngah, N. A. M. Isa, and I. L. Shuaib, “Breast mri tumour segmentation using modified automatic seeded region growing based on particle swarm optimization image clustering,” in *Soft Computing in Industrial Applications*. Springer, 2014, pp. 49–60.
- [4] L. Carreon, S. Glassman, J. Schwender, B. Subach, M. Gornet, and S. Ohno, “Reliability and accuracy of fine-cut computed tomography scans to determine the status of anterior interbody fusions with metallic cages,” *The Spine Journal*, vol. 8, no. 6, pp. 998–1002, 2008.
- [5] A. T. Eggebrecht, B. R. White, S. L. Ferradal, C. Chen, Y. Zhan, A. Z. Snyder, H. Dehghani, and J. P. Culver, “A quantitative spatial comparison of high-density diffuse optical tomography and fmri cortical mapping,” *Neuroimage*, vol. 61, no. 4, pp. 1120–1128, 2012.
- [6] G. Gratton and M. Fabiani, “Shedding light on brain function: the event-related optical signal,” *Trends in Cognitive Sciences*, vol. 5, no. 8, pp. 357–363, 2001.
- [7] D. W. McRobbie, *MRI from Picture to Proton, Chapter 3*. Cambridge University Press, 2007.
- [8] C. Wolters, A. Anwander, X. Tricoche, D. Weinstein, M. Koch, and R. MacLeod, “Influence of tissue conductivity anisotropy on eeg/meg field and return current computation in a realistic head model: a simulation and visualization study using high-resolution finite element modeling,” *Neuroimage*, vol. 30, no. 3, pp. 813–826, 2006.
- [9] P. E. Valk, *Positron Emission Tomography: Basic Sciences*. Springer, 2003.
- [10] D. L. Pham, C. Xu, and J. L. Prince, “Current methods in medical image segmentation 1,” *Annual Review of Biomedical Engineering*, vol. 2, no. 1, pp. 315–337, 2000.
- [11] T. L. McHugh, A. J. Saykin, H. A. Wishart, L. A. Flashman, H. B. Cleavinger, L. A. Rabin, A. C. Mamourian, and L. Shen, “Hippocampal volume and shape analysis in an older adult population,” *The Clinical Neuropsychologist*, vol. 21, no. 1, pp. 130–145, 2007.

- [12] P. A. Yushkevich, J. A. Detre, D. Mechanic-Hamilton, M. A. Fernández-Seara, K. Z. Tang, A. Hoang, M. Korczykowski, H. Zhang, and J. C. Gee, “Hippocampus-specific fmri group activation analysis using the continuous medial representation,” *Neuroimage*, vol. 35, no. 4, pp. 1516–1530, 2007.
- [13] D. Shen, S. Moffat, S. M. Resnick, and C. Davatzikos, “Measuring size and shape of the hippocampus in mr images using a deformable shape model,” *Neuroimage*, vol. 15, no. 2, pp. 422–434, 2002.
- [14] L. Wang, F. Beg, T. Ratnanather, C. Ceritoglu, L. Younes, J. C. Morris, J. G. Csernansky, and M. I. Miller, “Large deformation diffeomorphism and momentum based hippocampal shape discrimination in dementia of the alzheimer type,” *IEEE Transactions on Medical Imaging*, vol. 26, no. 4, pp. 462–470, 2007.
- [15] M. R. Hunsaker and D. G. Amaral, “A semi-automated pipeline for the segmentation of rhesus macaque hippocampus: Validation across a wide age range,” *PLoS One*, vol. 9, no. 2, p. e89456, 2014.
- [16] S. M. Nestor, E. Gibson, F.-Q. Gao, A. Kiss, and S. E. Black, “A direct morphometric comparison of five labeling protocols for multi-atlas driven automatic segmentation of the hippocampus in alzheimer’s disease,” *Neuroimage*, vol. 66, pp. 50–70, 2013.
- [17] G. P. Winston, M. J. Cardoso, E. J. Williams, J. L. Burdett, P. A. Bartlett, M. Espak, C. Behr, J. S. Duncan, and S. Ourselin, “Automated hippocampal segmentation in patients with epilepsy: Available free online,” *Epilepsia*, vol. 54, no. 12, pp. 2166–2173, 2013.
- [18] S. F. Eskildsen, P. Coupé, D. García-Lorenzo, V. Fonov, J. C. Pruessner, and D. L. Collins, “Prediction of alzheimer’s disease in subjects with mild cognitive impairment from the adni cohort using patterns of cortical thinning,” *Neuroimage*, vol. 65, pp. 511–521, 2013.
- [19] G. S. Flores, G. de Haan, R. Jasinschi, and O. Soldea, “Automatic segmentation of hippocampal substructures,” *Thesis Report, Technische Universiteit Eindhoven*, 2012.
- [20] J. Shi, P. M. Thompson, B. Gutman, and Y. Wang, “Surface fluid registration of conformal representation: Application to detect disease burden and genetic influence on hippocampus,” *Neuroimage*, vol. 78, pp. 111–134, 2013.
- [21] F. L. Bookstein, “Shape and the information in medical images: A decade of the morphometric synthesis,” in *Proceedings of the Workshop on Mathematical Methods in Biomedical Image Analysis*. IEEE, 1996, pp. 2–12.
- [22] T. F. Cootes, C. J. Taylor, D. H. Cooper, and J. Graham, “Active shape models—their training and application,” *Computer Vision and Image Understanding*, vol. 61, no. 1, pp. 38–59, 1995.
- [23] J. G. Csernansky, S. Joshi, L. Wang, J. W. Haller, M. Gado, J. P. Miller, U. Grenander, and M. I. Miller, “Hippocampal morphometry in schizophrenia by high dimensional brain mapping,” *Proceedings of the National Academy of Sciences*, vol. 95, no. 19, pp. 11 406–11 411, 1998.

- [24] S. C. Joshi, M. I. Miller, and U. Grenander, "On the geometry and shape of brain sub-manifolds," *International Journal of Pattern Recognition and Artificial Intelligence*, vol. 11, no. 08, pp. 1317–1343, 1997.
- [25] R. Hartley and A. Zisserman, *Multiple View Geometry in Computer Vision, Chapter 3*. Cambridge University Press, 2003.
- [26] S. M. Pizer, D. S. Fritsch, P. A. Yushkevich, V. E. Johnson, and E. L. Chaney, "Segmentation, registration, and measurement of shape variation via image object shape," *IEEE Transactions on Medical Imaging*, vol. 18, no. 10, pp. 851–865, 1999.
- [27] M. Styner, G. Gerig, J. Lieberman, D. Jones, and D. Weinberger, "Statistical shape analysis of neuroanatomical structures based on medial models," *Medical Image Analysis*, vol. 7, no. 3, pp. 207–220, 2003.
- [28] M. Styner, G. Gerig, S. Joshi, and S. Pizer, "Automatic and robust computation of 3d medial models incorporating object variability," *International Journal of Computer Vision*, vol. 55, no. 2-3, pp. 107–122, 2003.
- [29] C. Brechbühler, G. Gerig, and O. Kübler, "Parametrization of closed surfaces for 3-d shape description," *Computer Vision and Image Understanding*, vol. 61, no. 2, pp. 154–170, 1995.
- [30] L. H. Staib and J. S. Duncan, "Model-based deformable surface finding for medical images," *IEEE Transactions on Medical Imaging*, vol. 15, no. 5, pp. 720–731, 1996.
- [31] S. Mueller, L. Stables, A. Du, N. Schuff, D. Truran, N. Cashdollar, and M. Weiner, "Measurement of hippocampal subfields and age-related changes with high resolution mri at 4t," *Neurobiology of Aging*, vol. 28, no. 5, pp. 719–726, 2007.
- [32] P. A. Yushkevich, B. B. Avants, J. Pluta, S. Das, D. Minkoff, D. Mechanic-Hamilton, S. Glynn, S. Pickup, W. Liu, J. C. Gee *et al.*, "A high-resolution computational atlas of the human hippocampus from postmortem magnetic resonance imaging at 9.4 t," *Neuroimage*, vol. 44, no. 2, pp. 385–398, 2009.
- [33] R. La Joie, M. Fouquet, F. Mézenge, B. Landeau, N. Villain, K. Mevel, A. Pélerin, F. Eustache, B. Desgranges, and G. Chételat, "Differential effect of age on hippocampal subfields assessed using a new high-resolution 3t mr sequence," *Neuroimage*, vol. 53, no. 2, pp. 506–514, 2010.
- [34] L. Wisse, L. Gerritsen, J. J. Zwanenburg, H. J. Kuijf, P. R. Luijten, G. J. Biessels, and M. I. Geerlings, "Subfields of the hippocampal formation at 7t mri: In vivo volumetric assessment," *Neuroimage*, vol. 61, no. 4, pp. 1043–1049, 2012.
- [35] J. L. Winterburn, J. C. Pruessner, S. Chavez, M. M. Schira, N. J. Lobaugh, A. N. Voineskos, and M. M. Chakravarty, "A novel in vivo atlas of human hippocampal subfields using high-resolution 3t magnetic resonance imaging," *Neuroimage*, vol. 74, pp. 254–265, 2013.
- [36] K. Van Leemput, A. Bakkour, T. Benner, G. Wiggins, L. L. Wald, J. Augustinack, B. C. Dickerson, P. Golland, and B. Fischl, "Automated segmentation of hippocampal subfields from ultra-high resolution in vivo mri," *Hippocampus*, vol. 19, no. 6, pp. 549–557, 2009.

- [37] L. Shen, A. J. Saykin, S. Kim, H. A. Firpi, J. D. West, S. L. Risacher, B. C. McDonald, T. L. McHugh, H. A. Wishart, and L. A. Flashman, "Comparison of manual and automated determination of hippocampal volumes in mci and early ad," *Brain Imaging and Behavior*, vol. 4, no. 1, pp. 86–95, 2010.
- [38] E. Luders, P. M. Thompson, F. Kurth, J.-Y. Hong, O. R. Phillips, Y. Wang, B. A. Gutman, Y.-Y. Chou, K. L. Narr, and A. W. Toga, "Global and regional alterations of hippocampal anatomy in long-term meditation practitioners," *Human Brain Mapping*, vol. 34, no. 12, pp. 3369–3375, 2013.
- [39] F. P. Kuhl and C. R. Giardina, "Elliptic fourier features of a closed contour," *Computer Graphics and Image Processing*, vol. 18, no. 3, pp. 236–258, 1982.
- [40] G. Gerig, M. Styner, M. E. Shenton, and J. A. Lieberman, "Shape versus size: Improved understanding of the morphology of brain structures," in *Medical Image Computing and Computer-Assisted Intervention—MICCAI 2001*. Springer, 2001, pp. 24–32.
- [41] M. Styner, J. A. Lieberman, D. Pantazis, and G. Gerig, "Boundary and medial shape analysis of the hippocampus in schizophrenia," *Medical Image Analysis*, vol. 8, no. 3, pp. 197–203, 2004.
- [42] A. Kelemen, G. Székely, and G. Gerig, "Elastic model-based segmentation of 3-d neuroradiological data sets," *IEEE Transactions on Medical Imaging*, vol. 18, no. 10, pp. 828–839, 1999.
- [43] R. Hogan, L. Wang, M. Bertrand, L. Willmore, R. Bucholz, A. Nassif, and J. Csernansky, "Predictive value of hippocampal mr imaging-based high-dimensional mapping in mesial temporal epilepsy: preliminary findings," *American Journal of Neuroradiology*, vol. 27, no. 10, pp. 2149–2154, 2006.
- [44] N. Solowij, M. Walterfang, D. I. Lubman, S. Whittle, V. Lorenzetti, M. Styner, D. Velakoulis, C. Pantelis, and M. Yücel, "Alteration to hippocampal shape in cannabis users with and without schizophrenia," *Schizophrenia Research*, vol. 143, no. 1, pp. 179–184, 2013.
- [45] B. T. Wyman, D. J. Harvey, K. Crawford, M. A. Bernstein, O. Carmichael, P. E. Cole, P. K. Crane, C. DeCarli, N. C. Fox, J. L. Gunter *et al.*, "Standardization of analysis sets for reporting results from adni mri data," *Alzheimers Dement*, vol. 9, no. 3, pp. 332–337, 2013.
- [46] B. Fischl, D. H. Salat, A. J. van der Kouwe, N. Makris, F. Ségonne, B. T. Quinn, and A. M. Dale, "Sequence-independent segmentation of magnetic resonance images," *Neuroimage*, vol. 23, pp. S69–S84, 2004.
- [47] B. Patenaude, S. M. Smith, D. N. Kennedy, and M. Jenkinson, "A bayesian model of shape and appearance for subcortical brain segmentation," *Neuroimage*, vol. 56, no. 3, pp. 907–922, 2011.
- [48] G. G. Koch, "Intraclass correlation coefficient," *Encyclopedia of Statistical Sciences*, pp. 30–46, 1982.
- [49] A. Donner and J. J. Koval, "The estimation of intraclass correlation in the analysis of family data." *Biometrics*, vol. 36, no. 1, pp. 19–25, 1980.

- [50] J. L. Fleiss, *Design and Analysis of Clinical Experiments, Chapter 1*. John Wiley & Sons, 2011, vol. 73.
- [51] K. O. McGraw and S. Wong, “Forming inferences about some intraclass correlation coefficients.” *Psychological methods*, vol. 1, no. 1, p. 30, 1996.
- [52] L. Shen, S. Kim, J. Wan, J. D. West, and A. J. Saykin, “Fourier methods for 3d surface modeling and analysis,” *Emerging Topics in Computer Vision and Its Applications*, vol. 1, p. 175, 2011.
- [53] Z. Aktouf, G. Bertrand, and L. Perroton, “A three-dimensional holes closing algorithm,” *Pattern Recognition Letters*, vol. 23, no. 5, pp. 523–531, 2002.
- [54] E. W. Weisstein, “spherical harmonic.” from mathworldA Wolfram Web Resource,” <http://mathworld.wolfram.com/SphericalHarmonic.html/>, website Update Date: March 20, 2014; Last Date Accessed: April, 2014.
- [55] C. Brechbuhler, “Description and analysis of 3-d shapes by parametrization of closed surfaces,” *Ph.D. dissertation, The University of Utah*, 1995.
- [56] L. Shen, H. Huang, F. Makedon, and A. J. Saykin, “Efficient registration of 3d spharm surfaces,” in *Fourth Canadian Conference on Computer and Robot Vision*. IEEE, 2007, pp. 81–88.
- [57] M. K. Chung, S. M. Robbins, K. M. Dalton, R. J. Davidson, A. L. Alexander, and A. C. Evans, “Cortical thickness analysis in autism with heat kernel smoothing,” *Neuroimage*, vol. 25, no. 4, pp. 1256–1265, 2005.
- [58] L. Shen, A. J. Saykin, M. K. Chung, and H. Huang, “Morphometric analysis of hippocampal shape in mild cognitive impairment: an imaging genetics study,” in *Proceedings of the 7th IEEE International Conference on Bioinformatics and Bioengineering*. IEEE, 2007, pp. 211–217.

## APPENDICES



## A. DEMONSTRATE RESULTS

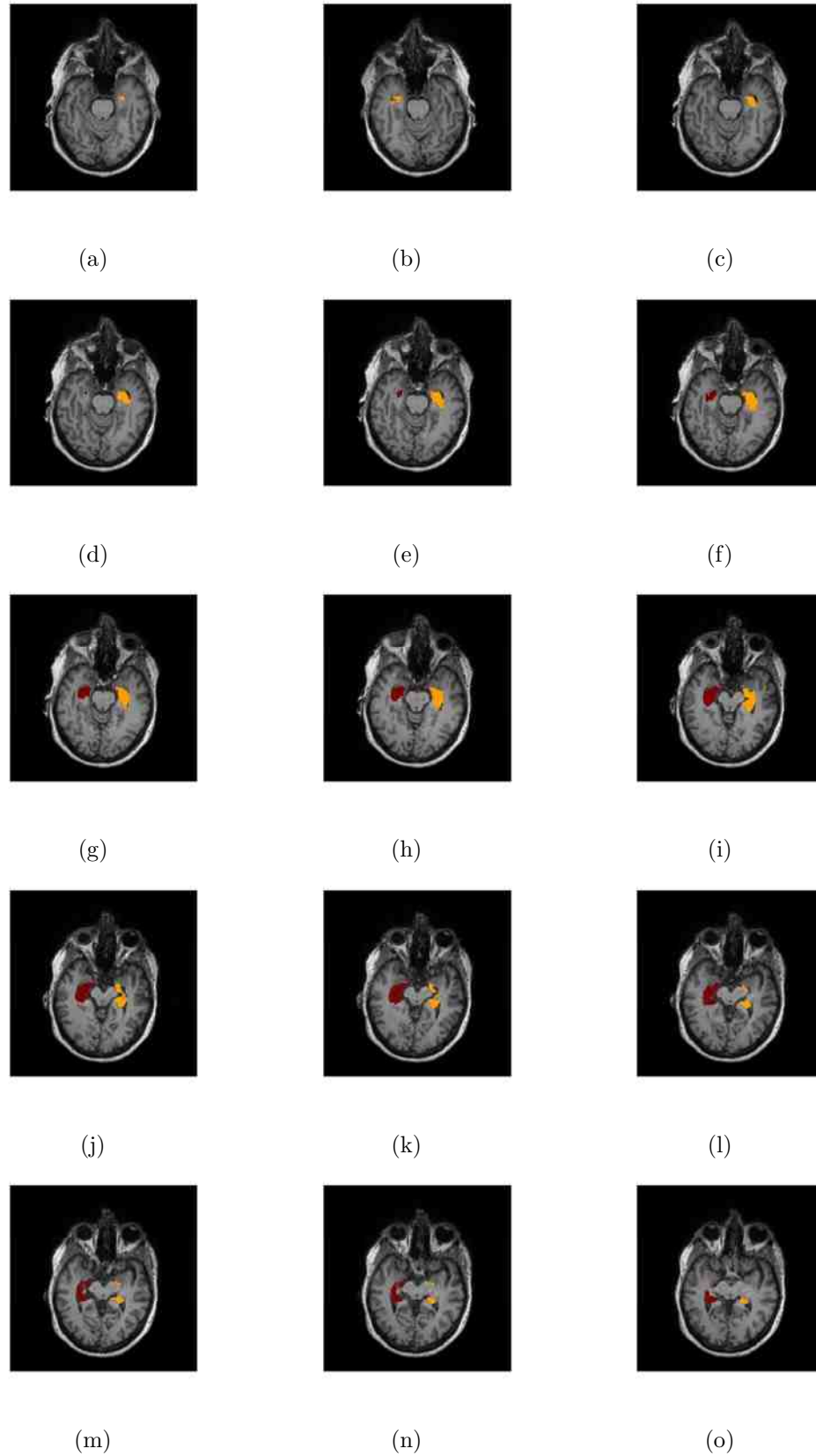


Fig. A.1.: Axial view of MRI scans with labeled left (red) and right (brown) hippocampi.

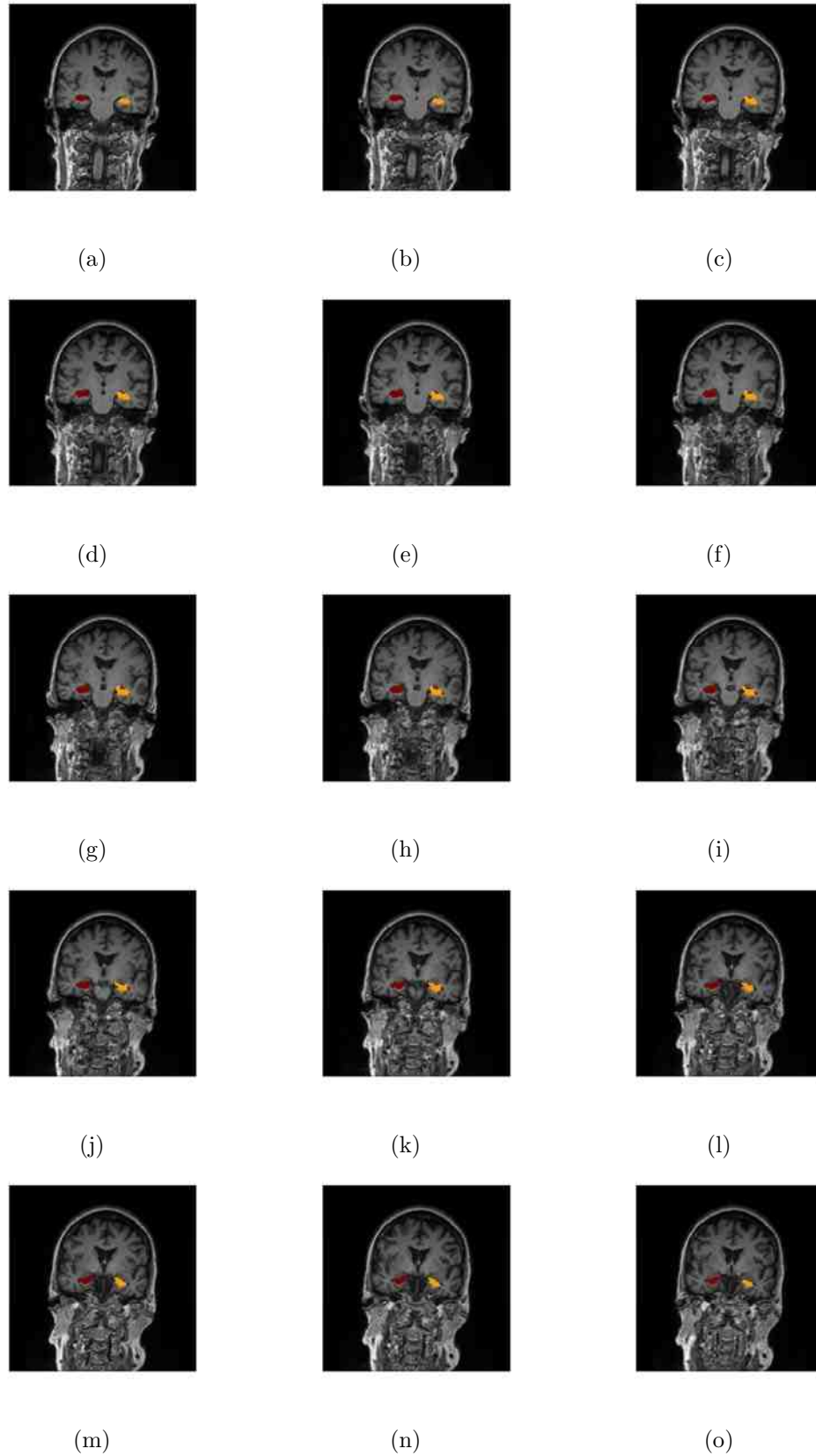


Fig. A.2.: Coronal view of MRI scans with labeled left (red) and right (brown) hippocampi.

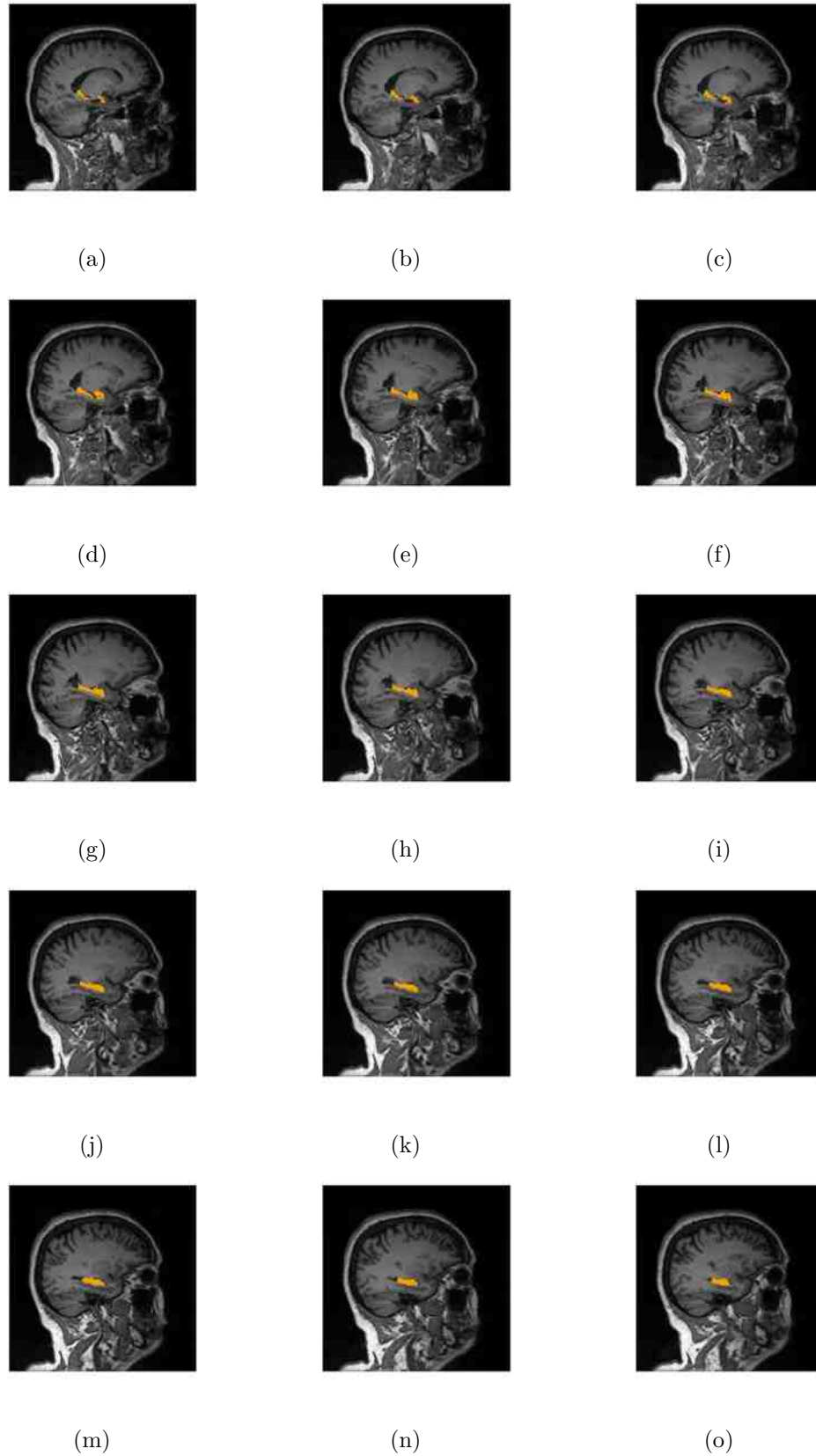


Fig. A.3.: Sagittal view of MRI scans with labeled right (brown) hippocampi.

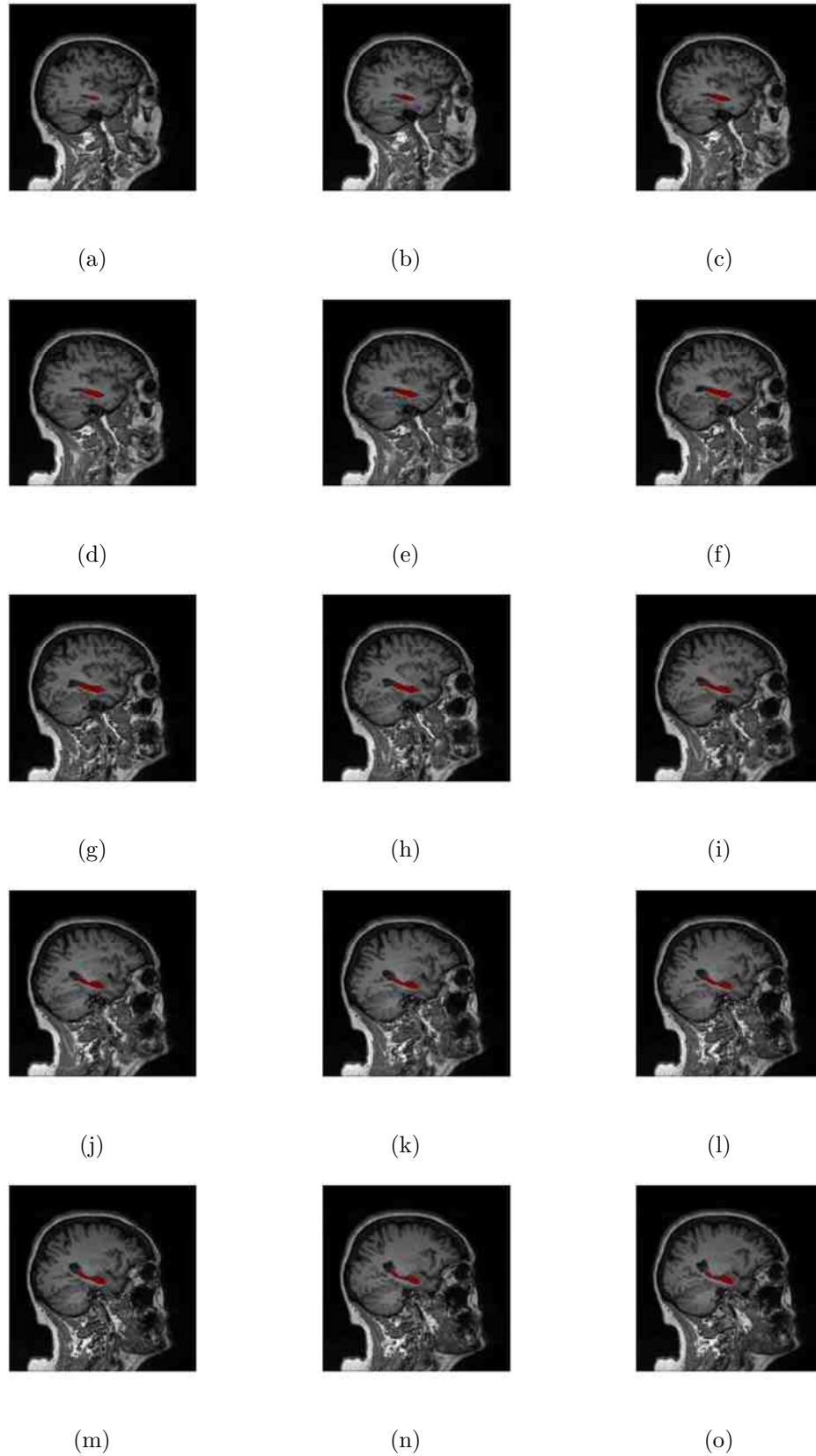
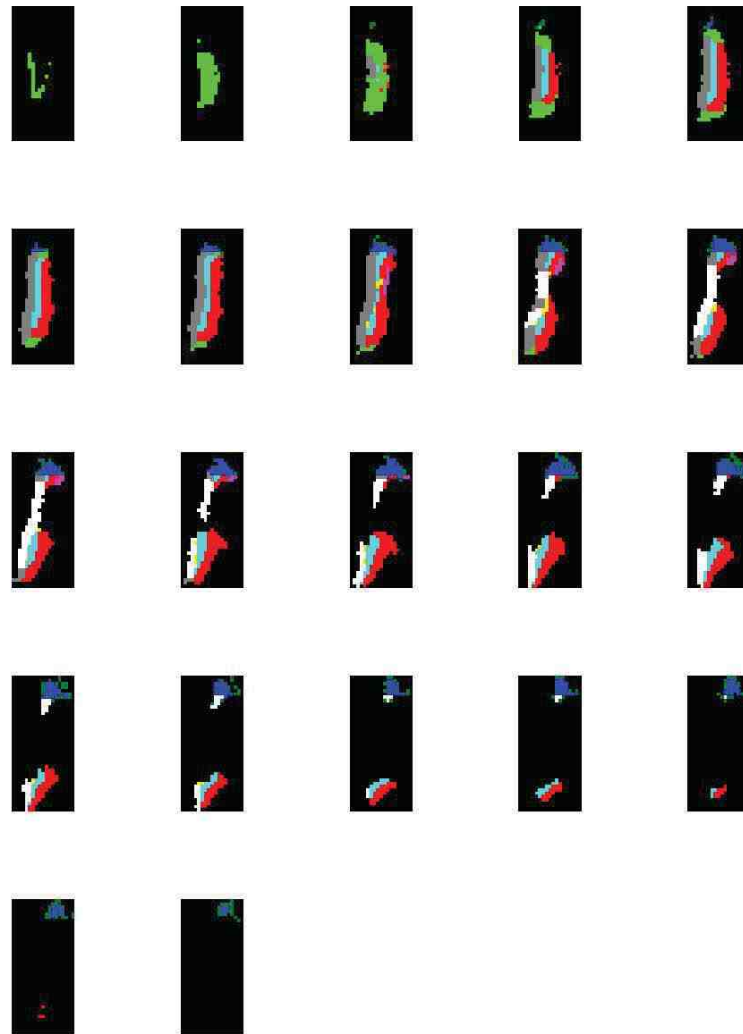


Fig. A.4.: Sagittal view of MRI scans with labeled left (red) hippocampi.



Subject: 00264262B-left-FS

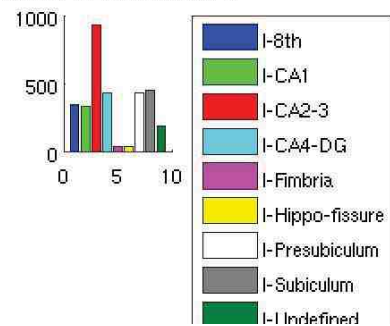


Fig. A.5.: Subfields masked by entire hippocampal segmentation result from FreeSurfer, noises can be viewed around the edges.

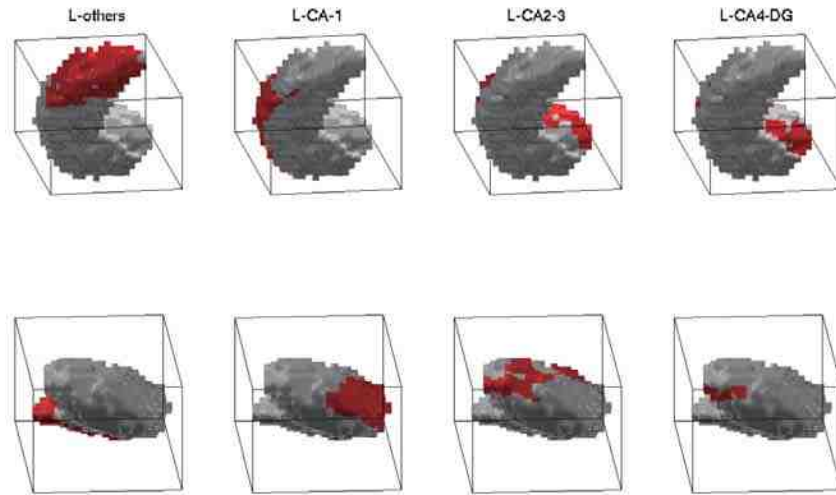


Fig. A.6.: Subfields masked by entire hippocampal segmentation result from FIRST, some unreasonable quantifications are made.

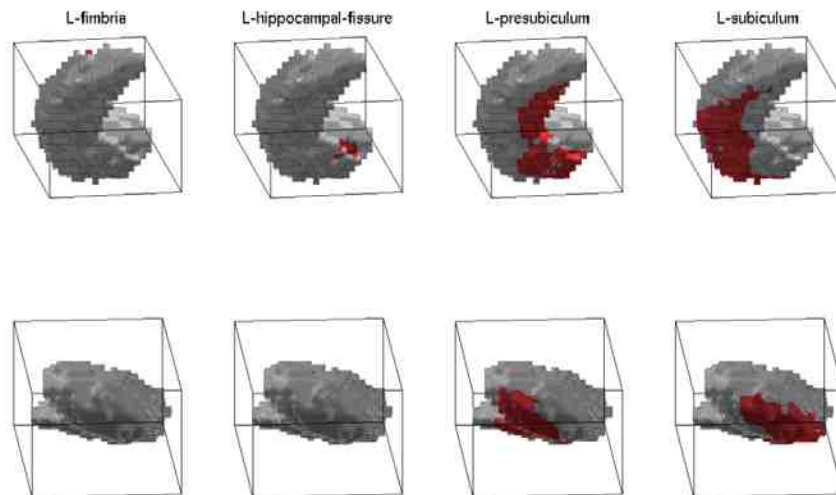


Fig. A.7.: Subfields masked by entire hippocampal segmentation result from FIRST, after Gaussin Kernel is applied.



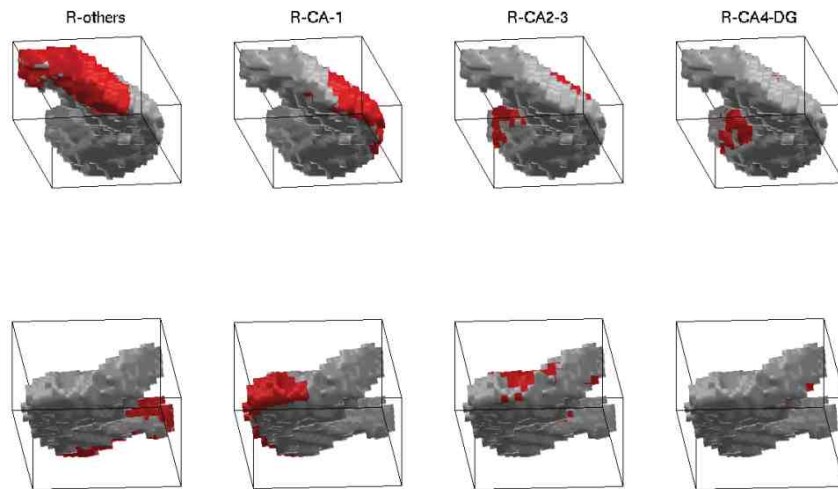


(a)

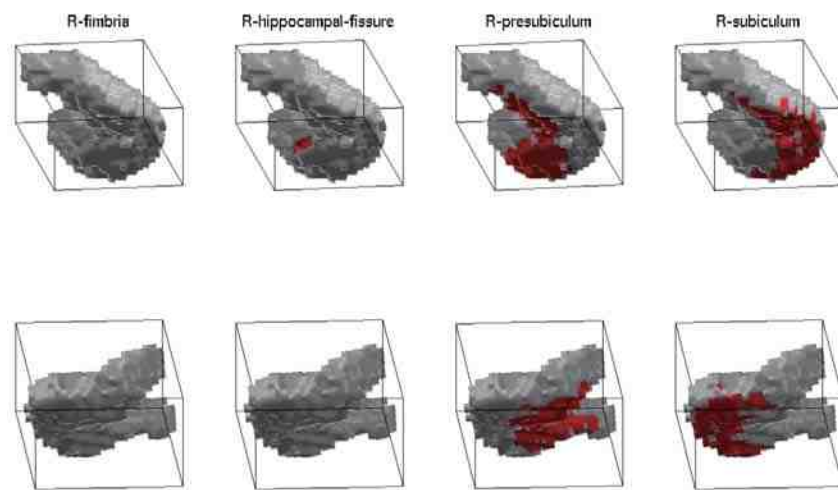


(b)

Fig. A.8.: The distributions of hippocampal subfields on the 3D surface (left hippocampi).

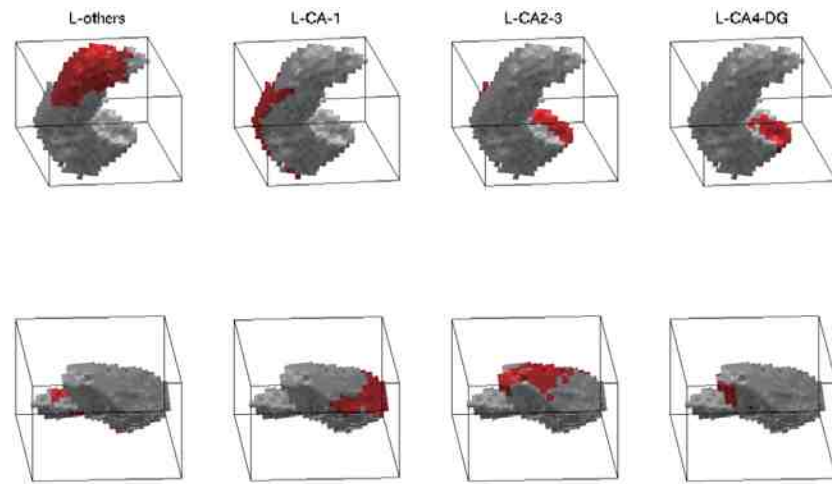


(a)

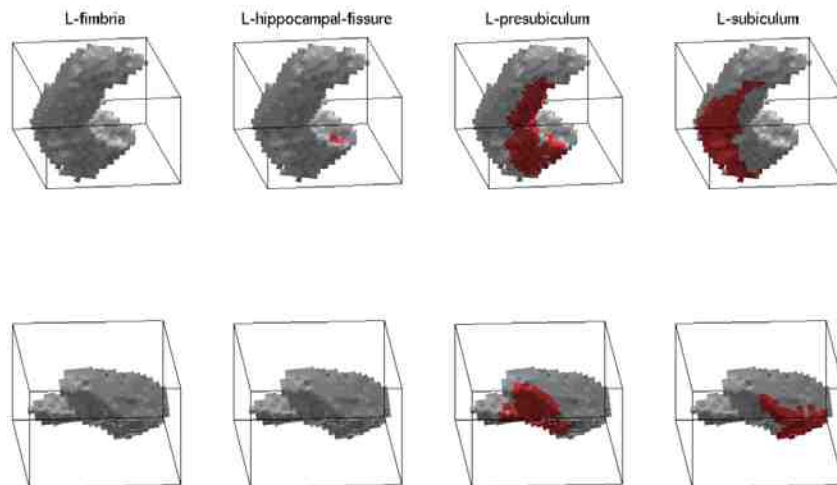


(b)

Fig. A.9.: The distributions of hippocampal subfields on the 3D surface (right hippocampi).

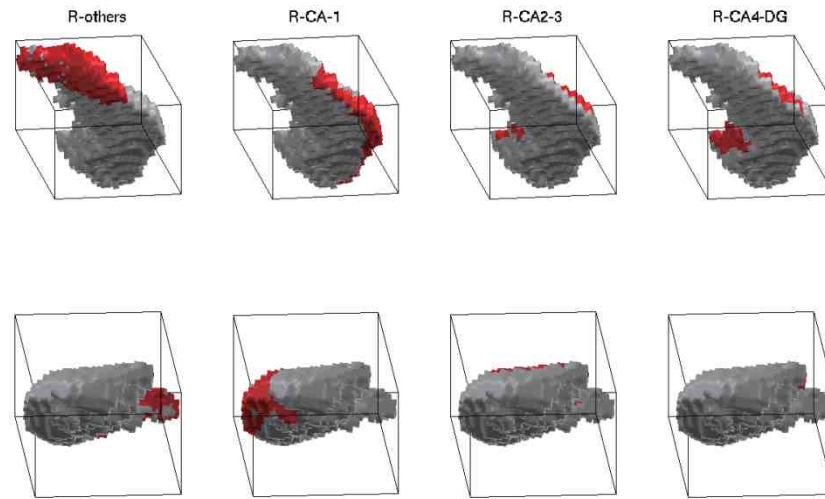


(a)

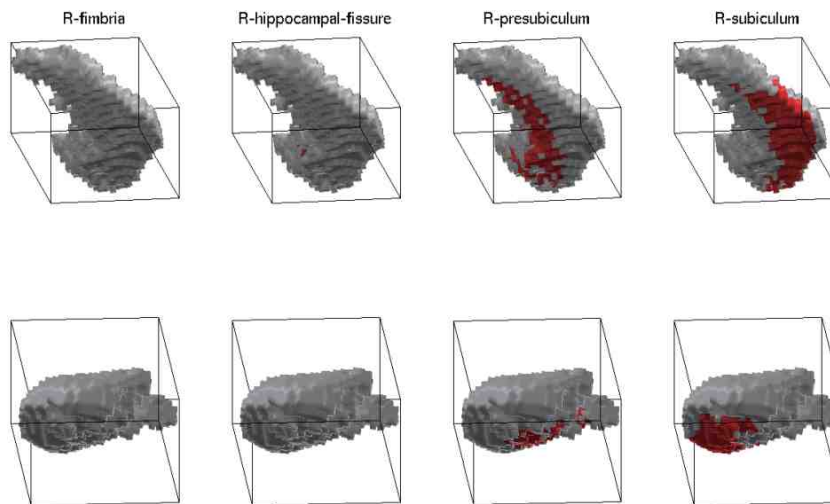


(b)

Fig. A.10.: The distributions of hippocampal subfields on the 3D surface (left hippocampi).

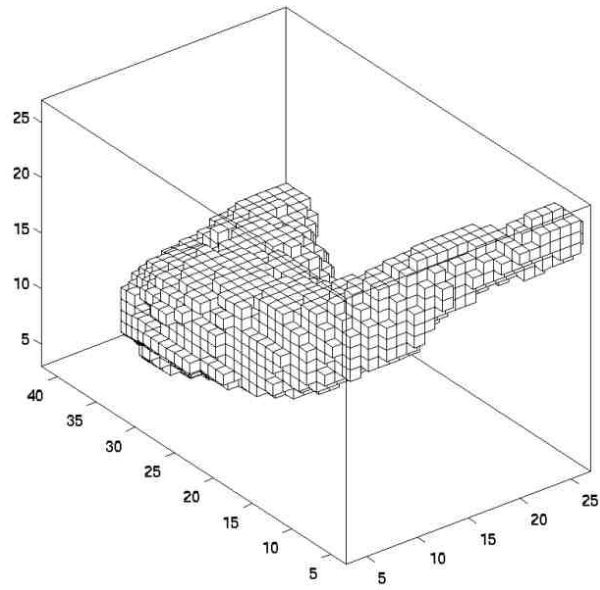


(a)

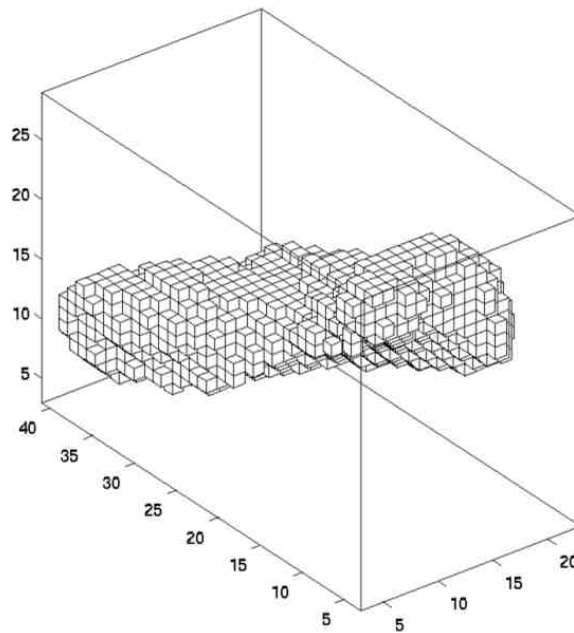


(b)

Fig. A.11.: The distributions of hippocampal subfields on the 3D surface (right hippocampi).

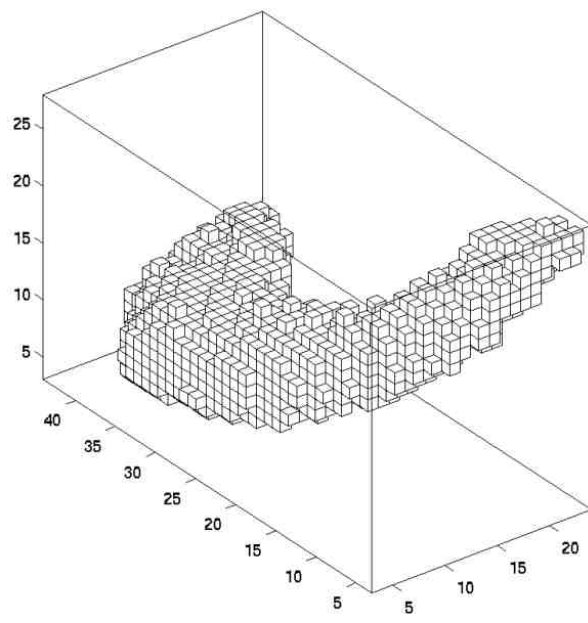


(a)

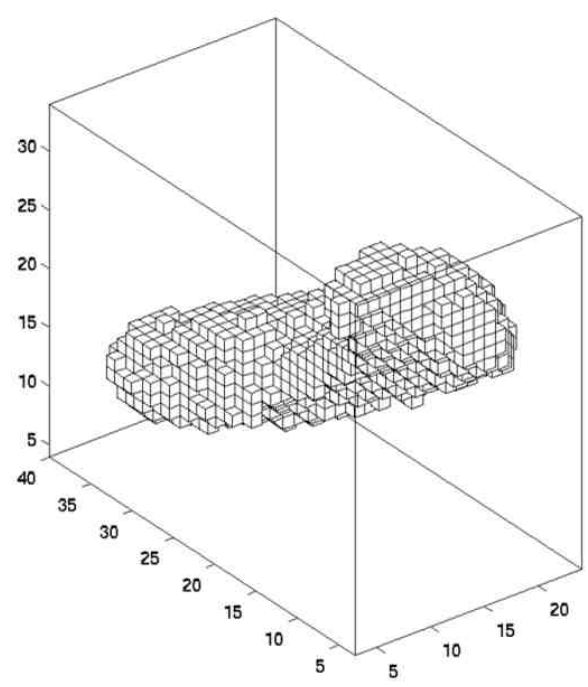


(b)

Fig. A.12.: The voxel-based structures after topology fix.

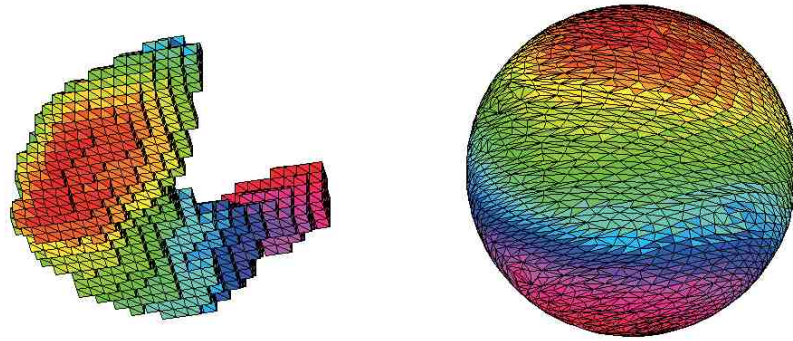


(a)



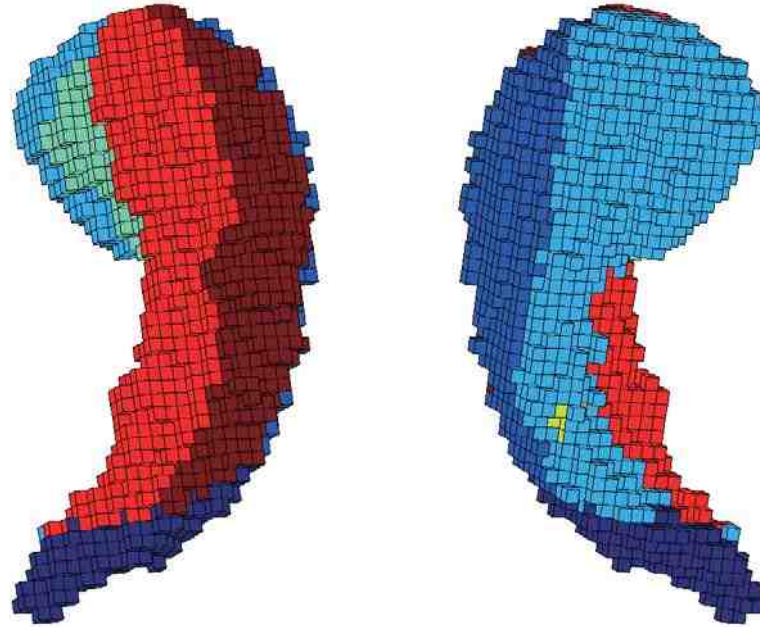
(b)

Fig. A.13.: The voxel-based structures after topology fix.

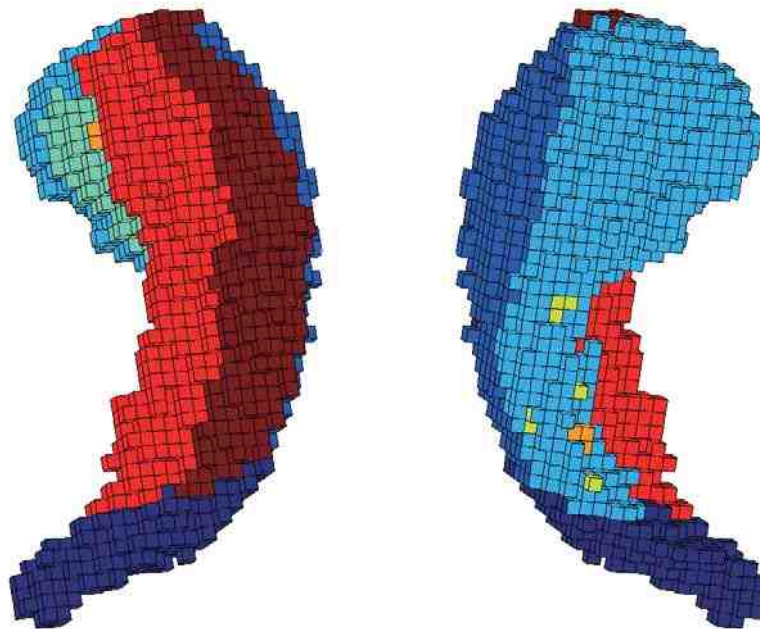


(a)

Fig. A.14.: SPHARM parameterization: bijective mapping from object surface to the surface of unit sphere.



(a)



(b)

Fig. A.15.: The hippocampal subfields distributions labeled on the surface, as each participant has two scans, (a) is obtained from group A and (b) is obtained from group B.



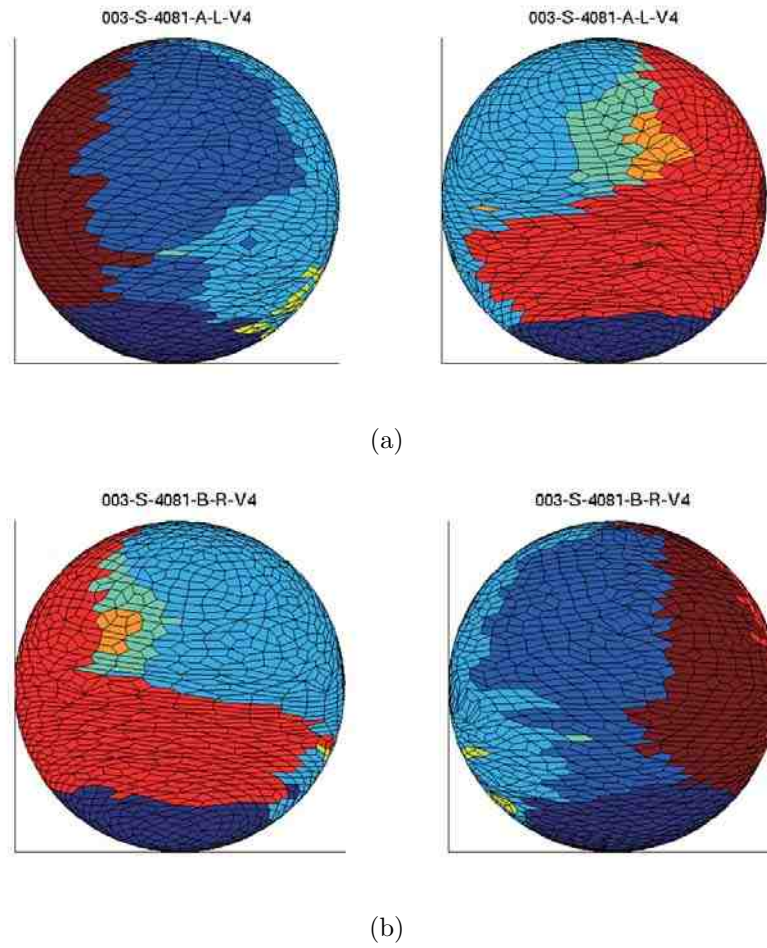
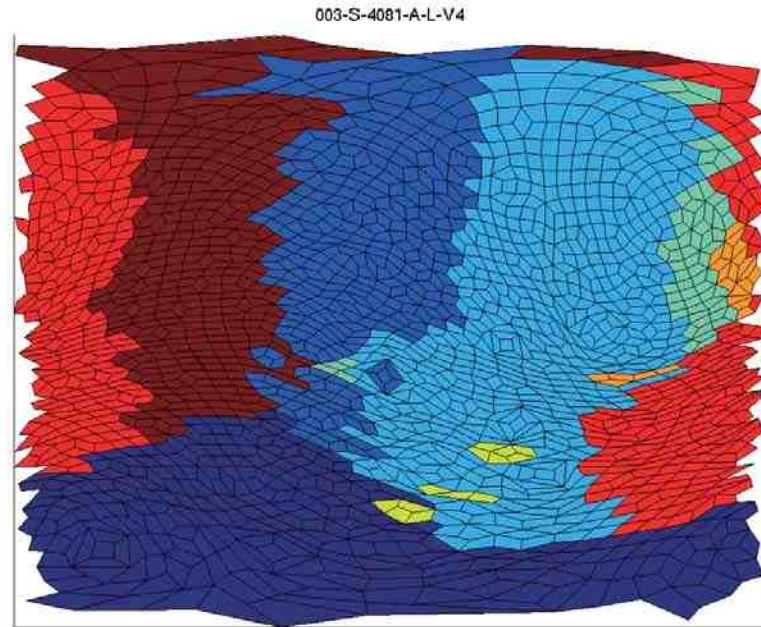
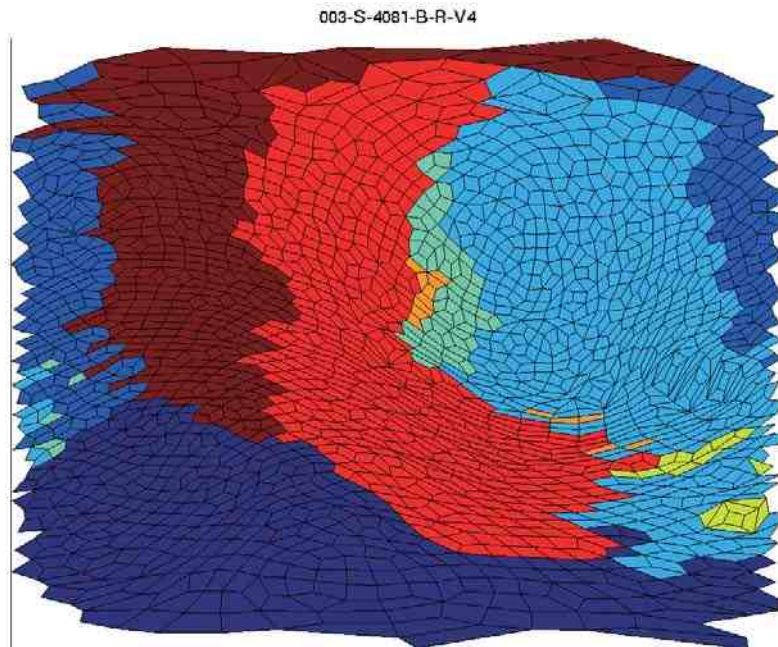


Fig. A.16.: Bijective mapping results from hippocampi surface to spherical surface: (a) is mapped from left hippocampi and (b) is mapped from right hippocampi.

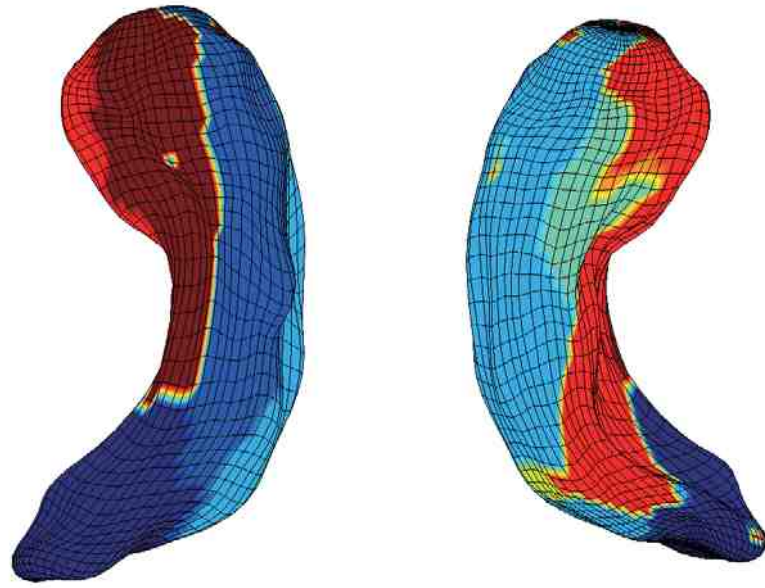


(a)

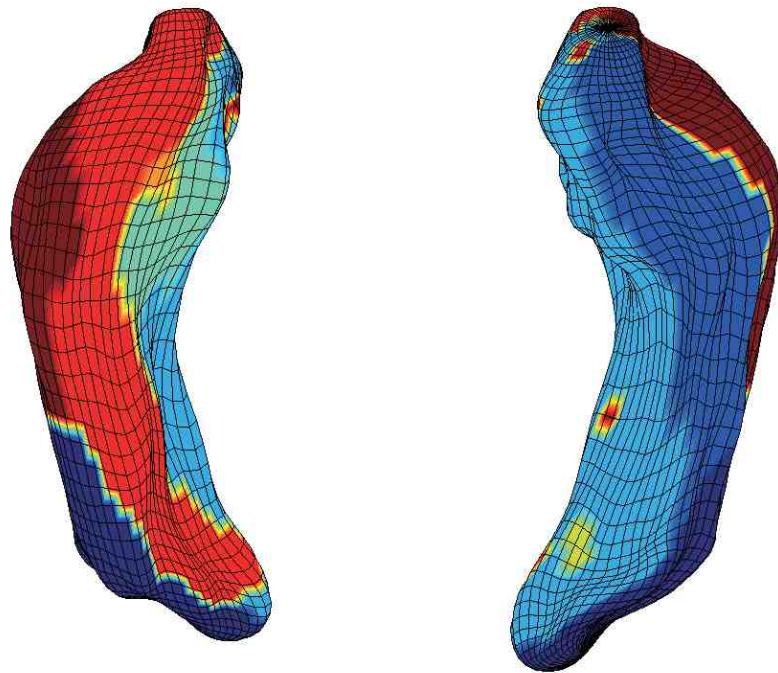


(b)

Fig. A.17.: The flat view of hippocampal subfields distributions labeled on the surface: (a) is obtained from left hippocampi and (b) is obtained from right hippocampi.



(a)



(b)

Fig. A.18.: The SPHARM expansion examples: (a) is obtained from left hippocampi and (b) is obtained from right hippocampi.

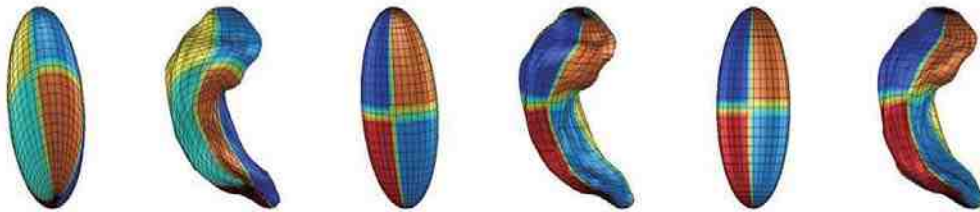


Fig. A.19.: SPHARM registration: fist group (first two images) is the original pose and parameterization, second group is aligned in parameter space, third group is aligned in object space.

## **B. DEMONSTRATE PROGRAMS**

## Subfield quantifications

```
clear all
close all
whole='/net/age3/ADNI_Hippo_FSL/FSL_seg_results/';
D0=dir(whole);
L0=length(D0);
hippo-fissure,left presubiculum,left subiculum\n');
for j=3:L0
parts=['/net/age3/ADNI_Hippo_FSL/freesurfersub/',D0(j).name, '/'];
D1=dir(parts);
L1=length(D1);
n=1;
m=1;
for i=3:L1
    t1=length(D1(i).name);
    t2=length(D0(j).name);
    if t1>11 && t2>11
        TF1=strcmp(D1(i).name(end-2:end),'nii');
        TF2=strcmp(D1(i).name(12),'l');
        TF22=strcmp(D1(i).name(12),'L');
        TF3=strcmp(D1(i).name(12),'r');
        TF33=strcmp(D1(i).name(12),'R');
        TF4=strcmp(D1(i).name(1),'r');
        TF5=strcmp(D1(i).name(end-4),'o');
        %%%%%%%%%%%%%%%%%%%%%%%%%%%%%%%%%%%%%%%%%%[[left part]]%%%%%%%%%%%%%%%%%%%%%%%%%%%%%%%%%%%%%%%%%
        if TF1==1 && TF4==1
            if (TF2 ==1 || TF22==1 ) && TF5==0
                if n==1
                    loadpath=[parts,D1(i).name];
```

```

        im1=load_nifti(loadpath);
        im11{1,n}=im1.vol/max(max(max(im1.vol)));
        im12=im1.vol/max(max(max(im1.vol)));
        max(max(max(im1.vol)));
        im11ref=im11{1,n};
        im12(im11ref~=0) = 1;
        n=n+1;
    else
        loadpath=[parts,D1(i).name];
        im1=load_nifti(loadpath);
        im11{1,n}=im1.vol/max(max(max(im1.vol)));
        max(max(max(im1.vol)));
        im12(im11{1,n}>im11ref) = n;
        im11ref(im11{1,n}>im11ref)=im11{1,n}(im11{1,n}>im11ref);
        n=n+1;
    end
end
end
%%%%%%%%%%%%%%%%%%%%%%%%%%%%%%%%%%%%%%%%%%%%%%%%%%%%%%%%%%%%%%%%%%%%%%%%[[left end]]%%%%%%%%%%%%%%%%%%%%%%%%%%%%%%%%%%%%%%%%%%%%%%%%%%%%%%%%%%%%%%%%%%%%%%%%
%%%%%%%%%%%%%%%%%%%%%%%%%%%%%%%%%%%%%%%%%%%%%%%%%%%%%%%%%%%%%%%%%%%%%%%%[[right part]]%%%%%%%%%%%%%%%%%%%%%%%%%%%%%%%%%%%%%%%%%%%%%%%%%%%%%%%%%%%%%%%%%%%%%%%%
if (TF3 ==1 || TF33==1) && TF5==0
    if m==1
        loadpath=[parts,D1(i).name];
        im2=load_nifti(loadpath);
        im21{1,m}=im2.vol/max(max(max(im2.vol)));
        im22=im2.vol/max(max(max(im2.vol)));
        max(max(max(im2.vol)));
        im21ref=im21{1,m};
        im22(im21ref~=0) = 1;
        m=m+1;
    else

```

```

        loadpath=[parts,D1(i).name];
        im2=load_nifti(loadpath);
        im21{1,m}=im2.vol/max(max(max(im2.vol)));
        max(max(max(im2.vol)));
        im22(im21{1,m}>im21ref) = m;
        im21ref(im21{1,m}>im21ref)=im21{1,m}(im21{1,m}>im21ref);
        m=m+1;
    end
end
end
end
end
end
%%%%%%%%%%%%%%%%%%%%%%%%%%%%%%%%%%%%%%%%%%%%%%%%%%%%%%%%%%%%%%%%%%%%%%%%%%[[right end]]%%%%%%%%%%%%%%%%%%%%%%%%%%%%%%%%%%%%%%%%%%%%%%%%%%%%%%%%%%%%%%%%%%%%%%%%%%
QL=[whole,D0(j).name, '/', D0(j).name, '-L_Hipp_corr_fix.mat'];
Whole_L=load(QL);
Whole_L11=Whole_L.bim;
Whole_L11(Whole_L11==1)=10;
QR=[whole,D0(j).name, '/', D0(j).name, '-R_Hipp_corr_fix.mat'];
Whole_R=load(QR);
Whole_R11=Whole_R.bim;
Whole_R11(Whole_R11==1)=10;
Lx_min=Whole_L.mins(1);
Ly_min=Whole_L.mins(2);
Lz_min=Whole_L.mins(3);
Lx_max=Whole_L.mins(1)+length(Whole_L.bim(:,1,1))-1;
Ly_max=Whole_L.mins(2)+length(Whole_L.bim(1,:,1))-1;
Lz_max=Whole_L.mins(3)+length(Whole_L.bim(1,1,:))-1;
Rx_min=Whole_R.mins(1);
Ry_min=Whole_R.mins(2);
Rz_min=Whole_R.mins(3);

```



```

Rx_max=Whole_R.mins(1)+length(Whole_R.bim(:,1,1))-1;
Ry_max=Whole_R.mins(2)+length(Whole_R.bim(1,:,1))-1;
Rz_max=Whole_R.mins(3)+length(Whole_R.bim(1,1,:))-1;
comb_L=im12(Lx_min:Lx_max,Ly_min:Ly_max,Lz_min:Lz_max)+Whole_L11;
comb_R=im22(Rx_min:Rx_max,Ry_min:Ry_max,Rz_min:Rz_max)+Whole_R11;
comb_L(comb_L<10 & comb_L>0) = 0;
comb_R(comb_R<10 & comb_R>0) = 0;          %% using FSL as mask
%%%%%%%%%%%%%%%%%%%%%%%%%%%%%%%%%%%%%%%%%%%%%%%%%%%%%%%%%%%%%%%%%%%%%%%%[[left part]]%%%%%%%%%%%%%%%%%%%%%%%%%%%%%%%%%%%%%%%%%%%%%%%%%%%%%%%%%%%%%%%%%%%%%%%%
WHL=comb_L;
[r1,c1,v1] = ind2sub(size(WHL),find(WHL >= 10));
[r11,c11,v11] = ind2sub(size(WHL),find(WHL == 10));
L1=length(r11);
L_tag=1;
R=1;
for i=3:L1
t11=length(D1(i).name);
t12=length(D0(j).name);
if t11>11 && t12>11
TF1=strcmp(D1(i).name(end-2:end),'nii');
TF2=strcmp(D1(i).name(12),'l');
TF22=strcmp(D1(i).name(12),'L');
TF3=strcmp(D1(i).name(12),'r');
TF33=strcmp(D1(i).name(12),'R');
TF4=strcmp(D1(i).name(1),'r');
TF5=strcmp(D1(i).name(end-4),'o');
if TF1==1 && TF4==1
if (TF2 ==1 || TF22==1 ) && TF5==0
loadpath=[parts,D1(i).name];
loadpath
im1=load_nifti(loadpath);

```



```

TF3=strncmp(D1(i).name(12),'r');
TF33=strncmp(D1(i).name(12),'R');
TF4=strncmp(D1(i).name(1),'r');
TF5=strncmp(D1(i).name(end-4),'o');
if TF1==1 && TF4==1
    if (TF3 ==1 || TF33==1) && TF5==0
        loadpath=[parts,D1(i).name];
        im1=load_nifti(loadpath);
        New_map=smooth_3(WHR,im1.vol(Rx_min:Rx_max,Ry_min:Ry_max,Rz_min:Rz_max));
        all_value{j-2,R}=New_map;
        R=R+1
    end
end
end
end
end
for i=1:Lr
    [value,label]=max([all_value{j-2,1}(rr1(i),cr1(i),vr1(i)),all_value{j-2,2}(rr1(i),...
    cr1(i),vr1(i)),all_value{j-2,3}(rr1(i),cr1(i),vr1(i)),all_value{j-2,4}(rr1(i),cr1(i),vr1(i)),...
    all_value{j-2,5}(rr1(i),cr1(i),vr1(i)),all_value{j-2,6}(rr1(i),cr1(i),vr1(i)),...
    all_value{j-2,7}(rr1(i),cr1(i),vr1(i)),all_value{j-2,8}(rr1(i),cr1(i),vr1(i))]);
    comb_R(rr1(i),cr1(i),vr1(i))=label+10;
end
end
%%%%%%%%%%%%%%%%%%%%%%%%%%%%%%%%%%%%%%%%%%%%%%%%%%%%%%%%%%%%%%%%%%%%%%%%%%[[right end]]%%%%%%%%%%%%%%%%%%%%%%%%%%%%%%%%%%%%%%%%%%%%%%%%%%%%%%%%%%%%%%%%%%%%%%%%%%

```

### Fixing holes with Gaussian Kernel

```
function W=smooth_3(mask,map)
```

```

L=1;
map=map./max(max(max(map)));

```

```

h = fspecial3('gaussian',9);
W = imfilter(map,h,'replicate');
while L>0
    K = imfilter(W,h,'replicate');
    test=W+mask;
    [r,c,v] = ind2sub(size(test),find(test == 10));
    L=length(r);
    W = K;
end
W(test < 10)=0;

```

Generating voxel-based structures and calculating vertex values

```

function [vertices, faces, mins, verind_table,num,name,mask_length] = gensfdata
mask_path='/net/age3/ADNI_Hippo_FSL/FSL_seg_results/copy_fix/fix';
mask_files = dir(sprintf('%s/*_fix.mat',mask_path));
mask_length=length(mask_files);
check_alignL=1;
check_alignR=1;
for m=1:mask_length
    loadpath=[mask_path,'/',mask_files(m).name];
    load(loadpath);
    bim(bim>0)=1;
    sub_path=['/net/age3/ADNI_Hippo_FSL/freesurfersub/',mask_files(m).name(1:end-13),'/Label'];
    sub_files = dir(sprintf('%s/*_V3.nii',sub_path));
    ifL=strncmp(mask_files(m).name(14),'L');
    ifR=strncmp(mask_files(m).name(14),'R');
    vertices=[];
    if ifL==1
        loadpath=[sub_path,'/',sub_files(1).name];
        im1=load_nifti(loadpath);

```

```

im1=im1.vol;
Lx_min=mins(1);
Ly_min=mins(2);
Lz_min=mins(3);
Lx_max=mins(1)+length(bim(:,1,1))-1;
Ly_max=mins(2)+length(bim(1,:,1))-1;
Lz_max=mins(3)+length(bim(1,1,:))-1;
im1=im1(Lx_min:Lx_max,Ly_min:Ly_max,Lz_min:Lz_max);
check=im1./9+bim;
im1(check<1)=0;
[rl1,cl1,vl1] = ind2sub(size(im1),find(check == 1));
L_holes=length(rl1);
if L_holes>0
fix_path=['/net/age3/ADNI_Hippo_FSL/freesurfersub/',...
mask_files(m).name(1:end-13),'/', 'New_map/'];
path1=[fix_path,'rposterior_lefthippo_r.nii'];
    if exist(path1)
        ob1=[fix_path,'rposterior_left_1hippo_r.nii'];
        cmd=['mv ', path1, ' ', ob1];
        system(cmd);
        pause(10);
    end
fix_holes = dir(sprintf('%s/rposterior_left*.nii',fix_path));
fix_length=length(fix_holes);
for m_1=1:fix_length
    loadme=[fix_path,fix_holes(m_1).name];
    tempk=load_nifti(loadme);
    all_value{m,m_1}=tempk.vol(Lx_min:Lx_max,Ly_min:Ly_max,Lz_min:Lz_max);
end
for i=1:L_holes

```

```

[value,label]=max([all_value{m,1}(r11(i),c11(i),v11(i)),...
all_value{m,2}(r11(i),c11(i),v11(i)),all_value{m,3}(r11(i),...
c11(i),v11(i)),all_value{m,4}(r11(i),c11(i),v11(i)),...
all_value{m,5}(r11(i),c11(i),v11(i)),all_value{m,6}(r11(i),...
c11(i),v11(i)),all_value{m,7}(r11(i),c11(i),v11(i)),...
all_value{m,8}(r11(i),c11(i),v11(i))]);
im1(r11(i),c11(i),v11(i))=label;
end
end
roi=im1;
DIM=size(roi);
roi = reshape(roi,DIM);
% make a work area so that all border voxels belong to the background
d = DIM+2; w = zeros(d);
w(2:d(1)-1,2:d(2)-1,2:d(3)-1) = roi;
temp_w=w;
temp_w(w~=0)=1;
% identifiy significant vertices (each vertice connects 8 adjacent voxels)
[xs, ys, zs] = meshgrid(1:d(1)-1,1:d(2)-1,1:d(3)-1);
len = prod(size(xs));
xs = reshape(xs,len,1);
ys = reshape(ys,len,1);
zs = reshape(zs,len,1);
nbsum = zeros(d);
inds = get_1d_ind(xs,ys,zs,d);
nbsum(inds) = sum([temp_w(inds),...
temp_w(get_1d_ind(xs+1,ys, zs, d)),...
temp_w(get_1d_ind(xs, ys+1,zs, d)),...
temp_w(get_1d_ind(xs+1,ys+1,zs, d)),...
temp_w(get_1d_ind(xs, ys, zs+1,d)),...

```

```

        temp_w(get_1d_ind(xs+1,ys,  zs+1,d)),...
        temp_w(get_1d_ind(xs,  ys+1,zs+1,d)),...
        temp_w(get_1d_ind(xs+1,ys+1,zs+1,d)),...
    ]');
vertinds = find(nbsum~=0 & nbsum~=8);
[xs1,ys1,zs1] = get_3d_ind(vertinds,d); % significant ones
vnum = length(vertinds);
if check_alignL==1
vertices = [xs1,ys1,zs1]; % remove the margin of the work area
vertices0 = vertices;
check_alignL=check_alignL+1;
else
    vertices = [xs1,ys1,zs1];
    [P,M] = align_icp(vertices,vertices0);
    vertices=P;
end
% identify square faces on the surface
vertinds = get_1d_ind(xs1,ys1,zs1,d); % values of x, y, z could be 0
verts(1:prod(DIM+1)) = NaN;
verts(vertinds) = 1:vnum;
tempind1 = find(temp_w(inds)==1 & temp_w(get_1d_ind(xs+1,ys,zs,d))==0);
faceind{1} = inds(tempind1);
tempind2 = find(temp_w(inds)==1 & temp_w(get_1d_ind(xs,ys+1,zs,d))==0);
faceind{2} = inds(tempind2);
tempind3 = find(temp_w(inds)==1 & temp_w(get_1d_ind(xs,ys,zs+1,d))==0);
faceind{3} = inds(tempind3);
tempind4 = find(temp_w(inds)==0 & temp_w(get_1d_ind(xs+1,ys,zs,d))==1);
faceind{4} = inds(tempind4);
tempind5 = find(temp_w(inds)==0 & temp_w(get_1d_ind(xs,ys+1,zs,d))==1);
faceind{5} = inds(tempind5);

```

```

tempind6 = find(temp_w(inds)==0 & temp_w(get_1d_ind(xs,ys,zs+1,d))==1);
faceind{6} = inds(tempind6);
faces = [];
for i = 1:6
    [x,y,z] = get_3d_ind(faceind{i},d);
    v1s = verts(get_1d_ind(x,y,z,d));
    switch i
    case 1
        v2s = verts(get_1d_ind(x,y-1,z,d));
        v3s = verts(get_1d_ind(x,y-1,z-1,d));
        v5s = verts(get_1d_ind(x,y,z-1,d));
        templabel=[x,y,z];
    case 2
        v2s = verts(get_1d_ind(x,y,z-1,d));
        v3s = verts(get_1d_ind(x-1,y,z-1,d));
        v5s = verts(get_1d_ind(x-1,y,z,d));
        templabel=[templabel; [x,y,z]];
    case 3
        v2s = verts(get_1d_ind(x-1,y,z,d));
        v3s = verts(get_1d_ind(x-1,y-1,z,d));
        v5s = verts(get_1d_ind(x,y-1,z,d));
        templabel=[templabel; [x,y,z]];
    case 4
        v2s = verts(get_1d_ind(x,y,z-1,d));
        v3s = verts(get_1d_ind(x,y-1,z-1,d));
        v5s = verts(get_1d_ind(x,y-1,z,d));
        inds2=get_1d_ind(xs+1,ys,zs,d);
        idx2=inds2(tempind4);
        x1=0;y1=0;z1=0;
        [x1,y1,z1]=ind2sub(d,idx2);
    end
end

```



```

        templabel=[templabel;[x1,y1,z1]];
    case 5
        v2s = verts(get_1d_ind(x-1,y,z,d));
        v3s = verts(get_1d_ind(x-1,y,z-1,d));
        V5s = verts(get_1d_ind(x,y,z-1,d));
        inds2=get_1d_ind(xs,ys+1,zs,d);
        idx3=inds2(tempind5);
        x1=0;y1=0;z1=0;
        [x1,y1,z1]=ind2sub(d,idx3);
        templabel=[templabel;[x1,y1,z1]];
    case 6
        v2s = verts(get_1d_ind(x,y-1,z,d));
        v3s = verts(get_1d_ind(x-1,y-1,z,d));
        V5s = verts(get_1d_ind(x-1,y,z,d));
        inds2=get_1d_ind(xs,ys,zs+1,d);
        idx4=inds2(tempind6);
        x1=0;y1=0;z1=0;
        [x1,y1,z1]=ind2sub(d,idx4);
        templabel=[templabel;[x1,y1,z1]];
    end
    faces(end+1:end+length(x),:) = [v1s; v2s; v3s; V5s]';
end
lx=templabel(:,1);
ly=templabel(:,2);
lz=templabel(:,3);
tempim=zeros(length(w(:,1,1)),length(w(1,:,1)),length(w(1,1,:)));
tempim(2:d(1)-1,2:d(2)-1,2:d(3)-1)=im1;
lx1=length(lx);
L_label=[];
for g=1:lx1

```

```

L_label(g)=tempim(lx(g),ly(g),lz(g));
end
temp_faces=[faces(:,1);faces(:,2);faces(:,3);faces(:,4)];
[count, bin] = histc(temp_faces, unique(temp_faces));
lc=length(count);
tempim=[];
verind_table=[];
% arrange files to be easily read
parts=['/net/age3/ADNI_Hippo_FSL/freesurfersub/',...
mask_files(m).name(1:end-13),'/'];
sw1=[parts,'rposterior_Left-Hippocampus.nii'];
sw2=[parts,'rposterior_Right-Hippocampus.nii'];
sw3=[parts,'rposterior_lefthippo_r.nii'];
if exist(sw1)
ob1=[parts,'rposterior_left_1hippo_r.nii'];
cmd=['mv ', sw1, ' ', ob1];
system(cmd);
pause(10);
end
if exist(sw2)
ob2=[parts,'rposterior_right_1hippo_r.nii'];
cmd=['mv ', sw2, ' ', ob2];
system(cmd);
pause(10);
end
if exist(sw3)
ob1=[parts,'rposterior_left_1hippo_r.nii'];
cmd=['mv ', sw3, ' ', ob1];
system(cmd);
pause(10);

```

```

end
% apply mask on subfields
tempim0=zeros(length(bim(:,1,1)),length(bim(1,:,1)),length(bim(1,1,:)));
for m_1=1:fix_length
    [m_1name,m_1add]=strtok(fix_holes(m_1).name,'.');
    loadme=[parts,m_1name, '.nii'];
    tempk=load_nifti(loadme);
    tt=tempk.vol(Lx_min:Lx_max,Ly_min:Ly_max,Lz_min:Lz_max);
    tempim0=tt./max(max(max(tt)))+tempim0;
end
tempim0=tempim0./(max(max(max(tempim0)))+1);
tt1=tempim0+bim;
[r11,c11,v11] = ind2sub(size(tt1),find(tt1 < 1)); %% tt1<1 delete
[r12,c12,v12] = ind2sub(size(tt1),find(tt1 == 1)); %% tt1==1 holes
L_hole=length(r12);
L_clean=length(r11);
for m_1=1:fix_length
    [m_1name,m_1add]=strtok(fix_holes(m_1).name, '.');
    loadme=[parts,m_1name, '.nii'];
    tempk=load_nifti(loadme);
    tm1=tempk.vol(Lx_min:Lx_max,Ly_min:Ly_max,Lz_min:Lz_max);
    loadme2=[fix_path,fix_holes(m_1).name];
    tempk2=load_nifti(loadme2);
    tm2=tempk2.vol(Lx_min:Lx_max,Ly_min:Ly_max,Lz_min:Lz_max);
    for g=1:L_clean
        tm1(r11(g),c11(g),v11(g))=0;
    end
    for g=1:L_hole
        tm1(r12(g),c12(g),v12(g))=tm2(r12(g),c12(g),v12(g));
    end
end

```

```

% finish fixing
% give probability to vertices
tempim{m_1}=zeros(length(w(:,1,1)),length(w(1,:,1)),length(w(1,1,:)));
tempim{m_1}(2:d(1)-1,2:d(2)-1,2:d(3)-1)=tm1;
tempim{m_1}=tempim{m_1}./max(max(max(tempim{m_1})));
for g=1:lx1
L_label1{m_1}(g)=tempim{m_1}(lx(g),ly(g),lz(g));
end
% assign values to verteces based on face values
verind_table{m_1}=zeros(lc,1);
verind_table_C{m_1}=zeros(lc,1);
for g=1:lx1
    verind_table{m_1}(faces(g,:),1)=verind_table{m_1}(faces(g,:),1)+L_label1{m_1}(g);
    verind_table_C{m_1}(faces(g,:),1)=verind_table_C{m_1}(faces(g,:),1)+1;
end
verind_table{m_1}=verind_table{m_1}./verind_table_C{m_1};
end
% compare vertices and give new label
for g=1:lc
    [value,label(g)]=max([verind_table{1}(g),verind_table{2}(g),...
    verind_table{3}(g),verind_table{4}(g),verind_table{5}(g),...
    verind_table{6}(g),verind_table{7}(g),verind_table{8}(g)]);
end
promap=verind_table;
verind_table=label';
saveto1=['/net/age3/ADNI_Hippo_FSL/submat/',mask_files(m).name(1:end-11),'_V5_fix.mat'];
bim=temp_w;
mins=mins-1;
face_table=L_label';
save(saveto1,'bim','mins','verind_table','face_table','vertices','faces','promap');

```

```

end
if ifR==1
    loadpath=[sub_path, '/', sub_files(2).name];
    im1=load_nifti(loadpath);
    im1=im1.vol;
    Lx_min=mins(1);
    Ly_min=mins(2);
    Lz_min=mins(3);
    Lx_max=mins(1)+length(bim(:,1,1))-1;
    Ly_max=mins(2)+length(bim(1,:,1))-1;
    Lz_max=mins(3)+length(bim(1,1,:))-1;
    im1=im1(Lx_min:Lx_max,Ly_min:Ly_max,Lz_min:Lz_max);
    check=im1./9+bim;
    im1(check<1)=0;
    [r11,c11,v11] = ind2sub(size(im1),find(check == 1));
    L_holes=length(r11);
    if L_holes>0
        fix_path=['/net/age3/ADNI_Hippo_FSL/freesurfersub/',...
            mask_files(m).name(1:end-13), '/', 'New_map/'];
        path1=[fix_path, 'rposterior_rightippo_r.nii'];
        if exist(path1)
            ob1=[fix_path, 'rposterior_right_1hippo_r.nii'];
            cmd=['mv ', path1, ' ', ob1];
            system(cmd);
            pause(10);
        end
        fix_holes = dir(sprintf('%s/rposterior_right*.nii',fix_path));
        fix_length=length(fix_holes);
        for m_1=1:fix_length
            loadme=[fix_path,fix_holes(m_1).name];

```

```

tempk=load_nifti(loadme);
all_value{m,m_1}=tempk.vol(Lx_min:Lx_max,Ly_min:Ly_max,Lz_min:Lz_max);
end
for i=1:L_holes
    [value,label]=max([all_value{m,1}(r11(i),c11(i),v11(i)),...
    all_value{m,2}(r11(i),c11(i),v11(i)),all_value{m,3}(r11(i),...
    c11(i),v11(i)),all_value{m,4}(r11(i),c11(i),v11(i)),...
    all_value{m,5}(r11(i),c11(i),v11(i)),...
    all_value{m,6}(r11(i),c11(i),v11(i)),...
    all_value{m,7}(r11(i),c11(i),v11(i)),...
    all_value{m,8}(r11(i),c11(i),v11(i))]);
    im1(r11(i),c11(i),v11(i))=label;
end
end
roi=im1;
DIM=size(roi);
roi = reshape(roi,DIM);
    % make a work area so that all border voxels belong to the background
    d = DIM+2; w = zeros(d);
    w(2:d(1)-1,2:d(2)-1,2:d(3)-1) = roi;
    temp_w=w;
    temp_w(w~=0)=1;
    % identifiy significant vertices (each vertice connects 8 adjacent voxels)
    [xs, ys, zs] = meshgrid(1:d(1)-1,1:d(2)-1,1:d(3)-1);
    len = prod(size(xs));
    xs = reshape(xs,len,1);
    ys = reshape(ys,len,1);
    zs = reshape(zs,len,1);
    nbsum = zeros(d);
    inds = get_1d_ind(xs,ys,zs,d);

```

```

nbsum(inds) = sum([temp_w(inds),...
                  temp_w(get_1d_ind(xs+1,ys,  zs,  d)),...
                  temp_w(get_1d_ind(xs,  ys+1,zs,  d)),...
                  temp_w(get_1d_ind(xs+1,ys+1,zs,  d)),...
                  temp_w(get_1d_ind(xs,  ys,  zs+1,d)),...
                  temp_w(get_1d_ind(xs+1,ys,  zs+1,d)),...
                  temp_w(get_1d_ind(xs,  ys+1,zs+1,d)),...
                  temp_w(get_1d_ind(xs+1,ys+1,zs+1,d)),...
                  ]');
vertinds = find(nbsum~=0 & nbsum~=8);
[xs1,ys1,zs1] = get_3d_ind(vertinds,d); % significant ones
vnum = length(vertinds);
if check_alignR==1
vertices = [xs1,ys1,zs1]; % remove the margin of the work area
vertices1 = vertices;
check_alignR=check_alignR+1;
else
    vertices = [xs1,ys1,zs1];
    [P,M] = align_icp(vertices,vertices1);
    vertices=P;
end
% identify square faces on the surface
vertinds = get_1d_ind(xs1,ys1,zs1,d); % values of x, y, z could be 0
verts(1:prod(DIM+1)) = NaN;
verts(vertinds) = 1:vnum;
tempind1 = find(temp_w(inds)==1 & temp_w(get_1d_ind(xs+1,ys,zs,d))==0);
faceind{1} = inds(tempind1);
tempind2 = find(temp_w(inds)==1 & temp_w(get_1d_ind(xs,ys+1,zs,d))==0);
faceind{2} = inds(tempind2);
tempind3 = find(temp_w(inds)==1 & temp_w(get_1d_ind(xs,ys,zs+1,d))==0);

```

```

faceind{3} = inds(tempind3);
tempind4 = find(temp_w(inds)==0 & temp_w(get_1d_ind(xs+1,ys,zs,d))==1);
faceind{4} = inds(tempind4);
tempind5 = find(temp_w(inds)==0 & temp_w(get_1d_ind(xs,ys+1,zs,d))==1);
faceind{5} = inds(tempind5);
tempind6 = find(temp_w(inds)==0 & temp_w(get_1d_ind(xs,ys,zs+1,d))==1);
faceind{6} = inds(tempind6);
faces = [];
for i = 1:6
    [x,y,z] = get_3d_ind(faceind{i},d);
    v1s = verts(get_1d_ind(x,y,z,d));
    switch i
    case 1
        v2s = verts(get_1d_ind(x,y-1,z,d));
        v3s = verts(get_1d_ind(x,y-1,z-1,d));
        v5s = verts(get_1d_ind(x,y,z-1,d));
        templabel=[x,y,z];
    case 2
        v2s = verts(get_1d_ind(x,y,z-1,d));
        v3s = verts(get_1d_ind(x-1,y,z-1,d));
        v5s = verts(get_1d_ind(x-1,y,z,d));
        templabel=[templabel; [x,y,z]];
    case 3
        v2s = verts(get_1d_ind(x-1,y,z,d));
        v3s = verts(get_1d_ind(x-1,y-1,z,d));
        v5s = verts(get_1d_ind(x,y-1,z,d));
        templabel=[templabel; [x,y,z]];
    case 4
        v2s = verts(get_1d_ind(x,y,z-1,d));
        v3s = verts(get_1d_ind(x,y-1,z-1,d));

```



```

        V5s = verts(get_1d_ind(x,y-1,z,d));
        inds2=get_1d_ind(xs+1,ys,zs,d);
        idx2=inds2(tempind4);
        x1=0;y1=0;z1=0;
        [x1,y1,z1]=ind2sub(d,idx2);
        templabel=[templabel;[x1,y1,z1]];
    case 5
        v2s = verts(get_1d_ind(x-1,y,z,d));
        v3s = verts(get_1d_ind(x-1,y,z-1,d));
        V5s = verts(get_1d_ind(x,y,z-1,d));
        inds2=get_1d_ind(xs,ys+1,zs,d);
        idx3=inds2(tempind5);
        x1=0;y1=0;z1=0;
        [x1,y1,z1]=ind2sub(d,idx3);
        templabel=[templabel;[x1,y1,z1]];
    case 6
        v2s = verts(get_1d_ind(x,y-1,z,d));
        v3s = verts(get_1d_ind(x-1,y-1,z,d));
        V5s = verts(get_1d_ind(x-1,y,z,d));
        inds2=get_1d_ind(xs,ys,zs+1,d);
        idx4=inds2(tempind6);
        x1=0;y1=0;z1=0;
        [x1,y1,z1]=ind2sub(d,idx4);
        templabel=[templabel;[x1,y1,z1]];
    end
    faces(end+1:end+length(x),:) = [v1s; v2s; v3s; V5s]';
end
lx=templabel(:,1);
ly=templabel(:,2);
lz=templabel(:,3);

```

```

tempim=zeros(length(w(:,1,1)),length(w(1,:,1)),length(w(1,1,:)));
tempim(2:d(1)-1,2:d(2)-1,2:d(3)-1)=im1;
lxl=length(lx);
L_label=[];
for g=1:lxl
L_label(g)=tempim(lx(g),ly(g),lz(g));
end
temp_faces=[faces(:,1);faces(:,2);faces(:,3);faces(:,4)];
[count, bin] = histc(temp_faces, unique(temp_faces));
lc=length(count);
verind_table=zeros(lc,1);
tempim=[];
verind_table=[];
parts=['/net/age3/ADNI_Hippo_FSL/freesurfersub/',...
mask_files(m).name(1:end-13),'/'];
sw1=[parts,'rposterior_Left-Hippocampus.nii'];
sw2=[parts,'rposterior_Right-Hippocampus.nii'];
sw3=[parts,'rposterior_lefthippo_r.nii'];
if exist(sw1)
ob1=[parts,'rposterior_left_1hippo_r.nii'];
cmd=['mv ', sw1, ' ', ob1];
system(cmd);
pause(10);
end
if exist(sw2)
ob2=[parts,'rposterior_right_1hippo_r.nii'];
cmd=['mv ', sw2, ' ', ob2];
system(cmd);
pause(10);
end
end

```

```

if exist(sw3)
ob1=[parts,'rposterior_left_1hippo_r.nii'];
cmd=['mv ', sw1, ' ', ob1];
system(cmd);
pause(10);
end
tempim0=zeros(length(bim(:,1,1)),length(bim(1,:,1)),length(bim(1,1,:)));
for m_1=1:fix_length
    [m_1name,m_1add]=strtok(fix_holes(m_1).name, '.');
    loadme=[parts,m_1name, '.nii'];
    tempk=load_nifti(loadme);
    tt=tempk.vol(Lx_min:Lx_max,Ly_min:Ly_max,Lz_min:Lz_max);
    tempim0=tt./max(max(max(tt)))+tempim0;
end
tempim0=tempim0./(max(max(max(tempim0)))+1);
tt1=tempim0+bim;
[r11,c11,v11] = ind2sub(size(im1),find(tt1 < 1)); %% tt1<1 delete
[r12,c12,v12] = ind2sub(size(im1),find(tt1 == 1)); %% tt1==1 holes
L_holes=length(r12);
L_clean=length(r11);
for m_1=1:fix_length
    [m_1name,m_1add]=strtok(fix_holes(m_1).name, '.');
    loadme=[parts,m_1name, '.nii'];
    tempk=load_nifti(loadme);
    tm1=tempk.vol(Lx_min:Lx_max,Ly_min:Ly_max,Lz_min:Lz_max);
    loadme2=[fix_path,fix_holes(m_1).name];
    tempk2=load_nifti(loadme2);
    tm2=tempk2.vol(Lx_min:Lx_max,Ly_min:Ly_max,Lz_min:Lz_max);
    for g=1:L_clean
        tm1(r11(g),c11(g),v11(g))=0;
    end
end

```

```

end
for g=1:L_holes
    tm1(rl2(g),cl2(g),vl2(g))=tm2(rl2(g),cl2(g),vl2(g));
end
tempim{m_1}=zeros(length(w(:,1,1)),length(w(1,:,1)),length(w(1,1,:)));
tempim{m_1}(2:d(1)-1,2:d(2)-1,2:d(3)-1)=tm1;
tempim{m_1}=tempim{m_1}./max(max(max(tempim{m_1})));

for g=1:lx1
L_label1{m_1}(g)=tempim{m_1}(lx(g),ly(g),lz(g));
end
verind_table{m_1}=zeros(lc,1);
verind_table_C{m_1}=zeros(lc,1);
for g=1:lx1
    verind_table{m_1}(faces(g,:),1)=verind_table{m_1}(faces(g,:),1)+L_label1{m_1}(g);
    verind_table_C{m_1}(faces(g,:),1)=verind_table_C{m_1}(faces(g,:),1)+1;
end
verind_table{m_1}=verind_table{m_1}./verind_table_C{m_1};
end
for g=1:lc
    [value,label(g)]=max([verind_table{1}(g),verind_table{2}(g),verind_table{3}(g),...
    verind_table{4}(g),verind_table{5}(g),...
    verind_table{6}(g),verind_table{7}(g),verind_table{8}(g)]);
end
promap=verind_table;
verind_table=label';
saveto1=['/net/age3/ADNI_Hippo_FSL/submat/',...
mask_files(m).name(1:end-11),'_V5_fix.mat'];
bim=temp_w;
mins=mins-1;

```

```

        face_table=L_label';
        save(saveto1,'bim','mins','verind_table','face_table','vertices','faces','promap');
    end
    h = figure;
    saveto=['/net/age3/ADNI_Hippo_FSL/subpics_V5/',mask_files(m).name(1:end-4),'_V5_ver'];
    hold on;
    subplot(2,2,1);title(strrep(mask_files(m).name(1:end-4),'_','-'));
    vertnum = size(vertices,1);
    facenum = size(faces,1);
    patches = patch('faces', faces, 'vertices', vertices, ...
        'FaceVertexCData', verind_table, ...
        'FaceColor', 'inter', 'EdgeColor', 'none', 'FaceAlpha', 1);
    FaceAlpha
    material([.3 .4 .2 10]);
    lighting phong;
    axis image;
    box on;
    view(37.5, 30);
    subplot(2,2,2);title(strrep(mask_files(m).name(1:end-4),'_','-'));
    vertnum = size(vertices,1);
    facenum = size(faces,1);
    patches = patch('faces', faces, 'vertices', vertices, ...
        'FaceVertexCData', verind_table, ...
        'FaceColor', 'inter', 'EdgeColor', 'none', 'FaceAlpha', 1);
    material([.3 .4 .2 10]);
    lighting phong;
    axis image;
    box on;
    view(217.5, 30);
    subplot(2,2,3);title(strrep(mask_files(m).name(1:end-4),'_','-'));

```

```

vertnum = size(vertices,1);
facenum = size(faces,1);
patches = patch('faces', faces, 'vertices', vertices, ...
                'FaceVertexCData', verind_table, ...
                'FaceColor', 'inter', 'EdgeColor', 'none', 'FaceAlpha', 1);
                FaceAlpha
material([.3 .4 .2 10]);
lighting phong;
axis image;
box on;
view(37.5, 210);
subplot(2,2,4);title(strrep(mask_files(m).name(1:end-4),'_','-'));
vertnum = size(vertices,1);
facenum = size(faces,1);
patches = patch('faces', faces, 'vertices', vertices, ...
                'FaceVertexCData', verind_table, ...
                'FaceColor', 'inter', 'EdgeColor', 'none', 'FaceAlpha', 1);
                FaceAlpha
material([.3 .4 .2 10]);
lighting phong;
axis image;
box on;
view(217.5, 210);
saveas(h, saveto, 'fig');
hold off;
close(h);
end
return;
%
% convert 1d index to 3d index

```

```
%  
function [xs, ys, zs] = get_3d_ind(is, d)  
xs = mod(is-1, d(1))+1;  
ys = mod((is-xs)/d(1), d(2))+1;  
zs = (is-xs-(ys-1)*d(1))/(d(1)*d(2))+1;  
return;  
%  
% convert 3d index to 1d index  
%  
function is = get_1d_ind(xs, ys, zs, d)  
is = (zs-1)*d(1)*d(2) + (ys-1)*d(1) + xs;  
return;
```